On Characterization and Optimization of Surface Topography in Additive Manufacturing Processes

AMOGH VEDANTHA KRISHNA

Department of Industrial and Materials Science
Chalmers University of Technology
Gothenburg, Sweden 2022

ABSTRACT

With its ability to construct components through the layer-by-layer deposition of material, Additive Manufacturing (AM), more commonly known as "3D printing", has revolutionized the manufacturing industries. Not only can AM produce complex lightweight designs, but it can also streamline the supply chain, allowing businesses to more quickly and easily meet customer demand. Additionally, with the rising demand for low-volume customized products, and sustainable production, manufacturers are increasingly compelled to adopt AM to remain competitive in the global economy. Despite its popularity, AM has several significant drawbacks, one of the most notable being its poor surface topography quality. Most product failures can be traced back to the initial surface conditions, making the surface texture a crucial factor in determining how well a product will perform. Hence, this thesis presents a study on the surface topography of various AM processes mainly to understand the surface behavior in relation to the factors affecting it.

Every manufacturing process including AM generates distinct surface features referred to as "footprints" or process signatures which substantially affect the surface quality and function. These process signatures vary based on changes in AM processes and their process settings, materials, and geometrical design. The accuracy of identifying and analyzing these features becomes crucial in defining their relationship with manufacturing process variables. Usually, the best practice for defining surface quality is through parametric characterization which provides a quantitative description of either the stochastic or deterministic nature of manufactured surfaces. However, the challenge with AM is that it generates surfaces that often contain both the aforementioned surface features which make it particularly difficult to identify the manufacturing "footprints" through the parametric description. Therefore, the surface topography of AM may often require novel characterization methods to fully interpret the manufacturing process and thereby predict and optimize its product performance.

The overall goal of this thesis is to provide an optimal approach toward the characterization of AM surfaces so that it gives a better understanding of the manufacturing process and also assists in process optimization to control the surface quality of the printed products. To realize this goal, the surface texture of AM processes was studied particularly Material Extrusion (MEX), Vat photopolymerization (VPP), and Powder Bed Fusion (PBF). These processes present topographical features that cover most of the surface scenarios in AM. Hence to explain these varied surface features, a diverse range of surface characterization tools such as Power Spectral Density (PSD), Scale-sensitive fractal analysis, feature-based characterization, and quantitative characterization by both profile and areal surface texture parameters were included in the analysis. Additionally, a methodology was developed using a statistical approach (Linear multiple regression) and a combination of the above-mentioned characterization techniques to identify the most significant parameters for discriminating different surfaces. Finally, the knowledge gained through the above-mentioned measurements and analysis is put to use to optimize the AM process to achieve enhanced surface quality. The results suggest that the developed approaches can be used as a guideline for AM users who are looking to optimize the process for gaining better surface quality and component functionality, as it works effectively in finding the significant parameters representing the unique signatures of the manufacturing process.

Keywords: additive manufacturing, vat-photopolymerization, fused deposition modeling, laser-based Powder bed fusion, surface metrology, power spectral density, scale-sensitive fractal analysis, feature-based characterization, profile parameters, areal surface texture parameters, and multiple regression.

ACKNOWLEDGEMENTS

APPENDED PUBLICATIONS

Paper 1: Amogh V. Krishna, O. Flys, V. V. Reddy, and B. G. Rosén, "Surface topography characterization using 3D stereoscopic reconstruction of SEM images," Surf. Topogr. Metrol. Prop., vol. 6, no. 2, 2018, doi: 10.1088/2051-672X/aabde1.

Contribution: Amogh Krishna initiated the study on 3D SEM reconstruction, performed surface measurements, developed a method for characterization, and wrote the paper. Olena Flys and Vijeth took part in the planning/discussion and provided inputs for the paper. Prof. BG Rosén reviewed the paper by providing his expert opinion.

Paper 2: Amogh V. Krishna, O. Flys, V. V. Reddy, A. Leicht, L. Hammar, and B. G. Rosen, "Potential approach towards effective topography characterization of 316L stainless steel components produced by selective laser melting process," Eur. Soc. Precis. Eng. Nanotechnology, Conf. Proc. - 18th Int. Conf. Exhib. EUSPEN 2018, June, pp. 259–260, 2018.

Contribution: Amogh Krishna initiated the study, developed the experimental design, performed surface measurements, developed analysis methods, and wrote the paper. Olena Flys and Vijeth Reddy took part in the planning/discussion and provided inputs for the paper. Leicht and Hammar manufactured the samples for the study. Prof. BG Rosén reviewed the paper.

Paper 3: Amogh V. Krishna, M. Faulcon, B. Timmers, Vijeth V. Reddy, H. Barth, G. Nilsson and B.-G. Rosén, "Influence of different post-processing methods on surface topography of fused deposition modelling samples," Surf. Topogr. Metrol. Prop., vol. 8, no. 1, p. 014001, Feb. 2020, doi: 10.1088/2051-672X/AB77D7.

Contribution: Amogh Krishna conceptualized the paper, developed the experimental design, performed analysis, and wrote the paper. Faulcon and Timmers produced samples and performed surface measurements. Vijeth Reddy, Henrik Barth, and Prof. B-G Rosén took part in the planning/discussion and provided inputs for the paper. Gunnar Nilsson provided a use case for proof of concept and Prof. BG Rosén acted as the reviewer of the paper.

Paper 4: Amogh V. Krishna, O. Flys, V. V. Reddy, J. Berglund, and B. G. Rosen, "Areal surface topography representation of as-built and post-processed samples produced by powder bed fusion using laser beam melting," Surf. Topogr. Metrol. Prop., vol. 8, no. 2, p. 024012, Jun. 2020, doi: 10.1088/2051-672X/ab9b73.

Contribution: Amogh Krishna and Olena Flys initiated the study. Amogh performed surface measurements, analyzed the data, and wrote the paper. Olena Flys and Vijeth took part in the planning/discussion and provided inputs for the paper. Johan Berglund and Prof. BG Rosén reviewed the paper by providing his expert opinion.

Paper 5: V. Reddy, O. Flys, A. Chaparala, C. E. Berrimi, **Amogh V. Krishna**, and B. G. Rosen, "Study on surface texture of Fused Deposition Modeling," Procedia Manuf., vol. 25, pp. 389–396, 2018, doi: 10.1016/j.promfg.2018.06.108.

Contribution: Vijeth Reddy and Amogh Krishna conceptualized the paper. Vijeth developed the experiments, analyzed the samples, and wrote the paper. Chaparala and Berrimi produced the samples and performed surface measurements. Amogh took part in the planning/discussion and provided inputs for the paper. Olena and Prof. BG Rosén reviewed the paper.

Paper 6: S. Dizdar and **Amogh V. Krishna**, "Microstructural and Mechanical Properties of Polylactic Acid/Tin Bronze Tensile Strength Bars Additive Manufactured by Fused Deposition Modelling," pp. 566–579, 2022, doi: 10.3233/atde220175.

Contribution: Senad Dizdar conceptualized the paper and is the main author of this paper. Amogh Krishna developed the experiments for 3D printing, optimized the process, and produced the samples. Amogh took part in the planning/discussion and was the co-writer of this paper. Senad Dizdar performed de-binding and sintering experiments and evaluated the samples.

Paper 7: Amogh V. Krishna, Vijeth V. Reddy, Dyall W Dexter, Dan-Åke Wälivaara, Peter Abrahamsson, B-G Rosen, and Jonas Anderud, "Quality assurance of Stereolithography based biocompatible materials for dental applications". Submitted to the Journal.

Contribution: The maxillofacial doctors Anderud, Abrahamsson, Dexter, and Wälivaara initiated the study. Amogh Krishna and Vijeth Reddy conceptualized the paper. Amogh developed the experiments, produced the samples, performed surface measurements, analyzed the data, and wrote the paper. All the co-authors took part in the planning/discussion and provided inputs for the paper. Prof. BG Rosén provided his expert advice in surface and dimensional analysis and reviewed the paper.

ADDITIONAL PUBLICATIONS

Paper 8: V. V Reddy, O. Flys, **Amogh. V. Krishna**, and B. Rosen, "Topography characterization of fused deposition modelling surfaces," Eur. Soc. Precis. Eng. Nanotechnology, EUSPEN 2017, October, pp. 5–8, 2017.

Paper 9: V. V. Reddy, **Amogh V. Krishna**, F. Schultheiss, and B. G. Rosén, "Surface topography characterization of brass alloys: lead brass (CuZn39Pb3) and lead-free brass (CuZn21Si3P)," Surf. Topogr. Metrol. Prop., vol. 5, no. 2, p. 025001, Apr. 2017, doi: 10.1088/2051-672X/AA612B.

Paper 10: V. V. Reddy, P. L. Tam, **Amogh V. Krishna**, and B. G. Rosén, "Characterization of subsurface deformation of turned brasses: lead brass (CuZn39Pb3) and lead-free brass (CuZn21Si3P)," J. Phys. Conf. Ser., vol. 1183, no. 1, p. 012006, Mar. 2019, doi: 10.1088/1742-6596/1183/1/012006.

x

LIST OF ABBREVIATIONS AND SYMBOLS

AM	Additive Manufacturing
SDG	Sustainable Development Goals
UN	United Nations
CT	Computed Tomography
PBF	Powder Bed Fusion
PBF-LB/M	Laser-Based Powder Bed Fusion of Metals
FDM	Fused Deposition Modeling
SLA	Stereolithography
VPP	Vat-photopolymerization
ABS	Acrylonitrile Butadiene Styrene
RQ	Research Questions
ML	Machine Learning
ASTM	American Society for Testing and Materials
ISO	International Organization of Standardization
BJT	Binder Jetting
DED	Directed Energy Deposition
LENS	Laser Engineered Net Shaping
EBW	Electron Beam Welding
MEX	Material Extrusion
MJT	Material Jetting
UV	Ultra-violet
PBF-LB/P	Laser-Based Powder Bed Fusion of Polymers
PBF-EB/M	Electron Beam Powder Bed Fusion of Metals
EBM	Electron Beam Melting
EBAM	Electron Beam Additive Manufacturing
SLS	Selective Laser Sintering
DMLS	Direct Metal Laser Sintering
SLM	Selective Laser Melting
SHL	Sheet Lamination
LOM	Laminated Object Manufacturing
UAM	Ultraviolet Additive Manufacturing
CAD	Computer-Aided Design
DLP	Digital Light Processing
CLIP	Continuous Liquid Interface Production
SGC	Solid Ground Curing
STL	Standard Triangle Language
LPS	Liquid Phase Sintering
LAF	Laser-Assisted Finishing

AVF	Acetone Vapour Finishing
$h(x, y)$ or $z(x,y)$	Surface height map
$h(x)$ or $h(\theta)$	Profile height
x	Linear displacement in x direction
y	Linear displacement in y direction
θ	Angular displacement
CSI	Coherence Scanning Interferometry
FP	Fringe Projection
$\emptyset$	Angle of the light projector in FP
α	Angle of the camera
p	Known Distance between the Projector and Camera
q	Unknown Distance of the point on the object's surface
C	Point on the surface
CM	Confocal Microscope
LSCM	Laser Scanning Confocal Microscope
FV	Focus Variation
CCD	Charge-Coupled Device
CF	Confocal Fusion
SEM	Scanning Electron Microscope
S-F	Surface obtained after applying F-operator
S-L	Surface obtained after applying L-filter
F-operator	Form operator
L-filter	Large-scale filter
S-filter	Small-scale filter
λs	Low pass micro-roughness filter
λc	High pass filter
P	Primary profile
R	Roughness profile
W	Waviness profile
S	Surface
V	Volume
GPS	Geometrical Product Specifications
PSD	Power Spectral Density
ASME	American Society of Mechanical Engineers
A	Area
F	Fourier Transform
FFT	Fast Fourier Transform
u	Lateral displacement in the spatial frequency domain in the x-direction
v	Lateral displacement in the spatial frequency domain in the y-direction
b	Breadth of the pixel
l	Length of the pixel
APSD	Areal Power Spectral Density
ANOVA	Analysis of Variance

SSFA	Scale-sensitive fractal analysis
SMFC	Scale of Maximum Fractal Complexity
R^2	Coefficient of determination
Lt	Layer thickness
α	Build inclination
Ra	Arithmetic mean deviation of roughness profile
Rp	Maximum peak height of roughness profile
Rz	Maximum height of roughness profile
Rdc	Roughness profile Section Height difference
Rv	Maximum valley depth of the roughness profile.
Rsm	Mean width of roughness profile elements
Rpc	Peak count on the roughness profile
Sa	Average Roughness
Sq	Root Mean Square Height
Ssk	Skewness
Sku	Kurtosis
Sz	Maximum height
Sp	Maximum peak height
Sv	Maximum valley depth
Smc	Inverse Material Ratio
Sal	Auto-Correlation Length
Str	Texture Aspect Ratio
Sdq	Root Mean Square Gradient
Sdr	Developed Interfacial Area Ratio
Vmc	Core Material Volume
Vvc	Core Void Volume
Vv	Void Volume
CDF	Cumulative Distribution Function
DOE	Design of Experiments
S/N	Signal to Noise ratio
LI	Low Infill in FDM process settings
MI	Medium Infill in FDM process settings
HI	High Infill in FDM process settings
HQ	High Quality in FDM process settings
MQ	Medium Quality in FDM process settings

LIST OF FIGURES

LIST OF TABLES

TABLE OF CONTENTS

Chapter 1

INTRODUCTION

This chapter presents the Introduction which begins with a background to the research field followed by the aim of the thesis. A research approach is presented which forms the basis of the structure followed in this thesis. Research questions are then formulated based on the research approach and finally, delimitations of the research are addressed.

1.1 BACKGROUND

Additive Manufacturing (AM) is the standardized term for what was formerly known as Rapid prototyping and what is popularly known as "3D printing" [1]. Rapid prototyping refers to the process of manufacturing a product relatively fast but created mainly for prototyping purposes. However, recent technological advancements have made it possible for this technique to be used more for end-user applications, and hence the international committee of standards has coined the term Additive Manufacturing [2]. The nature of manufacturing products by the deposition of materials layer by layer has given AM several sustainability advantages. AM provides industries with minimal carbon footprints for the products manufactured, the capability of repairing, remanufacturing, and reverse engineering products, opportunities for reducing energy consumption and manufacturing costs, and the capability of providing a significant reduction in wastage [1]. This technological advantage of AM is in line, particularly with 2 of the 17 Sustainable Development Goals (SDGs) of the United Nations (UN) [3] i.e. Industries, Innovation and Infrastructure, and Responsible Consumption and Production. The SDGs in the context of AM are discussed further in section 2.1.4.

Furthermore, the ability of AM to fabricate complex lightweight designs and internal structures has proved to be a real game-changer in manufacturing sectors. It is due to this reason that AM finds its application in automotive [4], aerospace [5], medical [6], and dental areas [7]. This disruptive nature of AM is not yet fully realized in industries mainly due to its inability to match the standards set by traditional manufacturing processes in terms of high product quality, reliability, repeatability, and product performance [8]. AM is often associated with post-finishing methods to bring the produced products to the required specifications. However, there is a continual effort to improve AM technology to reduce these gaps to ultimately help industries leverage the potential of this technique. Nonetheless, it is important to address these challenges so that it adds value to the knowledge base required for improving AM technology in the future and one such challenge pertaining to surface quality is discussed in this thesis.

Surface texture metrology provides insight into the physical phenomena that take place during AM process through investigation of the surface topography produced by the process [9]. Often the relationship between the physical phenomena and AM process control variables is studied to get an increased knowledge of the process to optimize and control the surface quality and its product function. The investigation of surface texture typically involves capturing the surface features and characterizing them. As a first step, it is important to capture the complete surface topography information using appropriate surface metrology methods. Previous studies have shown that the most widely used surface metrology method is contact stylus measurement with profile roughness parameters defining the AM surface topography [9][10]. Generally, profile

measurements provide insufficient data for optimization since they provide roughness information in only one measuring direction. On the contrary, areal surface measurements can be more advantageous since it provides the waviness and roughness information in both the lateral directions of the surface being measured [11]. It provides a better representation of the surface topography and could be more efficient in optimizing the surface quality and function. The real surface topography can also be captured by more sophisticated metrology instruments such as Computed Tomography (CT) instruments, which provide a voxel representation of the surface that ensures capturing the areal surface topography with thickness information [12] along with the re-entrant features [13][14] on the complex AM surfaces. This type of measurement can provide complete surface information required for optimization. The next step is to characterize the captured surfaces to selectively extract useful information that affects the surface quality and product function. The surface topography can be characterized either quantitatively or qualitatively or both through image analysis, roughness parameters analysis, and more advanced methods such as power spectral density, fractal analysis, feature-based characterization, and so on. Based on the nature of captured surfaces and as per the functional requirement an appropriate metrology and characterization method must be chosen for analysis. In this thesis, the areal surface topography of AM processes was captured by state-of-the-art metrology instruments (using mostly optical and contact stylus methods) and analyzed using both parametric and advanced characterization methods to interpret the AM surfaces. The following sections discuss in detail the research focus, structure, and approach which have been undertaken to ultimately reach the common goal of improving AM surface quality.

1.2 AIM OF THE THESIS

The focus of this thesis is to establish a framework for characterizing the Additive Manufacturing and post-processing surfaces and to enable the prediction and optimization of the surface topography quality to achieve its intended component function. This is accomplished by

- a. Employing scale-limited and multi-scale characterization of AM surface topography to identify the unique surface features representing the "footprints" of the manufacturing process.
- b. Developing a methodology to identify the most significant surface texture parameters that affect the quality of AM products.
- c. Employing statistical methods to establish the relationship between the AM process parameters and surface texture for prediction and optimization of surface quality
- d. Finally, the above-mentioned methods are employed in industrial and dental use cases to ensure high-quality AM end products.

1.3 RESEARCH APPROACH

This thesis presents a research approach that is based on the surface control loop system first published by Stout and Davis [15]. It mainly consists of three important facets namely, manufacturing, characterization, and function, as shown in Figure 1. These facets are looped together as their interdependency is crucial for achieving surface quality control for any manufacturing process. The surface characterization alone will be of little value if is not associated with any manufacturing process and product function. Hence, every manufacturing

process requires characterization to *interpret* its surfaces that can *predict* its functional behavior and knowing its function could enable *optimization* of the manufacturing process to again achieve its intended function efficiently.
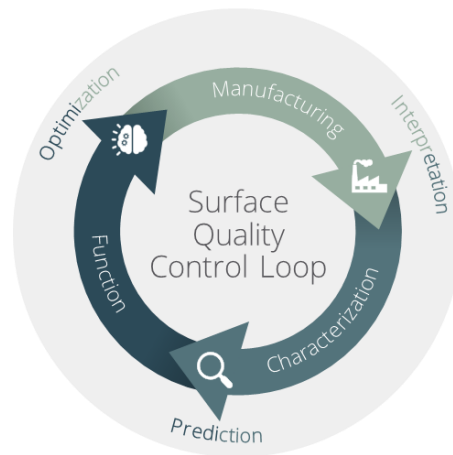
Figure 1. Control loop depicting the interdependence of three facets of surface quality control.

Based on the surface control loop, a detailed overview of the research structure is summarized visually in Figure 2. This thesis presents a compilation of many different AM processes, materials, post-AM processes, surface metrology, and characterization techniques, mainly utilized to establish the most effective method for characterizing AM surfaces. This leads to a better understanding of AM processes required for predicting and optimizing its product functional performance.

In this research, the surfaces belonging to three of the seven process categories [2] of AM namely Powder Bed Fusion (PBF) specifically the Laser-Based Powder Bed Fusion of Metals (PBF-LB/M) technology, Fused Deposition Modelling (FDM) under the Material Extrusion category, and finally, the Stereolithography (SLA) under the category of Vat-photopolymerization AM technology were utilized for analysis. These AM surfaces were produced by varying their respective process parameters such as layer thickness, infill density, print temperature, and so on. It must be noted that the influence of different AM build materials on the surface topography is not included in the study since the selection of materials vary with respect to the heating capacity of the machine [16]. Besides this thesis focuses on capturing the physical phenomena through surface analysis rather than studying the material influence on surface topography. In this thesis, Acrylonitrile butadiene styrene (ABS) material was utilized in FDM processes, Acrylic and epoxy-based resin material were used for the SLA process and 316L stainless steel was employed for studying the PBF-LB/M process. AM surfaces were also subjected to various post-processing methods as listed in Figure 2, and by varying their respective post-processing parameters different surface conditions were obtained. All the surfaces were then measured using various state-of-the-art tactile and optical metrology instruments. Several different topography characterization techniques were utilized to interpret the measured multi-scale and scale-limited AM surfaces. In addition, a statistical method (Linear multiple regression) was utilized for predicting the functional behavior and to understand its influence with respect to process parameters. The function in this context is defined based on the surface finish requirements obtained from the two use cases. The first use case is from the industry where the requirement is to produce AM surfaces close to the surface finish of the injection moulding component comprising a matte finish. The second use case is

from dentistry where importance was provided to producing surface topography suitable for bone regeneration. Finally, the developed approaches for interpretation, prediction, and optimization of AM processes were validated in the above-mentioned use cases to achieve the required function.
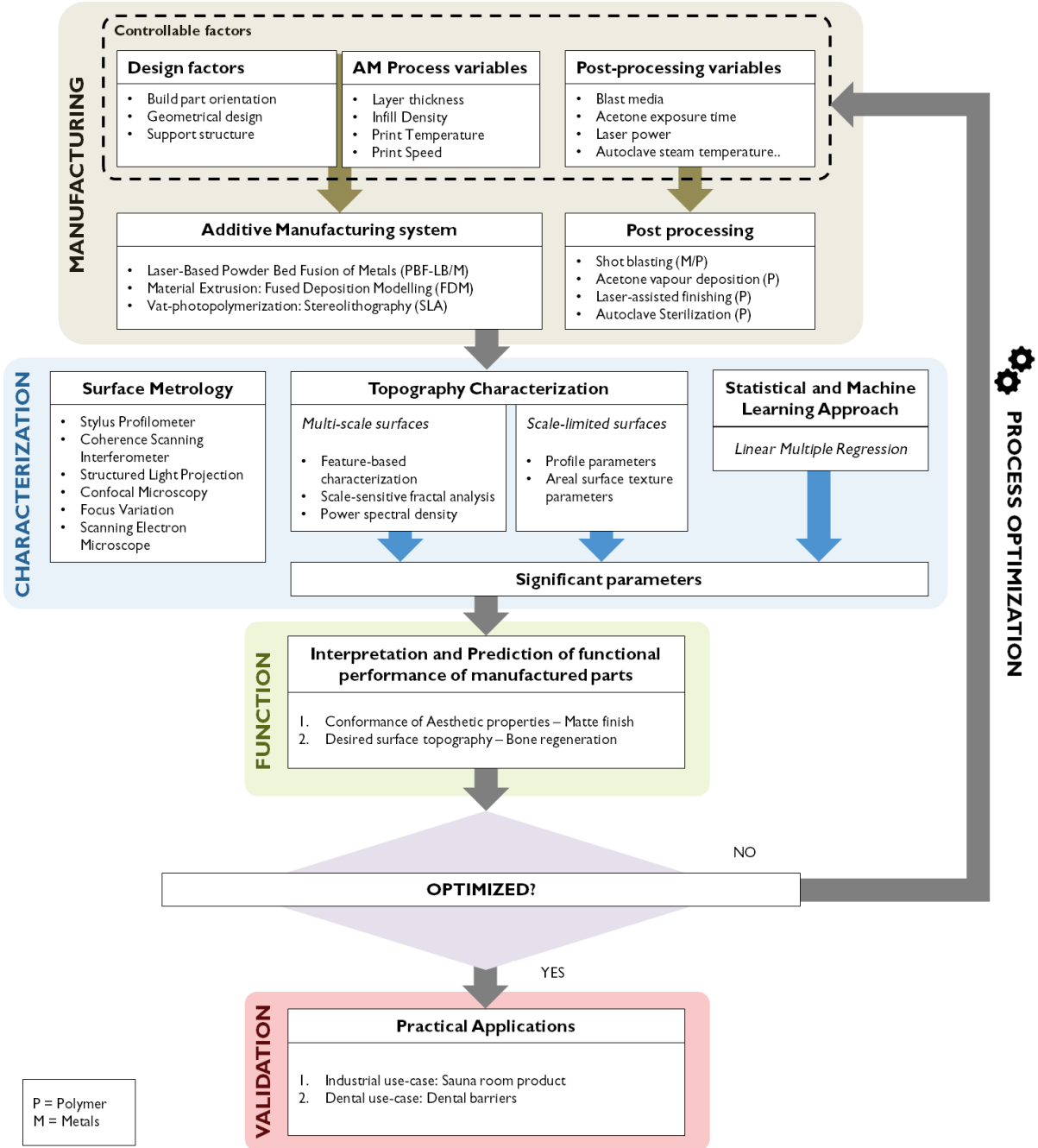
Figure 2. *Research workflow based on the surface control loop for the development of functional surfaces of the Additive Manufacturing process.*

1.4 RESEARCH QUESTIONS

This thesis is based on the following four Research Questions (RQs) that are designed to include the three facets of the surface control loop along with an additional validation step. The first three RQs address the characterization, manufacturing, and function facet of the control loop. The fourth RQ is designed to answer the validation step where the findings from the surface control loop are implemented and verified in an industrial and dental application.

1. What are the various topography characterization methods employed in this thesis that can be used to interpret scale-limited and multi-scale Additive Manufacturing surfaces?

2. How does the identification of significant roughness parameters improve the understanding of AM and post-processes?

3. How can the statistical data analysis method facilitate the optimization of the additive manufacturing processes for achieving its intended surface function?

4. How to validate the obtained research results in Industrial and Dental use cases?

The answer to these crucial research questions can be found in the appended research papers and Figure 3 shows the research questions classified as per the surface control loop associated with respective research papers.
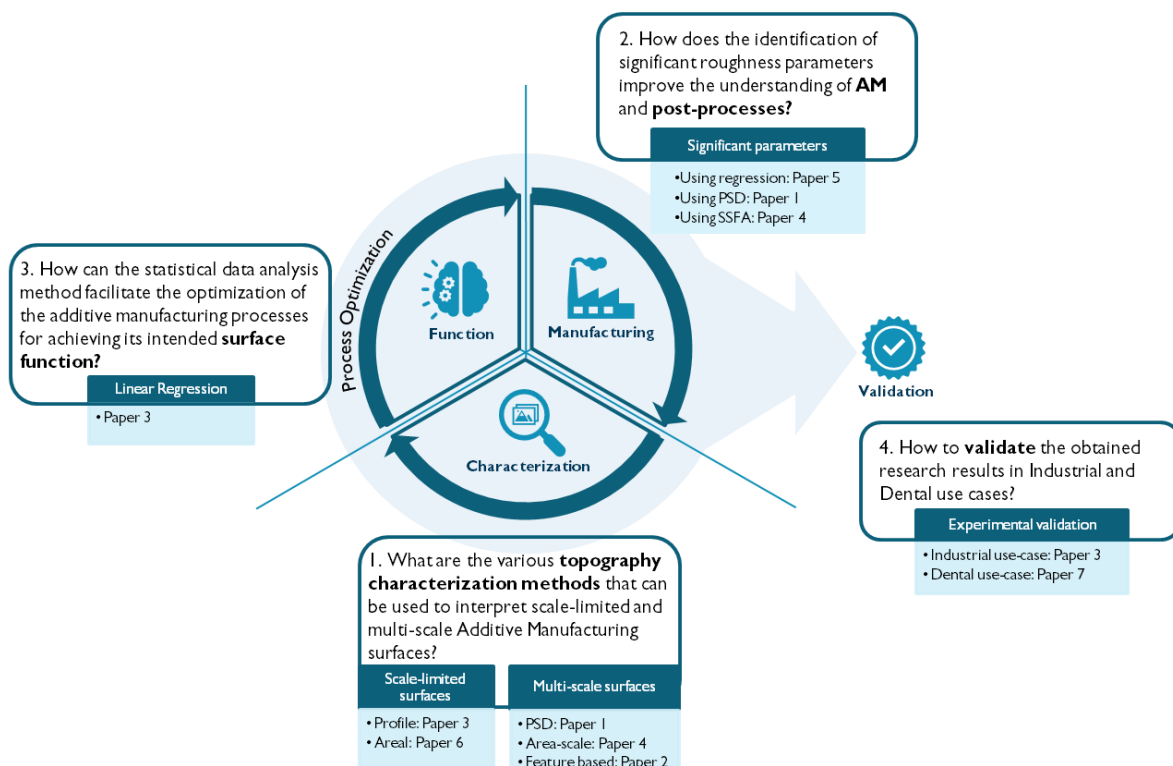
Figure 3. *Research questions as per the surface control loop*

1.5 DELIMITATIONS

- The surface analysis performed in this research is confined to parts produced by PBF-LB/M, FDM, and SLA techniques. However, several other AM methods produce surface features differently, and hence it may be necessary to explore other AM methods before generalizing the results from this study.
- In this thesis, the AM process is optimized to achieve its intended surface quality and function based on the established relationship between the surface texture parameters and the controllable process parameters (layer thickness, print temperature, and so on). However, the effect of the uncontrolled process parameters such as environmental temperature, vibrations during the printing process, humidity levels, etc. has to be studied to fully establish the AM process optimization.
- Surface analysis is strictly restricted to up-skin [17] or top surfaces of parts produced by AM processes partly due to the limitation of surface metrology employed in this thesis and also to avoid the influence of support structures which are often required to support down-skin surfaces.
- The surface measurements are based on tactile and optical methods which often fail to capture the re-entrant features [13], predominantly found on the down skin surfaces. It is necessary to use other surface metrology methods such as Computed Tomography (CT) to capture these re-entrant features and to explore the extent of their impact.
- The statistical method used in this research is confined to a linear approach to identify the influence of AM process settings on surface texture and to predict its functional behavior. A polynomial approach or Machine Learning methods with advanced algorithms would have to be explored to determine if they can improve the prediction of surface quality and function.

1.6 THESIS STRUCTURE

Chapter 1 presents a brief introduction discussing the background, aim, research approach, and thesis delimitations.

Chapter 2 includes an overview of Additive Manufacturing processes and post-processing methods along with their associated surface conditions.

Chapter 3 addresses the state-of-the-art in surface metrology for AM processes.

Chapter 4 describes topography characterization techniques used for AM surfaces.

Chapter 5 illustrates the research methodology.

Chapter 6 outlines the results based on the surface control loop.

Chapter 7 provides conclusions and future work.

Chapter 2

MANUFACTURING SYSTEMS

This chapter provides an overview of various Additive Manufacturing (AM) systems and post-processing methods utilized in this research along with their associated surface formations. It also includes a short discussion on the sustainability aspects of AM.

2.1   ADDITIVE MANUFACTURING PROCESSES

Additive Manufacturing (AM) widely known as 3D printing is a process of building an object by material deposition in layers [1]. As per ISO/ASTM 52900:2015 standard, AM is defined as the *"process of joining materials to make parts from 3D model data, usually layer upon layer, as opposed to subtractive manufacturing and formative manufacturing methodologies"* [2]. The unique technique of building parts layer by layer has provided industries with numerous advantages, which is why AM is considered the emerging next-generation technology in part manufacture. Not so long ago, the patents on the first generation of printers expired, which has led to explosive expansion in the additive manufacturing business [1]. Today, there are several types of AM technologies that are broadly classified into seven categories.

- *Binder Jetting (BJT)* is an AM fabrication process where binders (glue) material is selectively deposited that combines the powder materials to build the part [2]. The as-built parts are usually in the green state and require a consolidation step to fully achieve the required mechanical properties of the parts. Depending on the type of material, the consolidation step differs, typically for polymer materials, the build parts are left to cure in the printing chamber and for metallic materials, the sintering process or infiltration with metals that have low melting temperatures is performed after the printing process [1][18].
- *Directed Energy Deposition (DED)* is an AM process that utilizes thermal energy to melt the materials while they are being deposited [2]. Laser Engineered Net Shaping (LENS) [1][19] and Electron Beam Welding (EBW) c are two common techniques for both wire-based and powder-based DED systems; as the names imply, a powerful laser beam or electron beam is employed as a heating source to melt the material.
- *Material Extrusion (MEX)* is an AM process of building components by selectively depositing the material through a nozzle or orifice by the application of pressure [2]. There are two variations of the MEX method, one approach is to use temperature as the controlling mechanism for the material flow and the other uses a chemical reaction to solidify the material deposited for building the products. Examples of the former approach are Fused Deposition Modelling (FDM) [1][20][21] and the latter approach it is Contour Crafting [22][23][24] and Bio-printing [25][26][27].
- *Material Jetting (MJT)* is an AM process in which droplets of build material, typically photo-curable resins are selectively deposited [2]. The deposited photo-sensitive resin material is cured using a UV light source and the process is repeated layer by layer to build the part [28].
- *Powder Bed Fusion (PBF)* is an AM process where a product is built by using thermal energy that selectively fuses the powder particles in a powder bed arrangement [2]. As per the ISO/ASTM 52911:2019 standard [29], the PBF method that uses a laser to fuse polymer or metal powders is referred to as Laser-based Powder Bed Fusion of Polymers or Metals

(PBF-LB/P or PBF-LB/M). This technology is also known by many other non-conventional names provided by AM technology and service providers. Selective Laser Metal (SLM) and Direct Metal Laser Sintering (DMLS) are mostly suited for metal and metal alloys respectively [1][30], and Selective Laser Sintering (SLS) [31] is typically reserved for producing polymer-based products. The PBF method that utilizes an electron beam for its fabrication process is termed Electron-beam Powder Bed Fusion of Metals (PBF-EB/M). Since electrons are used as a thermal source it only works for metal and metal alloys materials. It is also popularly known as Electron Beam Melting (EBM) or Electron Beam Additive Manufacturing (EBAM) and it has relatively higher surface roughness and higher productivity in comparison to PBF-LB/M but has limited material availability [32].

- *Sheet Lamination (SHL)* is an AM process where multiple sheets of materials are fused together to build a product [2]. There are two variants of this technology namely Laminated Object Manufacturing (LOM) and Ultraviolet Additive Manufacturing (UAM). The LOM process first cuts the sheets of paper or plastic as per the cross-sectional layer of the CAD geometry and then laminates it together to build the object [33]. The UAM process uses ultrasonic vibrations to weld sheets of metal foils and then uses subtractive manufacturing methods to bring the product to its required shape [34].

- *Vat photopolymerization (VPP)* is an AM technique where the liquid resin or photopolymer material is solidified selectively upon the incidence of photons to build an object [1][2]. The most popular methods of this process category are the Stereolithography (SLA) [35] technique which uses UV laser for curing and Digital Light Processing (DLP) [36] which uses visible light from a projector for curing the resin materials. Other VPP methods include Continuous Liquid Interface Production (CLIP) [37] and Solid Ground Curing (SGC) [38] which are mostly designed to increase the production speed.

The steps for AM part preparation remain nearly the same for all the AM processes. It involves creating a 3D CAD model in the design software which is then exported into STL (Standard Triangle Language) file format and the model slicing procedure is performed to breakdown the continuous geometry of the CAD model into several discrete layers. Once the printer has all the necessary data, it may begin fabricating the model layer by layer. In the following sections, the relevant AM process technologies utilized in this thesis are explained in detail along with an overview of the formation of the surface topography obtained with each process.

2.1.1 Laser-Based Powder bed fusion of Metals (PBF-LB/M)

Figure 4 illustrates the working principle of the PBF-LB/M process. The main components of this process include a high-powered laser source, focusing mirrors, a powder bed with a powder distributor, and powder dispensing and collecting systems. The whole fabrication process takes place inside a closed chamber filled with an inert gas to reduce oxidation during the build process. The laser from the source with the aid of focusing/scanning mirrors selectively melts the powders distributed over the platform to build a part. Depending on the type of process and material utilized there are four main powder fusion mechanisms namely, full melting, liquid-phase sintering (LPS), chemically induced sintering, and solid-state sintering. Full melting refers to the melting of powder particles into a liquid which then cools down to form a solid object. LPS refers to the process of joining powder particles when only some amounts of the powder particles are melted in a powder bed, while the rest remain solid. The molten powder particles act like a binding agent to fuse the remaining solid particles. Chemically induced sintering uses a thermal source to trigger chemical reactions between different types of powders

that create a byproduct that binds the powder particles together. Solid-state sintering is a process of binding powder particles together at elevated temperatures without melting them. Further discussion on these sintering processes is described in [1].
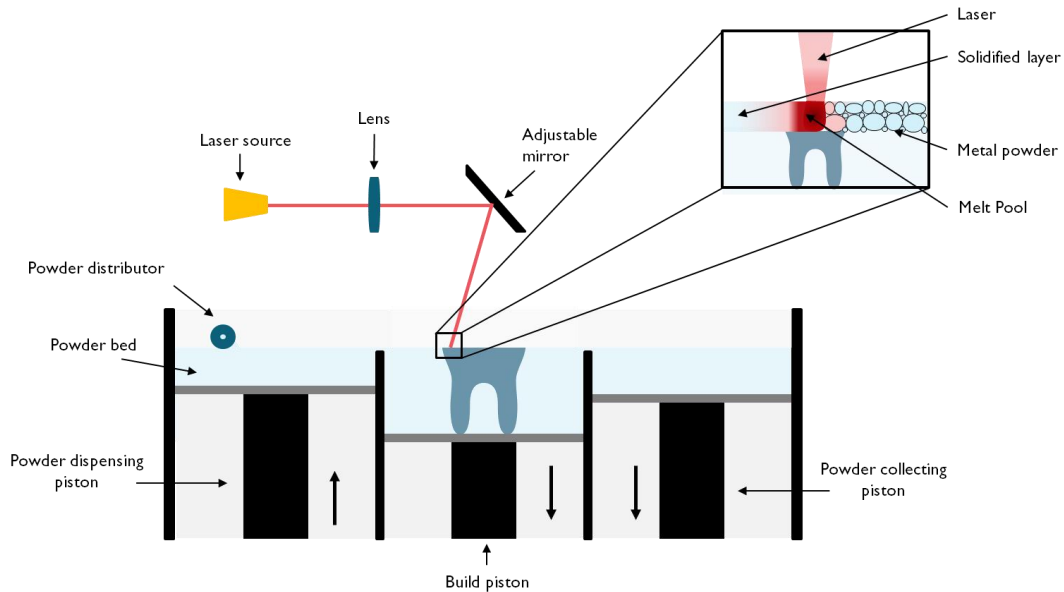
Figure 4. Illustration of Laser-based powder bed fusion of Metals (PBF-LB/M) process.

The formation of features on the surface topography of PBF-LB/M samples is a result of a complex cause-and-effect relationship between the process variables and corresponding physical phenomena [9]. The process variables or input parameters that affect the part quality are powder particle size, material composition and properties, laser beam spot size, energy deposition, scan speed, atmosphere, material homogeneity, linear track separation, vertical step height, powder reuse, part geometry, scanning strategy and errors caused due to motion & energy deposition [9]. The aforementioned process variables lead to the causation of the physical phenomena such as conduction heat transfer, phase changes, radiation heat transfer, denuding effect, balling effect, spatter, melt pool size, pore formation, Rayleigh instability, Marangoni circulation, the evolution of grain structure, thermal expansion & shrinkage, spatial variation in temperature (heat sinks), 'stair-step effect', raster pattern and residual stress [9][39]. Studying the surface topography can aid in determining the interrelationships between these variables, leading to more precise control of the manufacturing process and greater physical process stability [39].

Figure 5 illustrates the process of surface creation in the PBF-LB/M method. The stacking of layer upon layer during the fabrication process causes the formation of a "Stair-step" like feature on the surface and it is more pronounced on the slopes or curves of the sample. During the melting process, the powder particles in the powder bed adhere to the surface edges of each layer. On flat surfaces or surfaces at 0° build inclination, the laser melts most of the powder particles and so these surfaces contain mostly the footprints from the raster scanning of the lasers on its topography. On inclined surfaces, the "stair-step" formation occurs and as the build inclination or slope increases, the number of "stair-steps" increases, and additionally the adherence of powder particles to the surface also increases, increasing the surface roughness. However, at large slopes, the roughness decreases due to the reduced effect from the "stair steps" (see Figure 5c). This surface mechanism can be witnessed visually in Figure 6. It can be witnessed that surfaces contain raster (see 0° surface) and stair-step patterns (see 3° and 6° surface) at lower build inclinations and powder particles at higher build inclinations (beyond 15°).
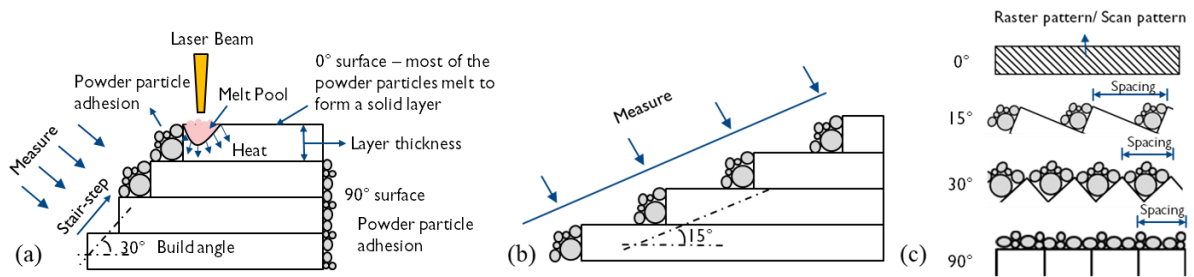
Figure 5. *Schematic representation of the PBF-LB/M process illustrating the mechanism of surface roughness development (a) at higher build inclination (b) lower build inclination and (c) visualization of surface roughness at various build inclinations.* [40]
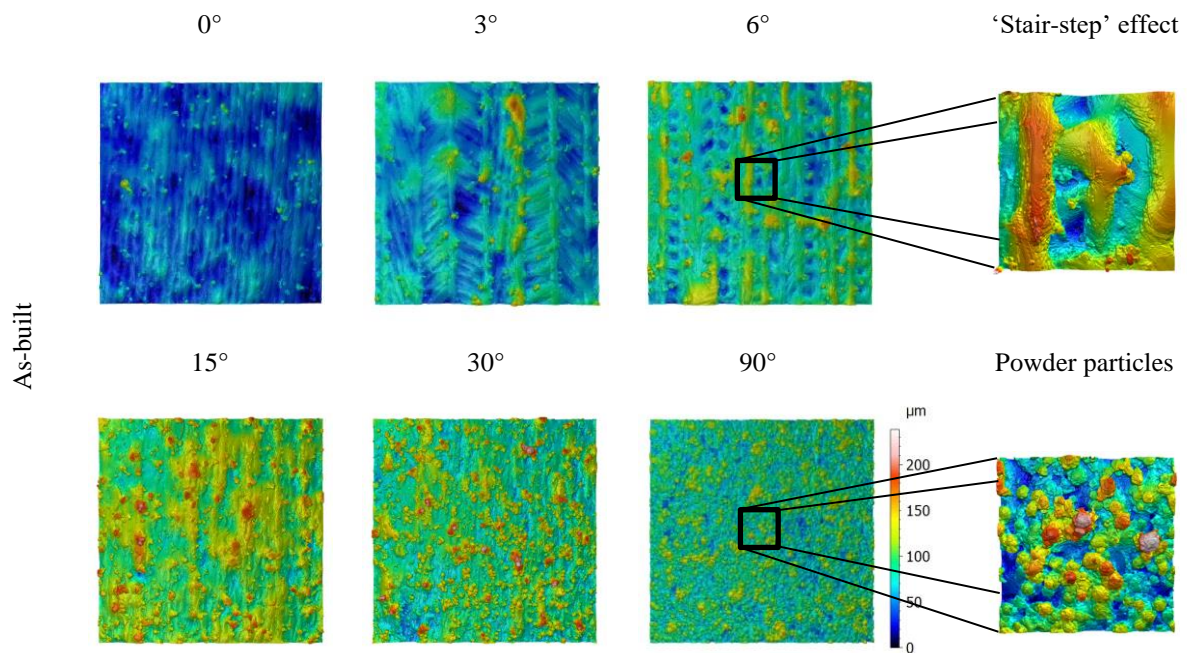
Figure 6. *3D topography view of as-built PBF-LB/M surfaces at various build inclinations. All surfaces have a measurement area of 2.5 mm×2.5 mm and the extracted surface has an area of 0.5 mm×0.5 mm.* [40]

2.1.2 Fused Deposition Modelling (FDM)

The most popular and widely used AM technique is the Fused Deposition Modelling (FDM) method, which is categorized under the Material Extrusion (MEX) process. Figure 7 illustrates a typical setup of the FDM process. The material feedstock in form of filaments or pellets is fed into the extruder mechanically. The material is then melted in the heated nozzle or the hotend fitted at the end of the extruder and then it is deposited selectively layer by layer to build the part. A complete description of the process, selection of materials, and applications are discussed in [1].
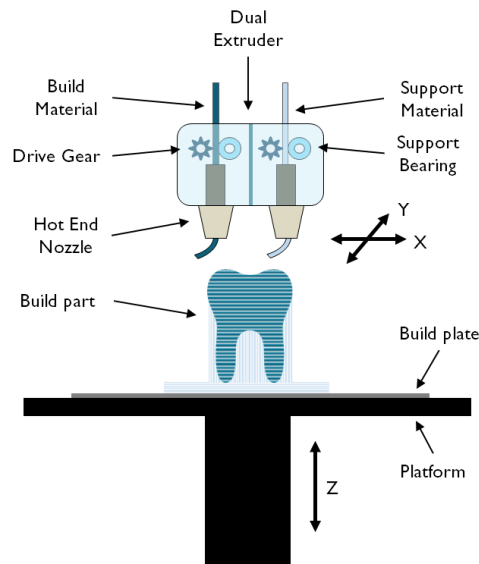
Figure 7. Illustration of the FDM process

The surface topography quality of the FDM samples is influenced by several factors during its fabrication process. Layer height, print temperature and speed, infill density and pattern, number of top layers, and so on are some of the many FDM process variables that affect the surface quality. Then there are the material properties, each material produces slightly different surface finish and geometrical design factors, for instance, the variation in build inclination or slopes impacts the surface quality. Finally, there are environmental factors such as surrounding temperature, humidity, vibrations, and so on which usually fall under uncontrolled factors. Research has shown that the geometrical design and FDM process variables, specifically the build inclination and layer height were the most influential factors on the surface topography quality of FDM samples [41][42]. The mechanism of surface formation in the FDM process is similar to PBF-LB/M which includes the formation of raster and "stair-step" patterns except the surfaces are free from powder particles [43], see Figures 8 and 9).
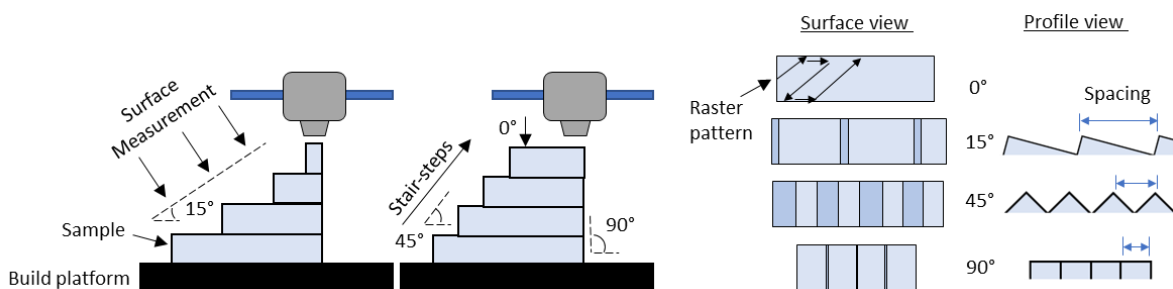
Figure 8. Working principle and mechanism of surface formation in the FDM process.
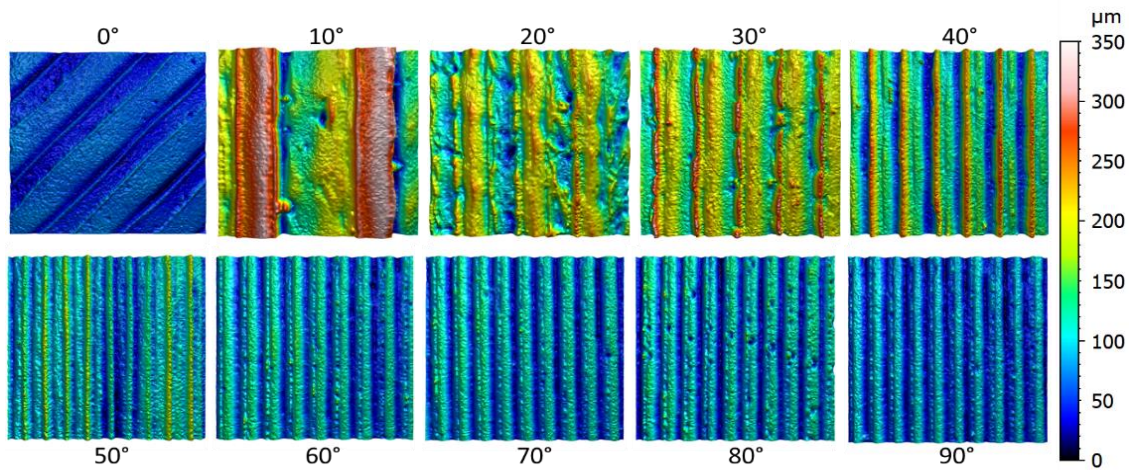
Figure 9. *Stair-step and raster patterns as seen in the areal surface topography of the as-built FDM sample due to varied build inclinations. All surfaces have a measurement area of 2.5×2.5 mm.* [44]

2.1.3 Stereolithography (SLA)

Stereolithography (SLA) is a type of Vat photopolymerization (VPP) AM process, where the photo-sensitive polymer solidifies undergoing a chemical reaction upon the incidence of Ultraviolet (UV) rays [2]. Figure 10 presents the working principle of the SLA process. It consists of a resin tank, a build platform, and a UV source. Photopolymer resins typically consist of liquid monomers or oligomers, photoinitiators, plasticizers, crosslinking monomers, and pigments [1]. The liquid monomers are usually a mixture of acrylic and epoxy-based monomers. The UV rays activate the photoinitiators that react chemically with monomers causing the formation of polymer chains. These polymer chains undergo a further reaction with crosslinking monomers to form a strong bond between them leading to the creation of a solid object [1]. After the object has been printed, it is taken out of the vat or resin tank, washed to get rid of any remaining resin, and UV-cured to further reinforce the polymer bonds.
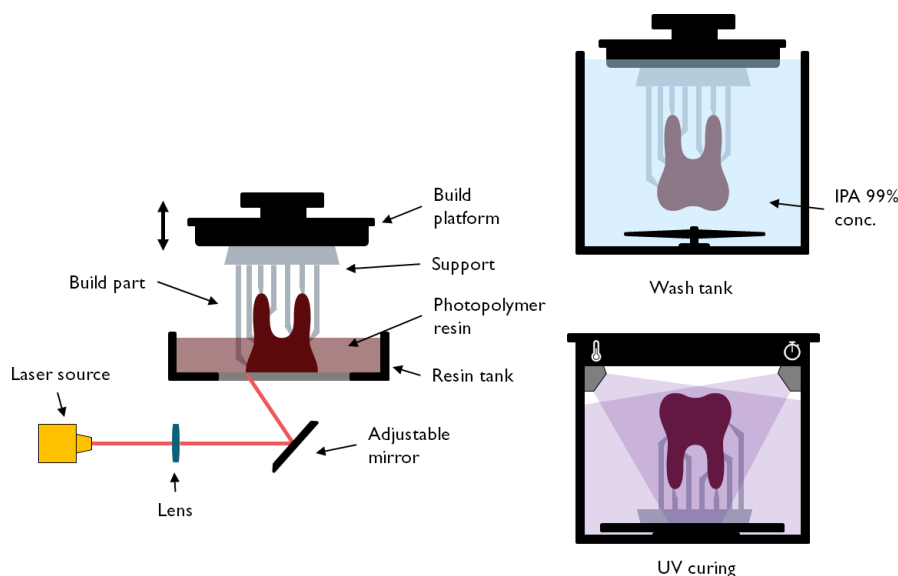
Figure 10. *Illustration of the SLA process*

12

Figure 11 illustrates a visualization of the surface creation process in the SLA process. Typically, in the SLA processes, unlike the Material Extrusion AM process, the raster pattern on the top surface layer is not apparent and it may be due to the following reason. Since all of the laser scannings happen inside the resin bath (vat), the patterns get filled in by resins to create a continuous smooth surface during the solidification process [1]. Furthermore, similar to all the AM processes, the SLA process also creates the "Stair-step" effect on the inclined or curved surfaces due to the stacking of layers during its fabrication process [45]. This phenomenon is evident significantly at lower build inclinations and progressively diminishes. This is mainly because the "stair-steps" are more widely spaced at lower build inclinations and get closer with an increase in build inclination. At high build inclination for instance at 90°, the layers are stacked exactly upon one another, bringing the layers together which are then masked by excess resin in the vat. Figure 12 displays the surface topography of the SLA process at various build inclinations.
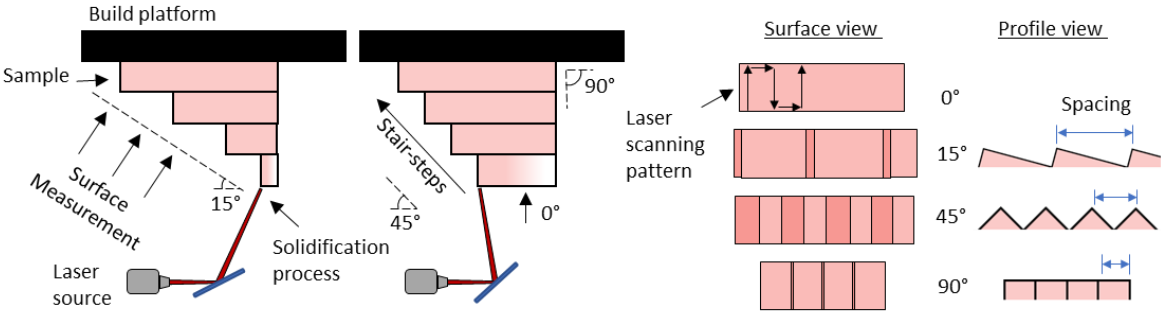
Figure 11. *Working principle and mechanism of surface formation in SLA process. Image taken from paper 7.*
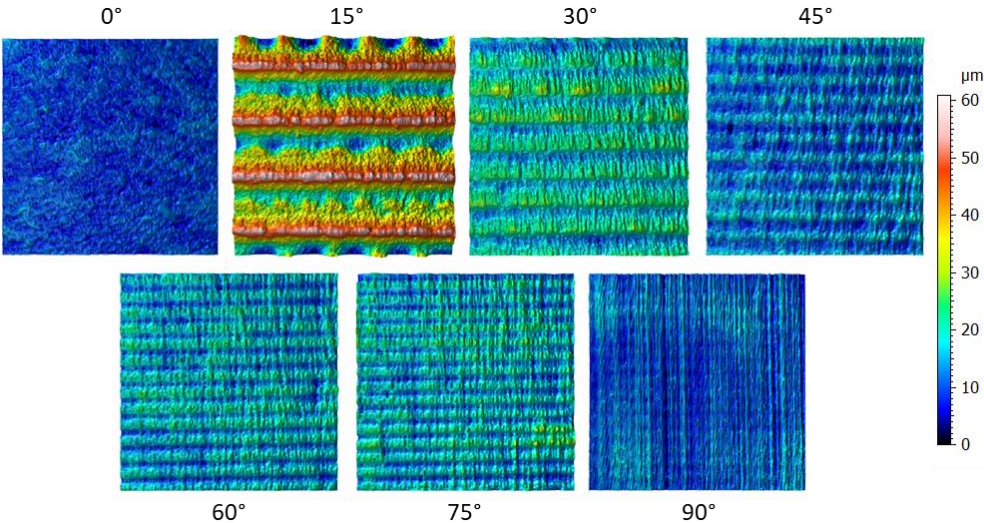
Figure 12. *The 3D view of the surface topography of the as-built SLA sample with varying build inclinations. Surfaces were measured using a 5.5X objective with a field of view of 1.56 mm×1.56 mm.*

2.1.4 Additive Manufacturing as Sustainable Manufacturing

The importance of sustainable manufacturing has recently been highlighted due to the increasing demand for manufactured goods and the declining amount of natural resources. It is crucial to conserve resources for establishing long-term financial and environmental benefits. Sustainable manufacturing is defined as a process of creating fabricated goods through economically viable methods that can reduce the detrimental effects on the environment whilst conserving natural resources and energy [46]. The development of Additive Manufacturing technologies has made it more feasible for industries to adopt sustainable business practices. With its ability to produce complex geometries and lightweight components, as well as to reduce inventory needs by producing parts on demand. Due to this reason, AM is being coined as the sustainable manufacturing of the future [47]. Figure 13 shows the 17 SDGs proposed by United Nation, in particular, the 12th SDG, responsible consumption and production [3] aligns well with the sustainability benefits observed with AM technology. However, much research is needed to address the challenges faced by AM technology before becoming the industry standard for manufacturing. The studies presented in this thesis are focused on improving one of the downsides of AM to encourage industries in embracing sustainable manufacturing through AM.

Figure 13. Sustainable development goals by the United Nations [3].

2.2 POST-PROCESSING

Post-processing methods have become an integral part of AM ecosystem since it mandates the requirement of several finishing steps before being accepted for industrial application. The term "post-processing" used throughout this thesis refers to the additional processing steps taken to improve the quality of the AM surface topography. Generally, most of the AM processes produce surface features that include raster patterns, stair-step effects, and other footprints of the process which deteriorates the overall surface quality. Optimizing the AM process settings can improve surface quality, but it can never eliminate these surface features due to the nature of its fabrication process. It is, therefore, necessary to employ post-processing methods to finish the surfaces, and knowledge of their effects on surface topography is crucial for achieving optimal process performance. In the following sections, an overview of various post-processing methods utilized in the thesis is presented.

2.2.1 Shot blasting

Shot blasting is a surface finishing method that utilizes a centrifugal wheel or compressed air to propel abrasive media onto the surface at high velocity. The type of abrasive media, the pressure of impact, and the blasting duration are some of the process settings that can be optimized to achieve the required finish on the surface. Several studies have been conducted to study the effects of abrasive flow machining [48], abrasive jet deburring [49], and abrasive finishing of internal channels [50][51] on surface topography quality.

(a) Sa = 20.8µm (b) Sa = 5.95µm

(c) Sa = 10.6µm (d) Sa = 9.5µm
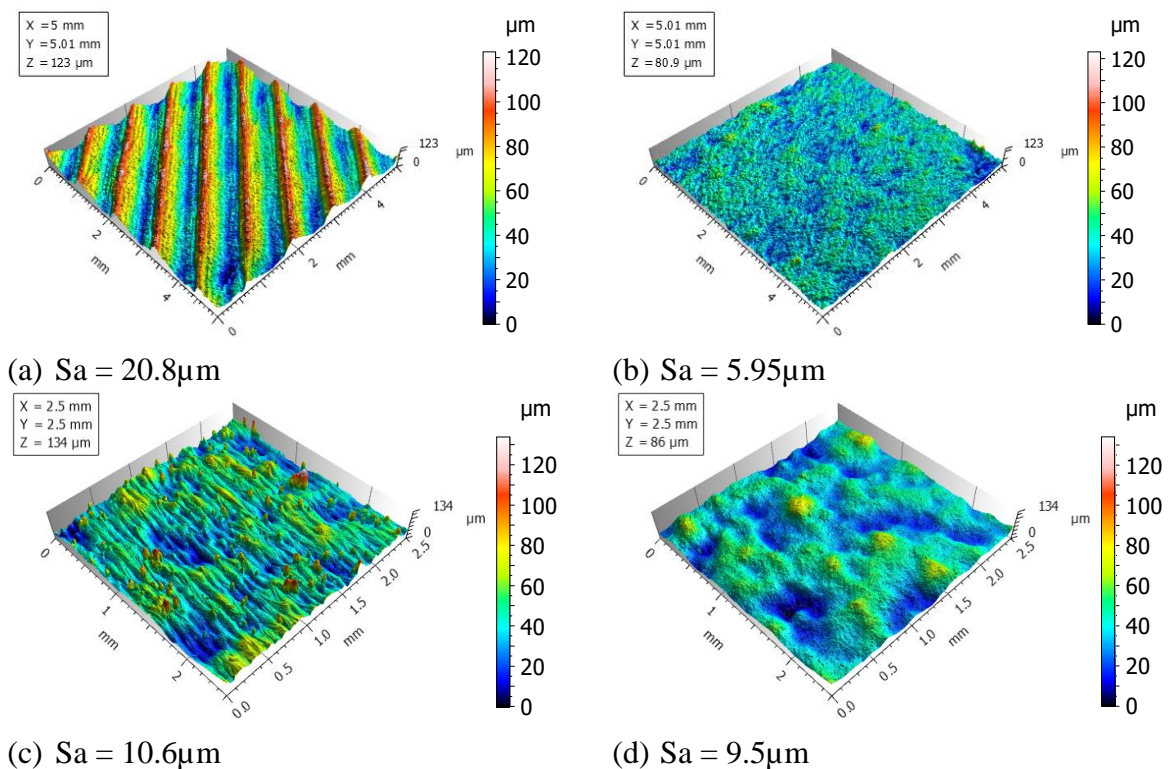
Figure 14*. Areal surface topography measured on 0° build inclination (a) as-built FDM surface, (b) shot-blasted FDM surface; (c) as-built PBF-LB/M surface, and (d) shot-blasted PBF-LB/M surface. [52]*

In this thesis, the shot blasting process was utilized to alter the surface texture of the as-built FDM and PBF-LB/M samples produced at various build inclinations. Figure 14 shows the surface images of as-built and shot-blasted surfaces for the two AM processes. Typically, the

abrasive media includes sand particles, glass or plastic beads, metal pellets, and so on. Depending on the material an appropriate abrasive media must be chosen, usually, sand particles have irregular grains that offer more abrasive actions resulting in higher material removal rates and a rough surface finish. The glass or plastic beads have more controlled circular-shaped grains that smoothen the surface texture [53]. It can be noticed from the figure that the raster and stair-step patterns are successfully eliminated due to the abrasive action imparted by the shot-blasting process.

2.2.2 Laser-assisted finishing

In paper 3, Laser-assisted finishing (LAF) was utilized to improve the surface topography quality of Acrylonitrile Butadiene Styrene (ABS) samples produced using the FDM process. The LAF process alters the surface structure using high-powered laser beams that melt and evaporates the portion of the surface in contact. The literature points out that the LAF process has been previously researched to study its effect on the surface finish of ABS samples produced using the FDM process [54]. The SLM surfaces have been subjected to Laser polishing [55] and Laser ablation methods [56] to improve their surface texture. Figure 15 provides the images of as-built FDM and laser-finished surfaces, it can be clearly witnessed that the raster patterns on the as-built surface are eliminated by the laser-finishing process. The extent of surface finishing with this process depends on several process parameters such as the Laser power, the Laser speed, the resolution of the laser, and so on.
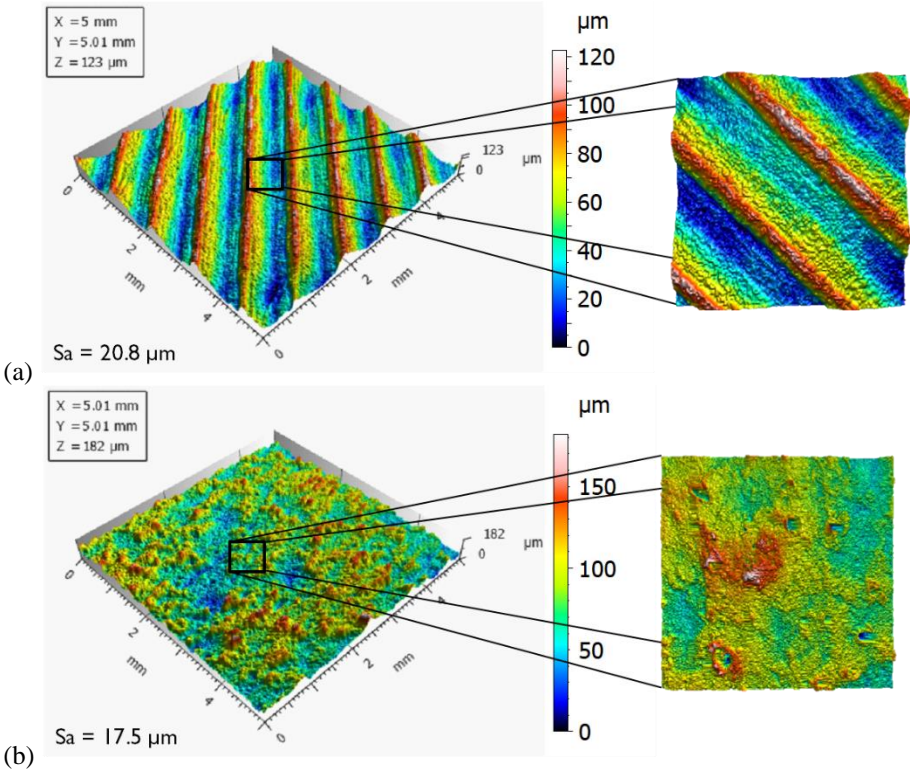
Figure 15. *Areal surface topography of the FDM process measured at 0° build inclination (a) as-built and (b) laser-finished surface.* [52]

2.2.3 Acetone vapor finishing

Acetone vapor finishing (AVF) is a surface treatment method that utilizes acetone to corrode the top surface layers of materials that are reactive to it, leaving behind a smooth surface texture [57]. To carry out this finishing method, FDM surfaces made of ABS material were exposed to acetone vapors for a timed duration inside a closed container. Over time, the ABS material undergoes a physical state change allowing the top solid surface layers of the thermoplastic polymer to slowly melt into a smooth and glossy surface layer. It is important to remove the sample in good time as long acetone exposure will deform the sample. Optimizing the acetone vapor exposure time, and the number of smoothening cycles is crucial in getting the best surface finishes without compromising the dimensional quality of the product. Figure 16 displays the as-built FDM and acetone vapor-finished surfaces.
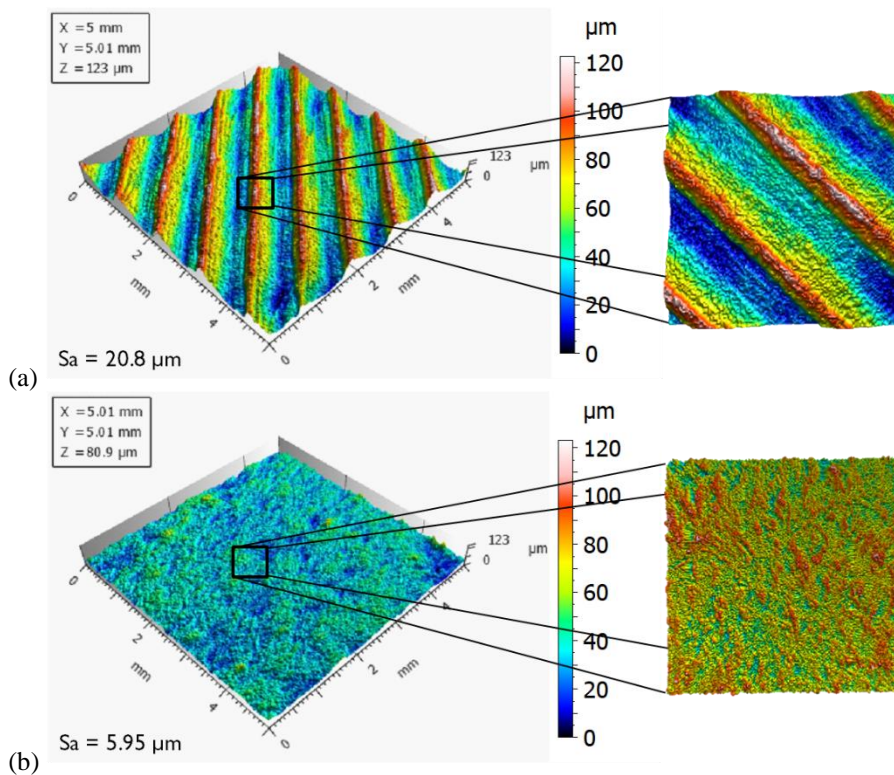
Figure 16. *The 3D view of surface topography of FDM surfaces at 0° build inclination (a) as-built and (b) Acetone-vapour finished surface.* [52]

2.2.4 Autoclave Sterilization

In this section, a different post-processing technique is utilized to modify the micro-roughness features necessary for investigating bone growth responses required for a dental application, whereas up until this point, the post-processes had been used to alter the macro-roughness features primarily to improve the overall surface texture to make it suitable for industrial application. In paper 7, biocompatible samples produced using the SLA method were studied before and after sterilization to understand their effects on surface topography.

Autoclave sterilization is commonly known as steam sterilization. The autoclave is mainly a container that is capable of withstanding high temperature and pressure, within which the surgical equipment is placed for sterilization [58][59]. The samples kept inside an autoclave are exposed to saturated steam under a vacuum for a specified period. At elevated temperatures and

pressure, the steam not only destroys the microorganisms by also disrupts the micro-roughness features on the surface topography. Figure 17 provides relocated surface images of FDM samples measured before and after the sterilization process. It can be seen visually that steam sterilization only alters the micro-roughness features without affecting the waviness and form of the surface. In this paper, the temperature of the steam was kept at 134°C and had a vacuum pressure of 0.1 Mbar and the SLA samples were kept in the autoclave for 3.5 minutes.
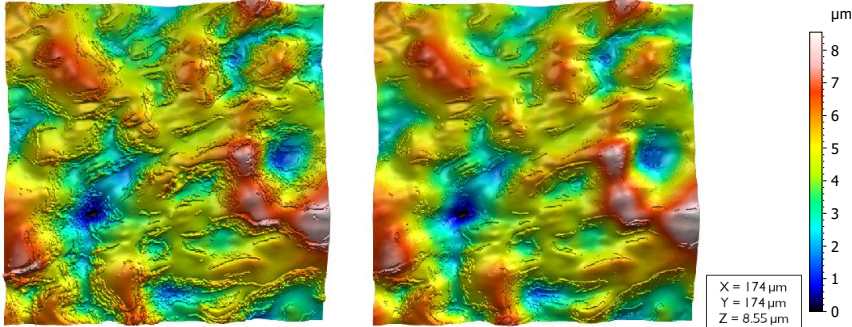
Figure 17. *Areal surface topography of SLA surfaces at 0° build inclination (a) as-built and (b) Sterilized surface. Image taken from paper 7.*

Chapter 3

METROLOGY SYSTEMS

This section describes in detail the state-of-the-art surface metrology instruments utilized in the thesis for analyzing the topography quality of Additive Manufacturing surfaces.

3.1   SURFACE METROLOGY

The term "surface metrology" refers to the practice of taking precise geometrical readings of surfaces to account for any deviations that occur due to the manufacturing process [60]. The geometrical information includes the shape and texture of the surface. In this context, the surface shape refers to form, which includes roundness, flatness, cylindricity, and straightness [61]. Surface texture refers to the manufacturing footprints or the geometrical irregularities excluding the form, that occur on the top surface layer during the manufacturing process [62]. The surface texture becomes increasingly complex with AM processes due to its nature of fabricating components layer by layer. Measuring such surfaces demand advanced surface metrology instruments. There are several surface measuring instruments that broadly fall under three categories. A complete taxonomy of surface metrology instruments is provided in ISO 25178-6:2010 [63]. According to the standard, the three techniques of measurement include line profiling, Areal-topography, and Area-integrating methods. In the following paragraphs, these methods are briefly introduced.

Line profiling metrology is a process of measuring the surface profile to retrieve the profile roughness information [63]. It is typically measured along a line scanned across the surface and mathematically expressed as a function of height $h(x)$ for a given displacement in the measuring direction. For circular profiles, the height information can be expressed as $h(\theta)$ where θ is the angular displacement [11]. Contact stylus profilometer [64], phase-shifting interferometry [65], circular interferometric profiler [66], and optical differential profiling [67] are some of the measurement methods that belong to this category.

The areal-topography method, as the name suggests, provides surface information by measuring the areal surface topography and is mathematically expressed as a function of height $h(x,y)$ for a given lateral displacement in the x and y direction [11][63]. It is also possible to get the areal topography data by combining several profile measurements, mathematically it can be formulated as $h(x)$ being a function of y. Confocal microscopy [17], coherence scanning interferometry [68], structured light projection [69], focus variation microscopy [70], digital holography microscopy, angle-resolved SEM, SEM stereoscopy [71], scanning tunneling microscopy, atomic force microscopy [72], optical differential profiler, point autofocus profiling are some the surface metrology instruments that fall under this category.

The area-integrating method is method does not involve generating profile data $h(x)$ or areal topography data $h(x,y)$ but rather measures a representative area of the surface that can generate numerical results to determine the surface texture [63]. For instance, the pneumatic flow measurement is a surface area-integrating method where fluid flows over the surface and its flow resistance is noted to calculate the roughness parameter [73]. Other examples include total integrated light scatter [74], angle-resolved light scatters [75], and parallel-plate capacitance [76].

Some of these above-mentioned optical surface metrologies have been briefly described elsewhere [77]. An overview of the various surface measurement techniques included in this thesis is provided below.

3.2 STYLUS PROFILOMETER

The stylus profilometer as per ISO 25178-601 [78], is described as a measurement of the surface topography using a probe system with contacting stylus whose displacement is converted into the signal as a function of position. Figure 18 presents an illustration of a stylus profilometer typically comprising a lateral scanning system and probing system. The lateral scanning systems include a drive unit responsible for moving the probing system or the surface to be measured along the x and y-axis. The probing system includes the stylus, the probe, and the digitizing system. The stylus is a mechanical component consisting of a tip used to measure the height data by traversing a predefined distance over the surface. The probe or transducer picks up these vertical displacements during the measurements and converts the height data into a signal. The digitizing system converts this analog signal to digital, thus the height data of the surface corresponding to the surface texture or roughness is measured.
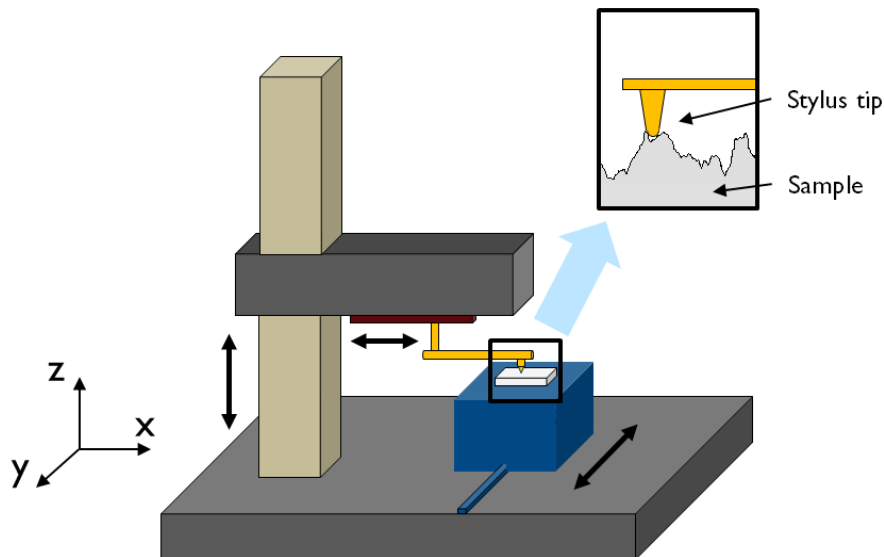
Figure 18. Stylus profilometer

The lateral axis movement in the stylus profilometer allows for capturing the areal surface topography by taking multiple parallel profile measurements. However, the measurement will considerably increase and elevates exponentially with an increase in measurement area and resolution. The design of the stylus tip and the tip radius determines the resolution of the profile whereas for the areal surface measurements the resolution depends not only on the tip design and the radius of curvature but also on the sampling interval. The stylus tips typically are made of diamond material with a tip radius ranging from 0.5 to 50 µm. Depending upon the nature of the surface under study, an appropriate stylus with a suitable tip radius must be chosen for determining the roughness. Furthermore, the use of the hard stylus tip for measurements often causes deformations on the surface, hence repeated measurements over the same spot are not advised [79]. The deformations can be substantial depending on the properties of the sample material, measurement speed, and load on the stylus tip all leading to uncertainty in measurements.

3.3 COHERENCE SCANNING INTERFEROMETER

Coherence Scanning Interferometer (CSI) is a surface measurement method wherein the surface is imaged based on the localization of interference fringes that occurs due to the variation in the optical path lengths during the scanning [77]. Figure 19 displays an illustration of a CSI instrument scanning an object surface with varied height features. The mechanical scanners allow for the movement of the objective in the z-direction for scanning the surface topography and usually, the scan length ranges from a few micrometers for piezo-electric scanners to several millimeters for motorized scanners. The illumination from the light source is controlled by the aperture and field stops, and the light beam is then focused onto the objective and camera with the help of a beam splitter. Typically, the interferometers are designed to contain special objectives that contain an internal beam splitter and a reference mirror. Figure 19 shows the setup of a Mirau interference objective, there are also other variations such as Michelson and Linnik type of objective which has a slightly different arrangement of reference mirror and beam splitter [77]. In the objective, the light is projected onto a reference mirror and the surface of the object with an internal beam splitter. The variations in the optical path lengths due to the differences between the topographical heights between the surfaces of the reference mirror and object causes the formation of interference fringes which are then imaged by the camera. During the scan, a computer records light-intensity data for each image point or pixel in successive camera frames. The areal surface topography can be constructed using the information of interference fringes.
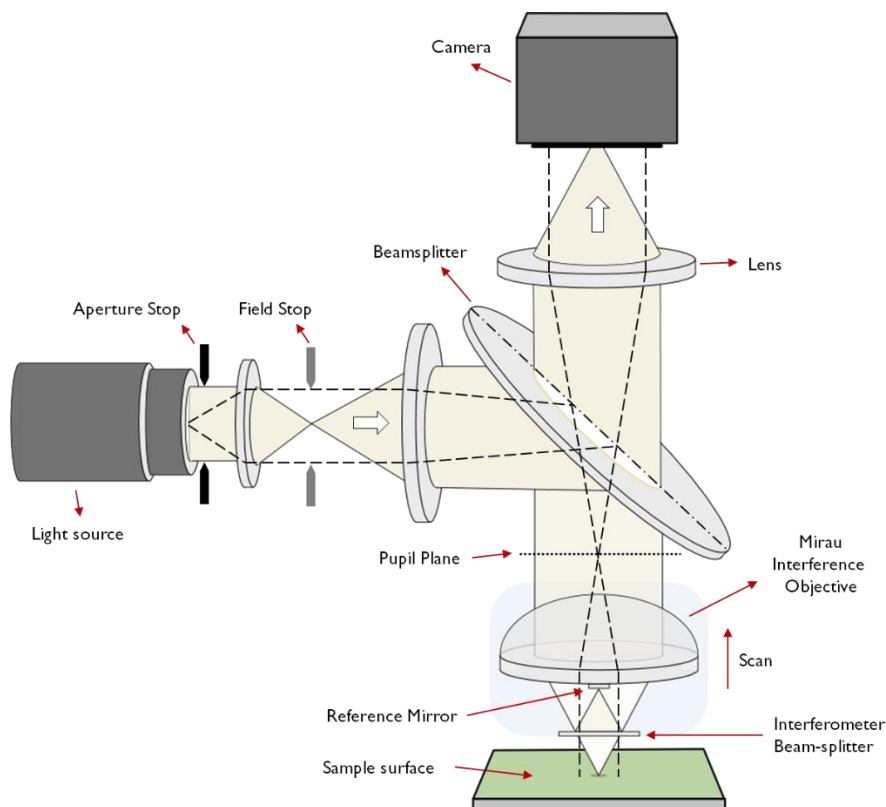
Figure 19. *Coherence Scanning Interferometer*

3.4 STRUCTURED LIGHT PROJECTION

Structured Light Projection or Fringe projection (FP) is a "*surface topography measurement technique whereby a light image with a known structure or pattern is projected on a surface and the pattern of reflected light together with knowledge of the incident structured light can determine the surface topography*" [63]. This measuring technique is named triangulation if the structured light is replaced with a single focused spot or fine line. Equation (1 presents a geometrical relationship between the projector, camera, and the point/spot on the object's surface defined by the triangulation principle [80].

$$p = q \ \frac{\sin \theta}{\sin(\theta + \alpha)} \tag{1}$$

Where,
C = Point on the surface
p = Distance of the point on the object's surface
q = Known Distance between the Projector and Camera
θ = Known angle of the light projector
α = Known angle of the camera
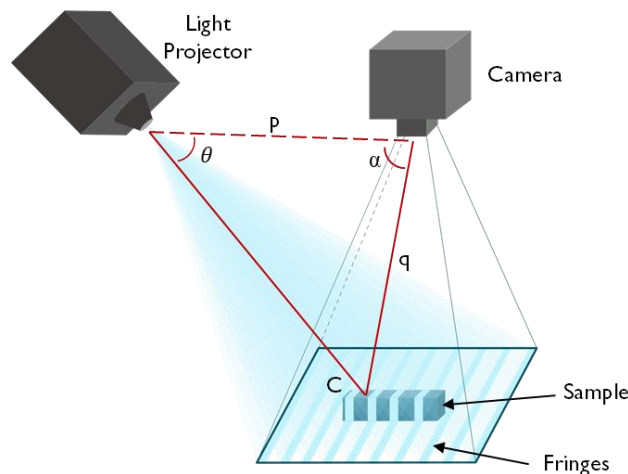
Figure 20. Structured Light Projection

Figure 20 displays the principle of this technique with an illustration of the triangulation method. A light source capable of illuminating the structured light pattern and a camera or image sensor to capture the images are needed. A light image of a known pattern or light fringes is projected onto the surface to be measured and a camera views the surface under different light pattern illumination. The pattern projected gets distorted due to the presence of surface features on the sample. This distorted image along with the original incident light pattern is utilized to reconstruct the height information of the surface under inspection. This technique succeeds in measuring the surface topography of a variety of materials very quickly but fails to capture the surface information on reflective or transparent surfaces. In such scenarios, using a replica or coating the surface is recommended. Furthermore, it is limited in resolution compared to other optical methods.

3.5 CONFOCAL MICROSCOPE

The metrological characteristics of non-contact especially confocal instruments are described in ISO 25178-602 [81]. The name confocal implies that both the illumination and detector have their optical path on a common focal point [77].
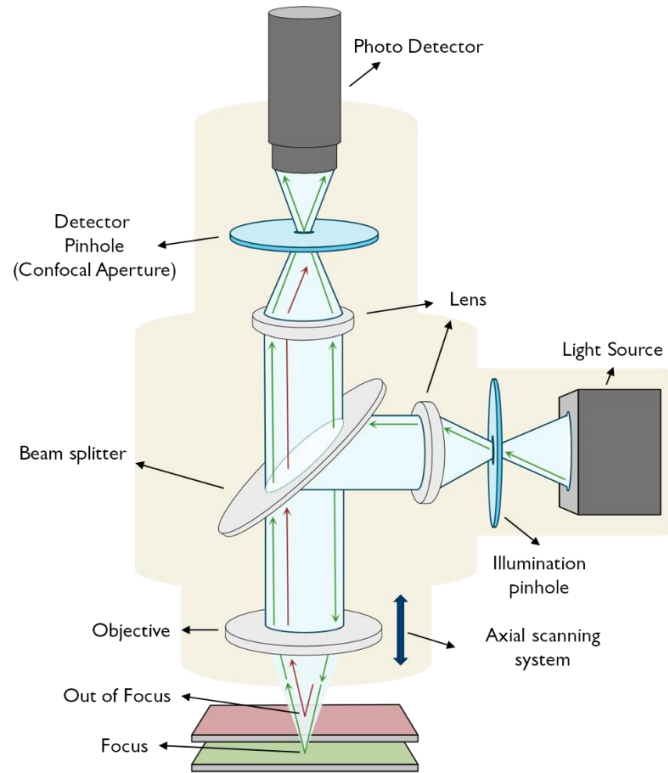
Figure 21. *Working principle of confocal microscopy*

Figure 21 illustrates the fundamental concept of confocal microscopy. It consists of two identically structured patterns along the optical axis, one of which is positioned near the light source and the other near the photodetector. The structured patterns are utilized mainly to minimize the size of illumination coming either from the light source or the backscattered light from the sample and these patterns can be in form of a single pinhole or set of pinholes, slits, or any other pattern [77]. Structured illumination is created when light from the source advances through the pinhole, which is then focused onto the objective and sample by the beam splitter. The purpose of the beam splitter is to divide the incident light beam from the source into transmitted and reflected light beams or in some cases it acts as a filter to remove a certain wavelength of visible light allowing the remainder to pass through onto the sample. The reflected or backscatter light from the sample passes through the same objective and beam-splitter and it is directed into the detector pinhole (confocal aperture), which allows only the focused light to reach the photodetector and rejects the out-of-focus light. This generates optically sectioned images of the surface being measured. An in-plane scanning mechanism captures these optically sectioned images and the scanning differs with the type of confocal setup, for instance, Laser Scanning Confocal Microscope (LSCM) [82] scans the surface point by point along the XY plane. Also, an axial scanning system allows the objective to move on a vertical path to capture a series of optically sectioned images of the sample surface at various heights. Finally, areal surface topography is reconstructed using these pixel-intensity maps (optically sectioned images) [77].

3.6 FOCUS VARIATION

The standard ISO 25178-6 [63] defines Focus Variation (FV) microscopy as a surface texture measurement technique where the sharpness of the surface image is used to construct the surface height at each position along the surface. Figure 22 presents the working principle of the FV measurement method.
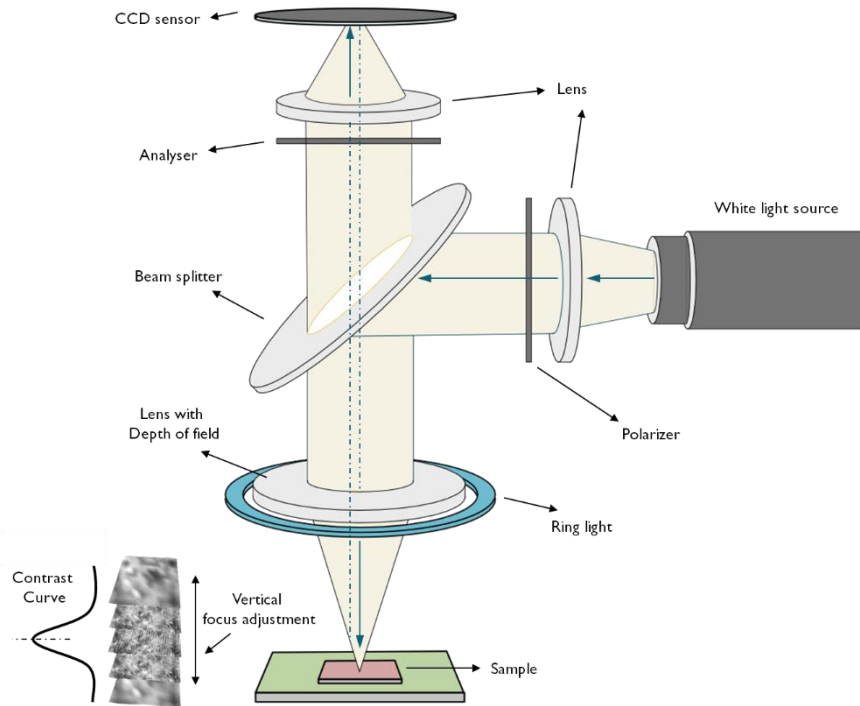
Figure 22. *Working principle of Focus variation microscopy*

Typically, a Focus variation instrument comprises an optical system with a limited depth of field for focus detection, a light source, a charge-coupled device (CCD) sensor, and a drive mechanism [77]. Through the beam splitter (semi-transparent mirror) light from the source is delivered to the objective and sample. The light gets scattered upon its incidence on the surface and some of the reflected light is captured by the CCD sensor. The vertical movement of the sample in relation to the objective alters the degree of focus of the sample surface, and this alteration in focus is responsible for the contrast change in the CCD sensor. By examining the contrast on the CCD sensor, the height information of the inspected surface can be reconstructed. This measurement approach enables FV to capture surfaces that contain features with steep slope angles [83].

3.7 CONFOCAL FUSION

Confocal fusion is a mode of measurement that combines both Confocal microscopy and Focus Variation methods for imaging the surface topography [84]. It is especially advantageous to use this technique for measuring surfaces with steep slopes and also surfaces that are highly reflective [84][85][86]. This technique was most suited for measuring the PBF-LB/M surfaces that contained reflective top surfaces and steep surface slopes due to the presence of powder particles at higher build inclinations. However, this technique along with the other "line of sight" instruments stated before (stylus profilometer, structured light projection, focus variation, and confocal microscopy), cannot capture the re-entrant features [13] present in PBF-LB/M samples.

3.8 SCANNING ELECTRON MICROSCOPE

The limitations of the optical microscope to resolve finer details are overcome by the electron microscope with its high lateral resolution, broad magnification range, and large depth of field due to the utilization of the shorter wavelength of electrons for imaging. A Scanning Electron Microscope (SEM) normally comprises a vacuum-operated electron gun, electromagnetic condenser lens, objective lens, deflection coils, sample mounting stage, and sets of electron detectors (secondary and backscatter electron detectors) [87]. The electron gun typically consists of a tungsten filament or Lanthanum- or Cerium hexaboride or a Field emission source from which electron beams are accelerated towards the specimen. The electron beam scans the sample in a raster fashion and a greyscale image is produced based on the intensity of signals obtained from the electron interaction with the sample. SEM is usually utilized for qualitative analysis since it produces two-dimensional false greyscale images, however, by the photogrammetry method, it is possible to obtain a three-dimensional image by reconstructing two or more grey-scale images captured at different angles [71]. In paper 1, 3D SEM was utilized for quantitative characterization of areal surface topography and in paper 6, SEM images were utilized for qualitative analysis of porosity in the FDM bronze sample.

Chapter 4

TOPOGRAPHY CHARACTERIZATION METHODS

In this chapter, various topography characterization methods utilized for defining surface quality of Additive Manufacturing (AM) and post-AM processes are described. It is followed by a presenting an overview of statistical methods utilized for analysis.

4.1 NATURE OF SURFACES

Surface metrology enables the capturing of the surface topography of manufactured samples. The captured surfaces can be subjected to analysis through qualitative or quantitative methods, in doing so, it is possible to optimize the manufacturing process for controlling the surface quality and function. The measured surfaces must be processed and refined before characterizing the topography data, since it may include form errors or other irregularities such as noise due to vibrations and so on. As mentioned earlier, every surface includes geometrical information about surface shape (Form and waviness) and texture (roughness) [62].

The form, waviness, and roughness of the measured surface are usually distinguished by measuring their surface wavelength [88]. Form errors have the largest wavelengths and they can occur when a surface containing a geometrical shape is measured. The rotary forms occur when the surface of a cylinder, cone, or sphere is measured and the planar form is due to tilting errors or when measured on a slope. Waviness surfaces have usually shorter wavelengths compared to form and can occur due to manufacturing process defects or in some cases due to the nature of fabrication itself. For instance, the "stair-step" effects in AM are considered to be waviness. The residual surface after filtering out the form and waviness surfaces provide the surface texture or the roughness surface. It must be noted that the separation of waviness and roughness features of the surface is arbitrary, an appropriate filter with a suitable nesting index must be chosen based on the required objective [88]. In the next chapter, a description of surface refining methods is presented.

In the following sub-sections, various topography characterization methods are discussed. These methods can broadly fall under two categories: Scale-limited and Multi-scale surfaces. Scale-limited surfaces refer to the surfaces measured at a particular scale of interest. ISO 25178-2:2021 [89] defines scale-limited surfaces as S-F or S-L surfaces. The S-F surface refers to the surface obtained after removing the form from the primary surface. The primary surface refers to the surface obtained after applying S-filter (small-scale filter) to the raw surface data. The S-L surface refers to the surface obtained after applying L-filter (Large-scale filter) to the S-F surface [89]. In short, the scale-limited surface is either a waviness or roughness surface captured at a particular scale. On the other hand, multi-scale surfaces are surfaces that are viewed at various scales of observation [90]. It can usually be obtained by filtering the surface using various nesting indexes.

4.2 SCALE-LIMITED SURFACE CHARACTERIZATION METHODS

4.2.1 Profile roughness parameters

The ISO 21920-2:2021 [91] cancels and replaces the previously known standard ISO 4287:1997 [92] that specifies the terms, and definitions for the profile roughness. Table 1 provides a list of parameters based on the roughness profile and highlights the parameters that existed in the old standard along with a set of new parameters as per the current standard. The profile parameters are categorized into various groups that define the characteristics of a measured profile based on height, spatial, hybrid, material ratio, function, and feature aspects. A brief explanation of various parameters can be found elsewhere [10][93].

***Table 1**. Classification of profile roughness parameters as per ISO 21920-2:2021 [91].*

Symbol	Unit	Parameter Group
Rq^a, Rt^a, Rp^a, Rv^a, Rz^a, Ra^a, Rpt^b, Rvt^b, Rzx^b	µm	**Height Parameters**
Rsk^a, Rku^a,	No unit	
Ral (s), Rsw	mm	**Spatial parameters**
Rdq^a, Rda, Rdt,	°	**Hybrid parameters**
Rdl	mm	
Rdr	%	
Rmr^a (c),	%	**Material ratio parameters**
Rdc^a (p,q), Rmc (p)	µm	
Rk, Rpk, Rvk, Rvq, Rpq	µm	**Functional parameters (Stratified surfaces)**
Rmrk1, Rmrk2, Rmq	%	
Rvm (p), Rvv (p), Rvmp (p), Rvmc (p,q), Rvvc (p,q), Rvvv (p)	µm³/mm²	**Functional parameters (Volume)**
Rsm^a, Rc^a,	µm or mm	**Feature parameters (Profile elements)**
Rpc^a	1/mm	
Rpd, Rmpc,	1/mm	**Feature parameters (watershed segmentation - Wolf pruning % of Rz)**
R5p, R5v, R10z, Rhhm, Rddm, Rhwm, Rdwm	µm or mm	
Rhvm, Rdvm	µm³	

ᵃParameters that were in the old ISO 4287:1996 standard
ᵇParameters that were previously termed as Rp1max, Rv1max, and Rz1max in ISO 4287:1996

The raw profile after the measurement is refined to eliminate noise by applying the low pass micro-roughness filter with certain cut-off (λs) specified in ISO 4288 [94], resulting in the Primary profile. The roughness and waviness profiles can be separated using the high-pass Gaussian filters with a cut-off in accordance with ISO 16610-21 [95]. The profile parameters

calculated on primary, roughness, and waviness profiles are denoted by prefixes P, R, and W respectively.

4.2.2 Areal surface texture parameters

The recently amended ISO 25178-2:2021 [89] presents a vast number of areal surface texture parameters defining several geometrical features of measured surface topography. Table 2 shows the list of all the areal surface texture parameters as per the new standard.

Table 2. Classification of areal surface texture parameters as per ISO 25178-2:2021 [89].

Symbol	Unit	Parameter Group
Sq[a], Sp[a], Sv[a], Sz[a], Sa[a], *Ssk[a], Sku[a],*	μm No unit	**Height Parameters**
Sal[a] (s), Ssw *Str[a] (s)* *Std[a]*	mm No unit °	**Spatial parameters**
Sdq[a] *Sdr[a]*	No unit %	**Hybrid parameters**
Smr[a] (c), *Sdc[a] (p,q), Smc[a] (p)*	% μm	**Functional parameters (Material ratio curve)**
Vm[a] (p), Vv[a] (p), Vmp[a] (p), Vmc[a] (p,q), Vvc[a] (p,q), Vvv[a] (p)	μm^3/mm^2	**Functional parameters (Volume)**
Sk[a], Spk[a], Spkx, Svk[a], Svkx *Svq[a], Spq[a], Smq[a]* *Smrk1[b], Smrk2[b], Sak1, Sak2*	μm No unit %	**Functional parameters (Stratified surfaces)**
Spc[a], Svc *Spd[a],* Svd *S10z[a], S5p[a], S5v[a]* Shh, Sdd *Sha[a], Sda[a]* *Shv[a], Sdv[a]* Shn, Sdn	1/mm 1/mm^2 μm mm^2 mm^3 No unit	**Feature parameters (Watershed segmentation - Wolf pruning % of Rz)**
Shrn, Shff, Shar, Sdrn, Sdff, Sdar Shed, Sded	No unit mm	**Feature parameters based on the shape (Watershed segmentation - Wolf pruning % of Rz)**

[a]*Parameters that were in the previous ISO 25178-2:2012 standard*
[b]*Parameters that were previously termed as Smr1, and Smr2 in ISO 25178-2:2012*

The areal surface texture parameters can broadly be classified into field and feature parameters. The field parameters are calculated from all the data points on a scale-limited surface, whereas, feature parameters are based on a subset of topographical information from a scale-limited surface [11]. They are further classified into several sub-groups as shown in Table 2, with each

group defining various geometrical aspects of the surface topography. The areal surface texture parameters are denoted by 'S' representing surface and 'V' for volume. In contrast to profile parameters, the notations (S or V) of the areal surface texture parameters do not indicate whether the measured surface is a waviness or roughness surface. The surface parameter values must therefore be associated with filtering conditions to understand the nature of the surface under investigation [11]. ISO 16610 series of standards presents various areal filtering methods that allow the separation of waviness and roughness features of the surface for analysis. Furthermore, it must be observed that most of the areal surface texture parameters are the direct counterpart of profile parameters [88] and therefore, both the characterization methods are comparable explaining similar geometrical features of the surface.

- *Height parameters* are a set of parameters that characterize topographic features normal to the surface (z-direction). Within the height parametric group, several parameters provide the complete specifications of amplitude features of the measured surface. The average roughness (Sa) parameter gives a measure of overall surface texture, Skewness (Ssk) provides the shape of the topography height distribution, and Kurtosis (Sku) indicates the sharpness of the surface height features. The parameter Sz gives the overall height of the surface topography features and Sp and Sv provide the maximum height of the peaks and valleys respectively. These parameters can be used to identify extremely sharp peaks and valleys, often caused due to measurement noise or surface defects. [11]

- *Spatial parameters* consist of mainly three parameters defining various characteristics of surface texture. Auto-correlation length (Sal) provides a quantitative measure of distance over the surface texture such that the new location has the least correlation or is statistically different from its original position. Standard texture direction (Std) is deduced by analyzing the Fourier spectrum of the surface being measured. It is utilized to indicate the direction or orientation of the dominant texture or lay on the surface topography. The texture aspect ratio (Str) provides the isotropy information of the surface. If the value of Str is closer to 0 the surface is anisotropic indicating the presence of dominant texture direction and when the Str value is closer to 1 the surface is isotropic [11]. The newly included parameter Ssw provides the dominant spatial wavelength of the surface topography [89].

- *Hybrid parameters* provide a measure of the complexity of the surface topography. It is mainly utilized to define surface features that depend on both the amplitude and spacing features such as slopes, curvatures, and so on. A brief explanation of these parameters is provided in [11].

- *Feature parameters* characterize specific features on the surface topography, and they play a crucial role in the functional behaviour of the product. They provide information on the height, density, curvatures, roundness, form factor, diameter, and aspect ratio of hills or peaks and dales or pits of the surface topography. The significant features can be identified by performing surface segmentation by the watershed method [89] followed by the pruning that helps in avoiding over-segmentation by setting a height threshold usually specified as a percentage of the total height parameter (Sz). [11]

- *Functional parameters* are defined based on the Abbott-Firestone curve, which is also known as the Bearing area or Material ratio curve. It is a graphical representation of the Cumulative Distribution Function (CDF) of surface amplitudes expressed in the percentage of material [93]. Functional parameters can be utilized to understand surface functional behaviour such as lubrication capacity, wear effects, and so on. Generally, using the Abbott-Firestone curve [96], certain functional height and volume parameters can be defined that

describes the quantity of material or void present between a predefined threshold or material ratios. Additionally, the functional behaviour of surfaces containing several textures imposed at different depths, often generated due to processing with distinct manufacturing procedures, can be described using *Stratified parameters* that fall under this category [11].

4.3 MULTI-SCALE SURFACE CHARACTERIZATION METHODS

4.3.1 Power spectral density

The ISO 25178-2:2021 [89] and ASME B46.1:2002 [97] standards define the Areal Power Spectral Density (APSD) as the magnitude square of the Fourier transform of the measured surface normalized by the pixel size. The Fourier transform decomposes the surface height distribution *z(x,y)* into individual frequency components. Equation 1 represents the Fourier transform of the measured surface.

$$F(u,v) = \iint_A z(x,y)e^{-2i\pi(ux+vy)} \, dx \, dy \tag{1}$$

Where, *z(x,y)* provides the surface amplitude data for lateral displacement in the *x* and *y* directions; *u* and *v* are the spatial frequencies in the x and y directions; *A* is the area of a pixel or the lateral resolution of the measured surface with a certain width or breadth *b* and length *l*.

As per the definition, APSD or 2D PSD is given by,

$$f_{APSD}(u,v) = \frac{1}{A}|F(u,v)\}|^2 \tag{2}$$

$$f_{APSD}(u,v) = \frac{1}{b \times l}\left|\int_{-b/2}^{b/2}\int_{-l/2}^{l/2} z(x,y)e^{-2i\pi(ux+vy)} \, dx \, dy\right|^2 \tag{3}$$

Usually, the lateral resolution of the optical microscopes is the same, and hence *b = l and A = l²*. Therefore,

$$f_{APSD}(u,v) = \frac{1}{l^2}\left|\iint_{-l/2}^{l/2} z(x,y)e^{-2\pi i(ux+vy)} \, dx \, dy\right|^2 \tag{4}$$

The power spectral density can be utilized to visualize the amplitude of the measured surface texture as a function of spatial frequency. The definition, applications, and comprehensive mathematical expression of APSD are provided elsewhere [98][99][100]. It is vastly adopted for characterizing optical and polished surfaces [99]. In this thesis, the PSD is utilized to describe the surface topography of PBF-LB/M and MEX processes for identifying the significant wavelength features influencing the surface quality and function. There are several types of power spectral density, hence, it is crucial to choose the right method, and other associated functions depending on the surface type before interpreting its results [101].

4.3.2 Scale-sensitive fractal analysis

Additive Manufacturing surfaces consist of topographical features of many sizes and scales but are mostly quantified at a single scale using the standard areal surface texture parameters. This could occasionally provide inaccurate results, particularly when identifying the correlation

between the surface and its functional performance. In such situations, the multiscale technique could be advantageous because it allows for surface analysis at several scales of observation. Scale-sensitive fractal analysis (SSFA) [89][90][102][103][104] is a type of multi-scale characterization method comprising two fractal methods namely the area-scale and length-scale analysis, where the former analyzes the areal features and the latter analyzes the profile length as a function of scales. In this thesis, the area-scale method is mostly utilized for analysis and in this method, the relative area and complexity of the surface topography can be calculated. The area-scale analysis involves creating a mesh of triangular tiles over the surface topography (see Figure 23) with each triangle having the same area representing a particular scale of measurement. The relative area at a certain scale is estimated by diving the calculated area by the nominal area at that scale. The calculated area is obtained by multiplying the number of triangular tiles covering the surface and the area of each triangle at a particular scale. The nominal area is obtained by calculating the area of the triangular tiles projected on the datum plane. The complexity of the surface topography is obtained by taking the slope of the relative area plot and multiplying it by the order of magnitude [11][105].
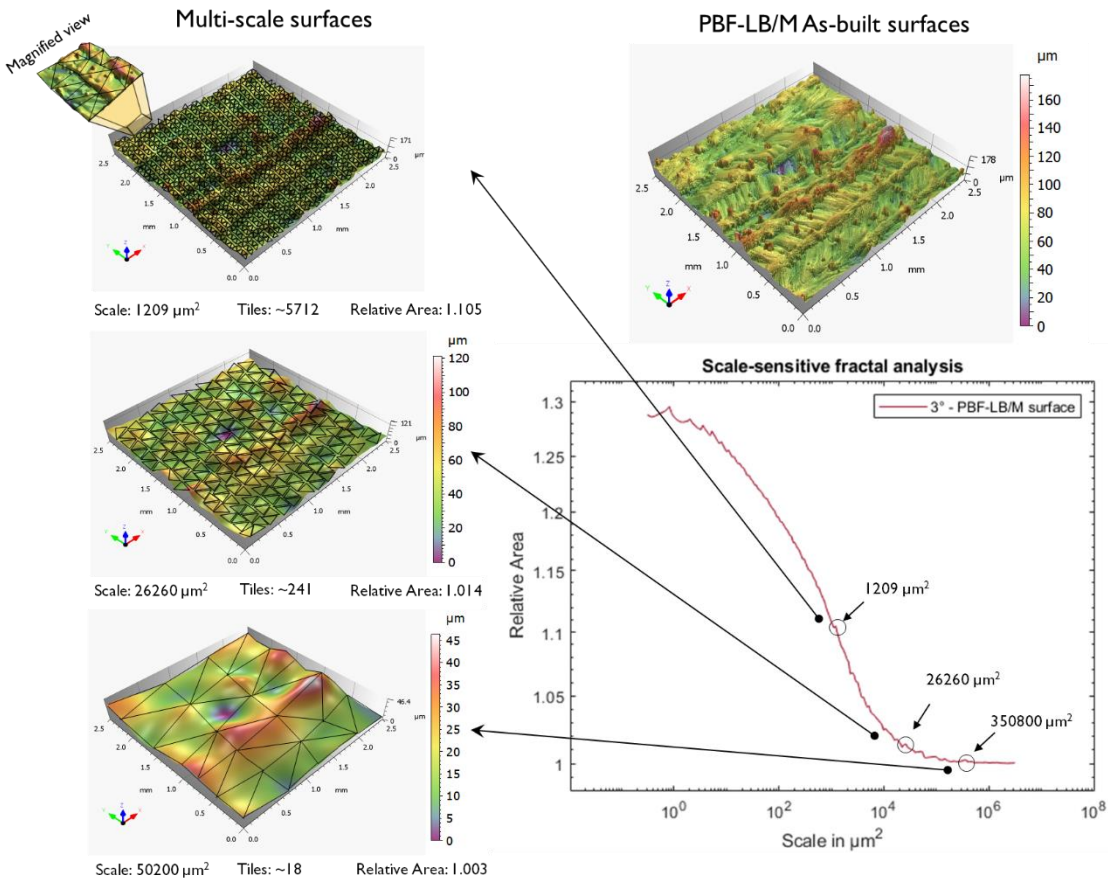
Figure 23. *Relative area plots show an example of a tiling algorithm performed on as-built PBF-LB/M surface. (a) Original surface (b) Relative area curve as a function of scale; (c-e) Surface topography representation at three different scales.* [52]

4.3.3 Feature-based characterization

Additive Manufacturing surfaces, particularly PBF-LB/M surfaces comprise several topographical features that include powder particles, melt tracks, and other manufacturing footprints. Characterizing them individually could give a better understanding of the AM

process for effective surface quality and function optimization and control. The literature points out several strategies for characterizing the surface features of AM samples [106][107], similarly, in this thesis, Feature-based characterization is discussed for the PBF-LB/M method. The feature-based characterization involves isolating the various significant surface features and then characterizing them individually to establish a complete understanding of the surface creation process for the chosen manufacturing process. In the present context, the surface features of the PBF-LB/M process were extracted in two of the following steps.

Firstly, the waviness from the measured surface topography was eliminated by applying a robust Gaussian filter (ISO 16610-71) with a suitable nesting index based on the characteristics of the measured surface. The isolated waviness surface would include the form caused due to the presence of powder particles, "stair-step" effects, and due to thermal conditions (shrinkages and swelling) during the printing process [108]. The roughness surface would include the powder particles and other manufacturing footprints.

Secondly, the powder particles present in the roughness surface were isolated using the binary thresholding function, which was achieved by moving a cutting plane from the highest point on the surface to the material ratio value corresponding to the Reduced peak height (Spk) of the surface. The residual surface thus obtained as a consequence of this operation includes the remaining footprints of the PBF-LB/M process, which along with the waviness surface can be parametrically characterized using areal surface texture parameters (ISO 25178-2). The isolated powder particles can be collectively characterized by measuring their volume. This methodology can be visualized in Figure 46, in section 6.5.2.

4.4 STATISTICAL APPROACHES

4.4.1 Regression

Regression, a statistical data analysis tool, is typically used to model interactions between dependent and independent variables [109][110]. Linear models are used in both simple linear regression (where only one independent variable is used) and multiple linear regression (when several independent variables are used) to predict the result of the dependent variable. In this thesis, a linear model is utilized to derive the correlations between the AM process settings or post-AM process settings and the surface parameters for optimizing the surface quality and product function. Furthermore, a special case of regression analysis is the Analysis of Variance (ANOVA) which explains the difference between the means of two or more data groups. It is important to understand the various factors involved in regression output to interpret the results required for process optimization and control.

- *Coefficient of determination (R^2)* describes the extent to which a given difference in one variable can be accounted for by the difference in another variable. In the context of surface analysis of AM processes, R^2 indicates the portion of the variance in the surface parameter readings that is predictable by the AM process settings. High R^2 values indicate a strong correlation between the dependent and independent variables. However, the R^2 assumes that all of the independent variables contribute to explaining the dependent variable. This may not always be true since some of the independent variables may not aid in forecasting the outcome of the dependent variables. Hence in such situations, the Adjusted R^2 can be

helpful since it pinpoints the exact set of independent factors responsible for explaining the dependent variables' variability. Usually, the adjusted R2 is preferred when there are many independent variables involved for analysis and if the difference between the R^2 and adjusted R^2 values is high, then it indicates that one or more of the independent variables may not adequately explain the variability in the surface parameter values. Excluding such independent variables or adding interaction effects can be some of the possible solutions to improve the accuracy of the model. The model fit may also be assessed with the help of the adjusted R^2.

- *Significance F* explains the trustworthiness of the data utilized in regression analysis. If the p-value associated with the F-test is less than 0.05, then there is a good chance that the measurements are accurate with respect to the process variables. It can also be utilized to determine the extent to which independent factors are reliable in predicting the variations of dependent variables.

- *P-value* in the regression output is utilized to determine the effects of independent variables on the dependent variables. In the present context, the independent variables refer to AM process variables and the dependent variables are the surface or profile parameters. The p-value is generally utilized in null hypothesis testing to determine whether the measured data is statistically different from the selected t-test. The null hypothesis usually suggests that there is no significant relationship between the two variables being measured. If the p-value is lower than 0.05, then the null hypothesis is rejected indicating a positive relationship between the measured variables.

- *Regression coefficients* in the regression output provide numerical values that can be utilized to model the relationship between the dependent and independent variables. The coefficients of the independent variables can be insignificant in determining the dependent variables if the associated p-values are more than 0.05. The coefficients can return positive or negative values indicating an increasing or decreasing relationship to the dependent variable.

Chapter 5

RESEARCH METHODOLOGY

Research methodology refers to systematic procedures or techniques followed to effectively achieve the stated research objective. In this chapter, an overall structure and description of the steps involved in the research methods are presented. It is followed by a brief discussion of the newly developed method for answering one of the research questions.

5.1 STRUCTURE OF RESEARCH METHODOLOGY

The main objective of this research is to find appropriate methods for characterizing the AM surfaces to fully understand the nature of the manufacturing process for optimizing the surface quality to achieve optimal product performance. It is important to reiterate this research objective to dissect this information mainly to establish the appropriate research methods required to achieve this goal. The research objective is as per the formulated research approach based on the three facets of the surface control loop previously discussed in section 1.3. Relevant research methods are established based on each facet as shown in Figure 24. Since this research is focused on process optimization, the study is mostly based on experimentation where the cause-and-effect relationship is studied between the process control variables and the surface topography formation, hence an experimental research methodology is employed.
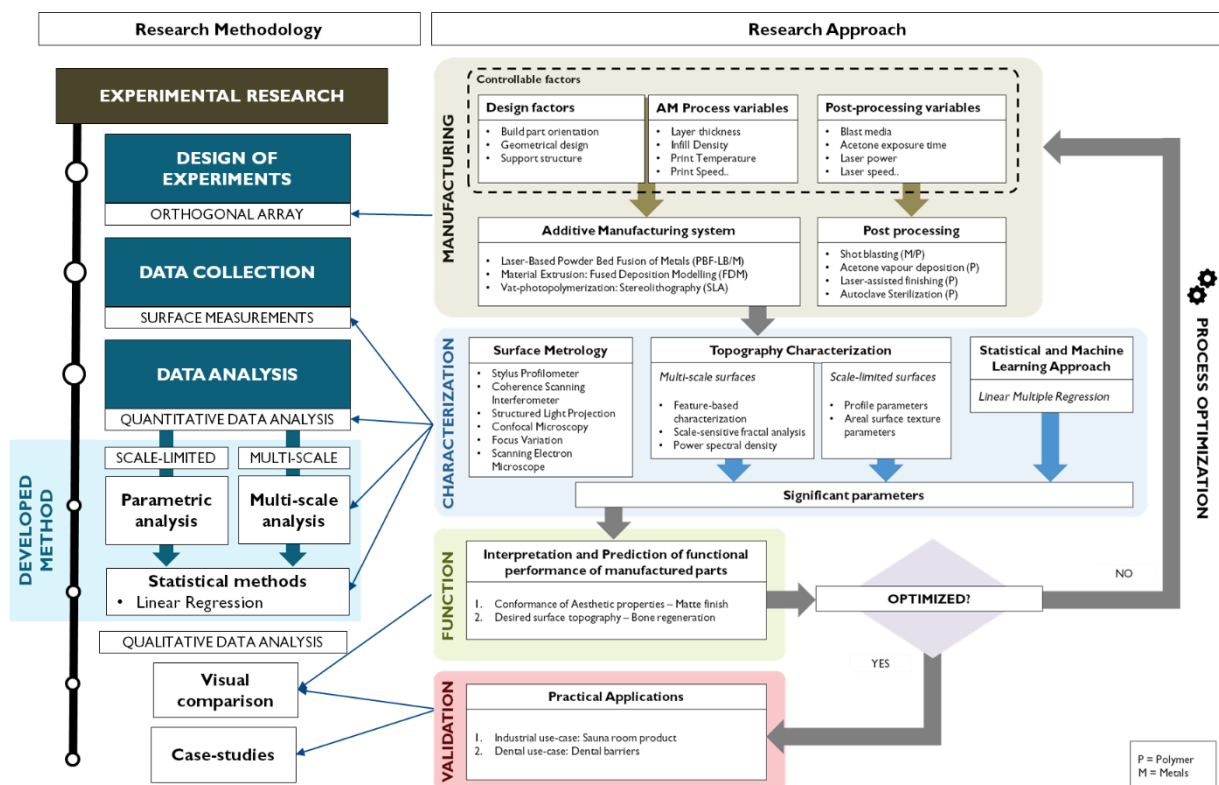
Figure 24. *Structure of research methodology as per the research approach*

5.2 EXPERIMENTAL RESEARCH METHODOLOGY

Empirical research is a type of research whose findings and conclusions rely on observed or experimental data or evidence rather than abstract theories and assumptions [111]. Empirical research is an umbrella term that includes a wide range of research methods such as interviews, observations, surveys, case studies, experiments, and so on, which are broadly classified into quantitative and qualitative methods [111]. A complete taxonomy of research methods and their definitions can be found in [112]. As mentioned earlier, in this thesis, the findings and conclusions are mostly based on performed experiments and hence an experimental research methodology is followed.

Experimental research follows a scientific approach attempting to prove or disprove a formulated hypothesis by performing laboratory or field experiments [113]. It usually involves experimentation to study the relationship between multiple-independent (AM process control variables) and dependent variables (roughness parameters). There are several types of experimental research methods but are broadly classified into two categories namely Laboratory experiments (True/Classical experiments) and Field experiments (Pre-experimental and Quasi-experimental designs) [113]. Laboratory and Field experiments are scientific methods of hypothesis testing involving cause-and-effect relationships, where the former is performed under controlled conditions and the latter is performed in natural settings representing real-world situations. The research work presented in this study is more inclined toward laboratory settings since the experimentations take place using controlled process variables. It would be necessary to include uncontrolled independent variables (Environmental temperature, humidity, vibrations, and so on), in order to gain more realistic conditions. However, previous research points out that in any research design it is difficult to establish inference conclusively due to various uncertainties involved in the process but laboratory experimentation provides the highest possibility of decisive inference since the tests are performed under controlled conditions [113].

Experimental research includes three important steps i.e. the Experimental design or Design of Experiments (DoE), Data collection methods, and Data analysis steps. The following sections discuss in detail these core concepts involved in experimental research along with a newly developed method to identify the significant roughness parameters and scale crucial for analyzing the manufacturing process and surface function.

5.2.1 Design of Experiments (DOE)

Design of Experiments (DoE) is defined as a statistical process of formulating a series of experiments based on independent variables to then analyze the empirically collected data mainly to discover and validate the objective information about a system under investigation [114]. Generally, DoE generates a number of experimental units consisting of a combination of "factors" and "levels" to determine its influence on the measured dependent variable. The word "factors" refer to two or more independent variables in a system and "levels" refer to several layers within each factor. For example, in the present research context, the factors are the AM process control variables such as layer thickness, print speed/temperature, infill density, and so on. Each factor has layers, for example, layer thickness for an FDM process can be chosen as anything between 0.1µm to 0.4 µm (the numerical values of layer thickness can vary from one

AM system to another) which are termed "levels". The dependent variables are the obtained surface/profile parameter reading from the surface topography measurements.

The major constraint of this research method is that the causal inferences made on the experimental results highly depend on the chosen DoE [115]. It is, therefore, important to consider randomization, replication, and blocking while designing the experiments before drawing any inferences or conclusions from the results. In doing so, it improves the accuracy and precision of estimating the effects of factors on dependent variables. Randomization refers to a random selection and ordering of experimental units, Replication refers to multiple runs of experimental units comprising of same factor-level combination. Blocking refers to segregating or grouping similar experimental units to reduce the effect of uncontrolled factors.

There are several types of DoE and its complete taxonomy with explanation can be found in [114][115][116]. A summary of only a fraction of the classical DoE is presented in this thesis mainly to point out the typically followed procedure of conducting experiments in the appended papers. This research follows two main steps in DoE i.e., Screening Experiments, and either Full or Fractional factorial designs using Taguchi's Orthogonal Arrays [115].

Screening experiments form the initial stage of experimental design, typically used when there is a large set of factors involved. This is mainly done to vaguely establish a boundary between the factors that affect and the factors that do not affect or influence the dependent variable. It can also be used as a way to test the limits of the manufacturing process and note the most important factors influencing the outcome. After identifying the factors, subsequent experiments may be necessary to fully establish the relationship between independent and dependent variables. In this thesis, the experiments are designed either based on established knowledge (previously published papers or expert opinion) or from the experience gained during the experimental screening process.

A *full factorial design* provides all possible experimental units for factor-level combination in experimental design. It can evaluate multiple factors with multiple levels which provide complete information about the process under investigation. A full factorial design is used when there is a limited number of factors and levels mainly due to the investment of time that is required to run all experiments. Hence, *fractional factorial designs* are often used to overcome the time constraint. It is a subset of full factorial designs that are carefully selected to represent the whole experimental design. One type of fractional factorial design is *Taguchi's orthogonal array* [115] which allows selecting a balanced subset of multiple factors with multiple levels that ensure providing unbiased designs by considering all levels and factors equally.

Furthermore, more advanced methods such as *Response Surface Methods (RSM)* [116] and *Monte-Carlo simulations* [117] can be used to study the non-linear relationship between the independent and dependent variables of a complex system.

In this thesis, a linear model developed using relatively simplistic experimental designs seemed to be sufficient for investigating the surface topography of AM processes.

5.2.2 Data Collection

Data collection is a process of acquiring information by measuring factors of interest that either answer an underlying research objective, tests a hypothesis, or simply evaluate an outcome [118]. In the present research study, the data collection mainly refers to measuring topography

information of AM surfaces for conducting detailed data analysis to establish credible evidence for predicting and optimizing AM processes required to achieve its product function. The surface data collected is mostly primary data since it is directly collected from the researcher by performing experiments.

The surface topography of AM processes is measured using state-of-the-art surface metrology instruments as discussed in *Chapter 3.* To study any manufacturing process, it is crucial to select appropriate surface metrology methods since they dictate the outcome of the study. Every surface measuring instrument produces surface information differently, some are comparable while others provide distinct surface data. The data extracted can either be used for qualitative or quantitative purposes depending on the defined research objective. However, for any surface data to be meaningful, several things need to be considered.

- *The calibration* procedure is imperative for any surface metrology instrument to ensure the certainty of the data measured. It is a process of configuring the instrument so that the measured surface information lies within the acceptable range of the standard reference specimen [119].
- *Sampling size* broadly implies *the number of surface measurements* made on a particular specimen to get a representative roughness value for that specimen. The definition of sampling size differs with the type of measurement. For instance, in profile measurements, each measurement made is termed as the evaluation length upon which the profile parameters are defined. The evaluation length is usually segmented into 5 equal parts (by default as per ISO 4288:1996) and each part is called a sampling length [94]. To summarize, five sampling lengths make one evaluation length which represents one profile measurement made on a surface, and the number of such evaluation lengths measured gives the sampling size. With surface or areal measurements, the default as per ISO 25178-2:2021 is one sampling area per evaluation area [89] and a number of such sampling or evaluation areas gives the sampling size. In this study, the sampling size varies from one AM surface to the other. Usually, an average of 5 to 10 measurements are taken to get statistically reliable parameter readings.
- The choice of *magnification* is vital for analysis but largely depends on the research objective. For instance, if the area of interest is to study the function such as wear, then macro-roughness features could be more relevant for the study which can then be measured using low magnification. Magnification gives the possibility of observing surface features at various scales.
- Every optical microscope has an *objective lens* associated with a certain magnification which when focused onto the specimen surface, an image of a certain area of the surface can be captured. This area captured is called *the field of view* or *measurement area*. The measurement area can be the area corresponding to either a single magnification measurement or a stitched area of several measurements. Each measurement area comprises several pixels and the size of each pixel is termed as the *resolution* for a given magnification. Whereas in profile measurements, the magnification corresponds to the resolution which is the same as the size of the stylus tip radius.
- It must be noted that in areal surface measurements, the evaluation area or sampling area is the same as the measurement area or field of view, however, several of such measurements are considered as sampling size.
- Other *confounding factors* such as environmental temperature, humidity, and so on can also influence surface measurement factors.

The exact values of chosen surface metrology specifications for each of the appended papers are presented in the results and discussion section.

5.2.3 Data Analysis

After the collection of data, the next step would involve analysis to extract meaningful information required for the study. The surface measurements can be either a profile or areal surface data. In areal surface measurements, the captured surfaces contain geometrical features that typically correspond to surface shape and texture formed as a result of the manufacturing process. The surface shape corresponds to form and waviness, and the texture is termed roughness. As per the ISO 25178-2:2021 [89] standard, the measured surface is called the raw or unrefined surface containing the aforementioned irregularities, and a primary surface is extracted from the raw surface after applying the S-filter removing the small-scale lateral features that correspond to noise in the measurements. The form is removed from the primary surface by applying the F-operator and the resulting surface is labelled as the S-F surface to put simply the term "S-F" refers to the surface obtained after removing the form. Further, the waviness or the large-scale components are removed by applying L-filter to the S-F surface resulting in an S-L surface denominated as roughness or texture.

Similarly, ISO 4288 [94] standard defines the refining procedure for the profile measurements, the primary profile is obtained after the application of a low pass micro-roughness filter (λ_S). The form errors mostly correspond to tilt or shape correction of the measured profile and the high-pass filter (λ_C) as per ISO 16610-21 [95] separates the waviness and roughness profiles. All the captured surface profiles or images are processed using the software MountainsLab, a 3D imaging, and analysis tool from Digital Surf. Once the surfaces or profiles are refined, they can be subjected to various topography characterization methods (refer to *Chapter 4*).

Form removal

In this study, the form is removed mostly using the levelling operator by the least-squares method that can be applied to both profile and areal surface texture measurements. There are other types of form removal techniques based on various algorithms, for instance, tilt errors can be removed using levelling line by line and levelling by partition, and polynomial approximation with higher orders can be used to remove any shape from the measured surface topography. The selection of the type of form removal operator depends on the nature of the surface under investigation.

Filtering

After removing the form from the surface, various metrological filters such as Gaussian filter, spline filter, morphological filter, motif method, wavelet transform, Fast Fourier transform (FFT) filters, and spatial filters can be utilized to separate the waviness from the roughness features [120]. These filters can also be used to remove the measurement noise from the surface data. A brief explanation of these filters can be found in [101]. In this thesis, the robust Gaussian filters (ISO 16610-71) were most commonly used and in one case FFT filters were utilized for analysis. The accuracy of separation of waviness and roughness components of the surface or profile mainly depends on the type of filter utilized along with the selection of nesting index or cut-off value. The term nesting index is commonly associated with areal surface texture measurement and cut-off values with profile measurements [121]. It decides the way the chosen

filter separates the surface features at a particular scale or wavelength based on its parameter value. ISO 16610 series of standards specifies the metrological characteristics of various areal and profile filtering methods to refine the surface data for analysis.

Other operations

Generally, the topography measurement of any manufactured surfaces results in either a few non-measured points or outliers in the form of sharp peaks or valleys, this may be due to the surface complexity or material transparency, and reflectivity issues of the sample. This challenge is particularly pronounced in optical measurements and can be handled by processing the image in the software. The software fills in these non-measured points by measuring the neighboring data points or by filling them with a constant value. The outliers can be removed by using image dilation [122].

5.2.4 Developed methodology

Additive Manufacturing (AM) surfaces contain various intricate features that constitute their surface roughness. The surface features are due to the physical phenomena that occur as a consequence of its manufacturing process and its process variables [9]. The surface features, for instance in metal AM, include melt pool tracks, stair steps, the spattering of powder particles, the balling effect due to the agglomeration of powder particles, and so on [9][123]. To achieve a complete geometrical description of these surface features, more than one and often several roughness parameters are required. It is also important to note that these features on the surface topography can be of many scales and sizes [124]. However, not all of these surface features will affect the functional performance of the AM part [15]. It is, therefore, necessary to identify the important parameters and scales that describe those specific surface features that affect functional behaviour. The following sub-chapters present two developed methodologies, the first is an approach to identify significant roughness parameters for scale-limited surfaces and the second is to identify the significant scales and their corresponding roughness parameters for multi-scale surfaces. These methodologies are utilized in this study to have an improved interpretation of AM surfaces and for effective optimization of the AM process to achieve its intended function.

Identification of significant roughness parameters using regression

For the scale-limited surfaces, regression analysis is utilized for identifying the significant parameters. Regression analysis is a statistical data analysis tool for modelling and predicting the relationship between the dependent and independent variables [109][125]. The regression analysis used in this context is based on a linear model with multiple dependent and independent variables and hence it is called Multiple Linear Regression (MLR) [126]. In this study, the dependent variables are surface or profile roughness parameters and the independent variables are the process control variables from various AM processes (layer thickness, print temperature, etc.), Post-processes (Shot blasting media, laser engraving power, etc.), and design factors (build inclination, part orientation, etc.). Figure 25 presents a workflow that is followed to not only identify the significant parameters but also to determine the influence of process control variables on the identified parameters.

The surface topography of various AM processes was measured and characterized using profile/surface roughness parameters as per the ISO standards. The roughness parameters were

then linearly regressed with AM process variables as per the selected design of experiments and analysis of the resulting regression output reveals the relevant roughness parameters. In this study, the four factors such as coefficient of determination (R^2), Significance F, P-value, and regression coefficients are considered to be important. The first three factors are more concerned with the validity of the results while the last is used for modelling the relationship between the roughness parameter and AM process variables. A complete description of various factors in the regression output can be found in chapter 4, section 4.4.1. However, a brief explanation is presented for ease of understanding of the developed method. The following steps describe the parameters selection criteria.
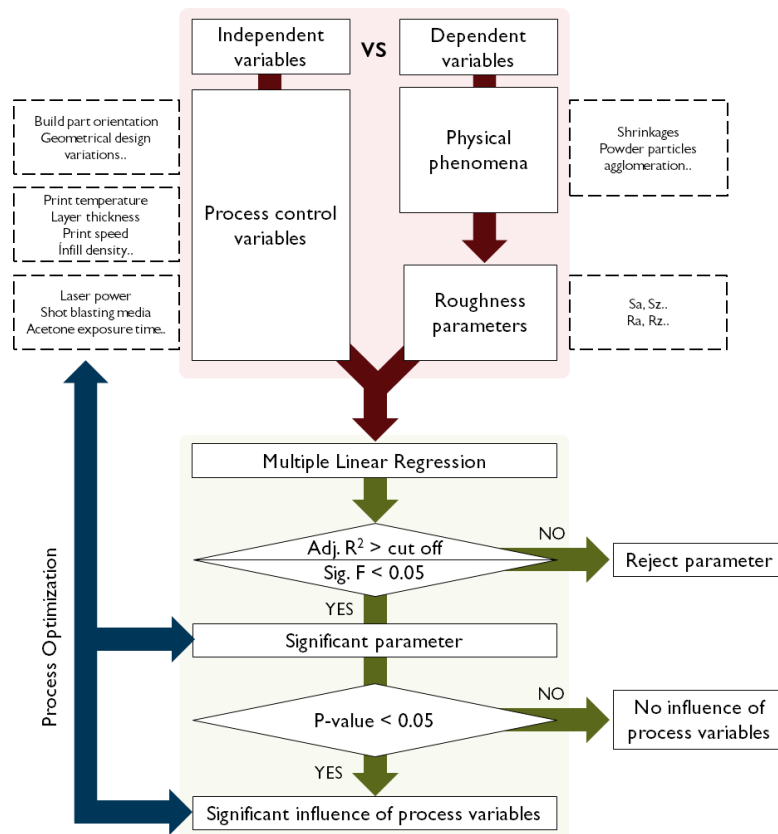
Figure 25. Identification of significant parameters using regression

1. The first step of the parameters selection criteria is to observe the *Coefficient of determination, R^2* value in the regression output. The R^2 provides information on the goodness of fit to show how well the chosen regression model fits the observed results [126]. The higher the value of R^2 the higher will be the goodness of fit and the better will be the accuracy of prediction. The low values of R^2 indicate that the chosen linear model may be insufficient in describing the variations between the dependent and independent variables. The adjusted R^2 is utilized when there are several independent variables. In this study, a certain cut-off value of R^2 or adjusted R^2 is set as a threshold to filter out the parameters that do not agree with this condition.

2. The second step is to examine the *Significance F* value. This provides information on the reliability of the regression data. From the regression output, any roughness parameter that has a significance F value less than 0.05, indicates that the probability of measurements made with respect to the process variables is not random. This is the final step in the

selection of relevant parameters, the parameters that agree with steps 1 and 2 are termed as significant.

3. After establishing all the significant parameters, the next step is to identify which of the many independent variables used in the study has a significant influence on surface parameters. For this purpose, the *P-value* from the regression output is analyzed. Any independent variable whose p-value from the regression output is less than 0.05 does not have any influence on the roughness parameter. This step establishes the relationship between the roughness parameters and the process control variables, and this relationship can be modelled using the *Regression coefficients*. Thus, the obtained model can be used to predict the values of the significant roughness parameter for various values of independent variables or process control variables, thereby, enabling process optimization.

Method limitations

The identification of significant parameters and the derived relationship between process control variables and roughness parameters are based on the linear regression model. It may be necessary to investigate other complex models to test the accuracy of the developed method. Furthermore, the threshold value set for the coefficient of determination, R^2 is mostly arbitrary, however, the choice of selection depends on the nature of the surface and its manufacturing process. Nonetheless, thresholding allows the selection of a robust set of parameters that can explain the occurrences of surface features effectively.

Identification of significant scales using a multi-scale characterization approach

The multi-scale characterization approach is a way of analyzing the captured surface topography at various scales of observation. The captured surface may contain topography features at different scales and by applying a filter with various nesting indices, surface wavelengths corresponding to the nesting index can be separated resulting in multiple surfaces. This yields an opportunity to identify the most significant scales affecting the surface function and thereby identify the most influential parameters for analysis. In this study, Power Spectral Density (PSD) and Scale-Sensitive Fractal Analysis (SSFA) are utilized for the identification of crucial scales and parameters. The PSD method analyzes the surface features as a function of spatial frequency and SSFA analyzes surfaces at scales of interest based on fractal methods [89].

This section presents two different methods based on two different scenarios present in the appended papers. These methods were developed specifically for the research presented in those papers. However, there is a possibility to generalize these techniques by extending them to other scenarios where the focus is to compare the surface topography quality of two or more manufacturing processes and for comparing the capabilities of multiple surface metrology instruments in capturing the surface topography information.

Scenario 1 – comparing two processes

In this case, SSFA through the Area-scale method is utilized for analysis, however, PSD can also be applied to get similar results. This method is best suited for comparing the surface of two processes with a smaller number of independent variables or process parameters. For instance, in paper 4, the surface topography of the samples produced from the PBF-LB/M process (process A) was compared before (as-built) and after the shot-blasting process (process B) for various build inclinations (only one independent variable), and this comparison is

performed at various scales. Figure 26 shows the workflow to identify the significant scales and parameters.

The as-built and shot-blasted surfaces for all build inclinations were measured and complexity plots were generated. As previously described, complexity plots provide the rate of change of surface intricacy as a function of scale. The ratio of the complexity plots of as-built to that of shot-blasted conditions was taken for each build inclination to explain the differences between the two processes. The resulting plot from this operation was termed a "Transfer Function" and the region where the difference between the two processes is maximum was considered to be the most significant scale range. The surface features corresponding to the identified significant scale range were extracted from the original surface (as-built surface) by applying a bandpass filter using the robust Gaussian method [127]. The filtered surface contains surface features that are mostly affected by the shot-blasting process, any alterations in the independent variables or process control variables will likely affect the surface features corresponding to this scale range. Furthermore, to select the most significant roughness parameters within the selected scale regions, the coefficient of determination (R^2) is utilized for this purpose. The R^2 is calculated between the complexity values and roughness parameters obtained for process A at each scale (mostly for as-built surfaces since it contains all the surface information). The obtained R^2 values for each parameter are plotted for each scale and the parameters with R^2 values more than the predetermined threshold inside the selected scale range are considered to be significant parameters.
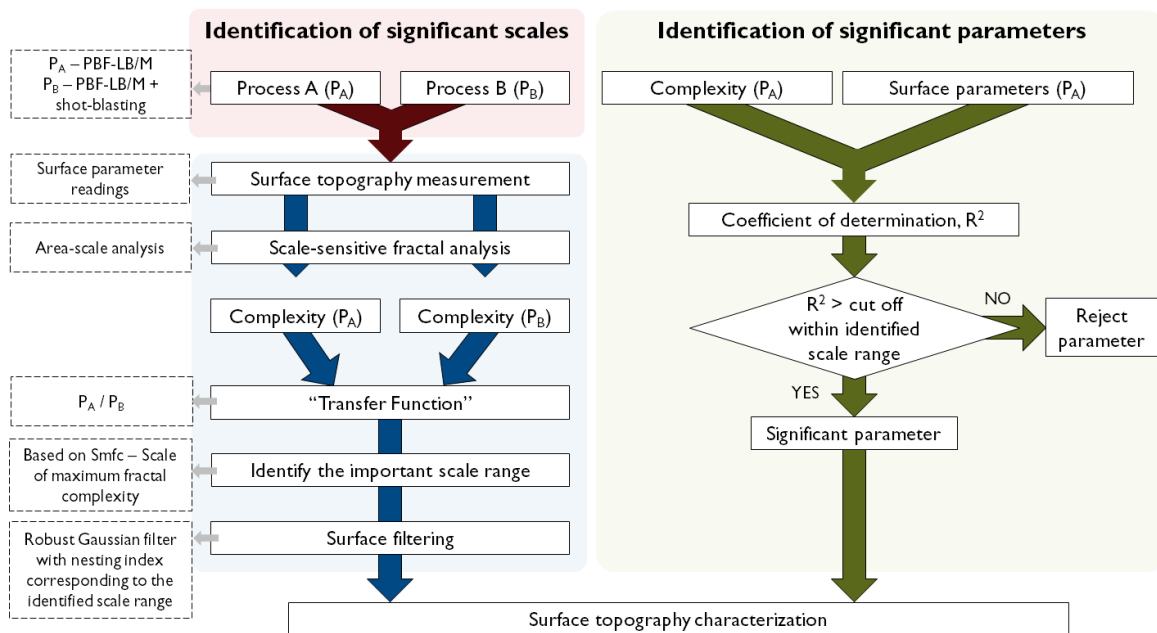
Figure 26. *Identification of significant scale and parameters using area-scale analysis*

Method limitations

Note that this method can be extended to various other scenarios to compare different manufacturing or post-processes and identify their effects on surface topography. However, the use of the "Transfer Function" in the methodology allows for comparing only two processes at any given time. Nonetheless, the complexity plots can still be applied to multiple manufacturing processes to vaguely visualize the difference between them through surface analysis. For establishing a more accurate difference "Transfer function" can be utilized. Also, the selection

of a threshold value based on R^2 for identifying the significant parameters is again arbitrary. Similar to the previous method, it depends on the nature of surface topography and processes that are being compared.

Scenario 2 – comparing multiple surface metrology instruments

In this scenario, Power Spectral Density (PSD) was utilized to identify the significant region of interest that helps in discriminating the surfaces that are measured using different surface metrology instruments. This method was first developed in paper 1 where the focus was to compare the CSI and 3D SEM measurements performed on a roughness calibration standard. The objective of this paper was to use PSD to test the fidelity of 3D SEM measurements when compared to CSI measurements. Typically, SEM images provide false grey scale 2D images that are mostly used for qualitative analysis, but with the development of algorithms and software, it is now possible to reconstruct a 3D image by viewing the surface at different angles. Using this 3D SEM image, it is possible to calculate the surface roughness parameters, however, the accuracy of these readings is still a question. In paper 1, the 3D reconstruction of SEM images was obtained from two different algorithms namely Piazzesi Model Function (PMF) [128] and the Triangulation Algorithm (TA) [129]. Although the PMF and TA methods are algorithms for the 3D reconstruction of SEM images, they are considered separate measuring instruments for ease of interpretation of the developed method.

The surface topography of the roughness standard sample was measured and relocated using CSI and SEM instruments. After relocating the images, surface parameter readings were taken for both CSI and SEM algorithms and the PSD was plotted. The PSD represents surface features as a function of spatial frequency and the PSD plot will reveal the regions in the frequency spectrum where the differences and similarities can be found between various measuring devices. The selection of a significant region depends on the objective of the research. With this method, one can choose similar regions in the frequency spectrum to convey the fidelity of 3D SEM measurements to the CSI measurements. On the other hand, the differences in the frequency spectrum reveal the deviation in capturing the surface information with respective metrology devices. Once the significant region is identified, a suitable bandpass filter can be utilized to filter out the surface features and parametric characterization can be performed to get the quantitative differences or similarities between the different measuring instruments.

The significant parameters can be identified by calculating the percentage difference of each surface parameter for each measuring instrument before and after the filtration process. The parameters that have a percentage difference of less than the set cut-off threshold for every surface measuring instrument are considered significant for the identified region of interest. It is also possible to identify the significant parameters by understanding the underlying mathematical expression utilized for calculating each surface parameter. For instance, the average height parameter (Sa) is defined based on the surface height information and so it mostly depends on larger wavelength regions in the frequency spectrum. Hence any filtration in the lower end of the frequency spectrum i.e., removal of shorter wavelengths will not affect the Sa parameter largely. Therefore, if the identified region of interest is in the larger wavelength region, then the Sa parameter is likely to have lower percentage differences thereby termed as significant.

Method limitations

The identification of significant regions in the frequency spectrum is mostly visual where the spatial frequency curves of various measuring devices are observed and the nesting indices for bandpass filtering are identified. Also, the PSD curve differs based on the nature of the surface under inspection, for instance, the anisotropic surfaces will have 2D PSD that produces two peaks one for each dominant wavelength in the frequency spectrum. Hence, analyzing multiple PSD curves becomes tedious. One way to overcome this challenge is to use a 2D isotropic PSD that averages the 2D PSD (anisotropic) over an azimuthal angle [119].
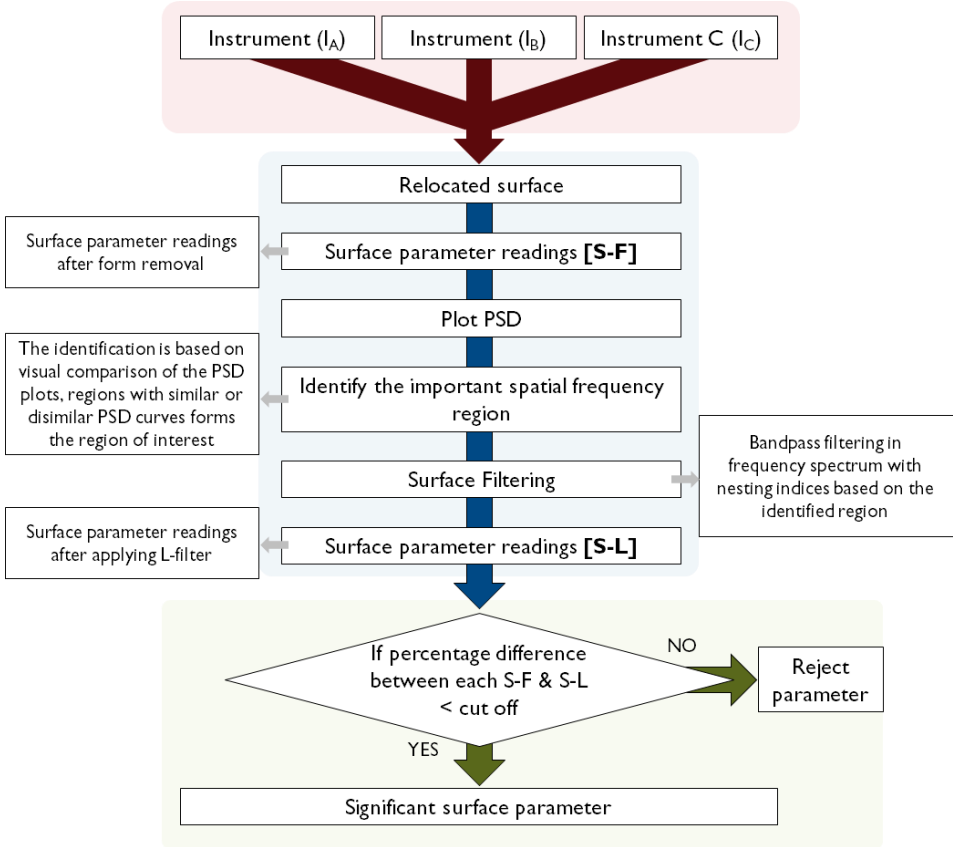
Figure 27. *Identification of significant spatial frequency regions and parameters using Power Spectral Density*

Chapter 6

RESULTS AND DISCUSSION

The chapter on results and discussion presents the main findings from the various appended papers to answer the raised research questions. This chapter begins by providing an overview of the structure used to show the organization of the appended papers into their relevant research questions and it is followed by providing a summary of relevant results.

6.1 FRAMEWORK OF RESEARCH RESULTS

In this research, four important research questions are formulated to answer the underlying research objective. The first three research questions are designed around the three facets of the surface control loop namely Characterization, Manufacturing, and Function. The fourth research question introduces the Validation step which intends to verify the results obtained from testing the surface control loop by applying them to a real-world application. A total of 7 appended papers comprising various research methods, analyses, and results were utilized to answer the 4 listed research questions, but it is important to sort and classify these papers for the realization of the stated research objective. For this purpose, Figure 28 provides an overview of the structure of the research questions and relevant papers. The first research question is designed to include all the appended papers and hence a brief introduction for each paper is presented before proceeding with the discussion on the relevant topic. Whereas for the remaining research questions, the results are directly presented. The following sections present the results from the listed research papers.
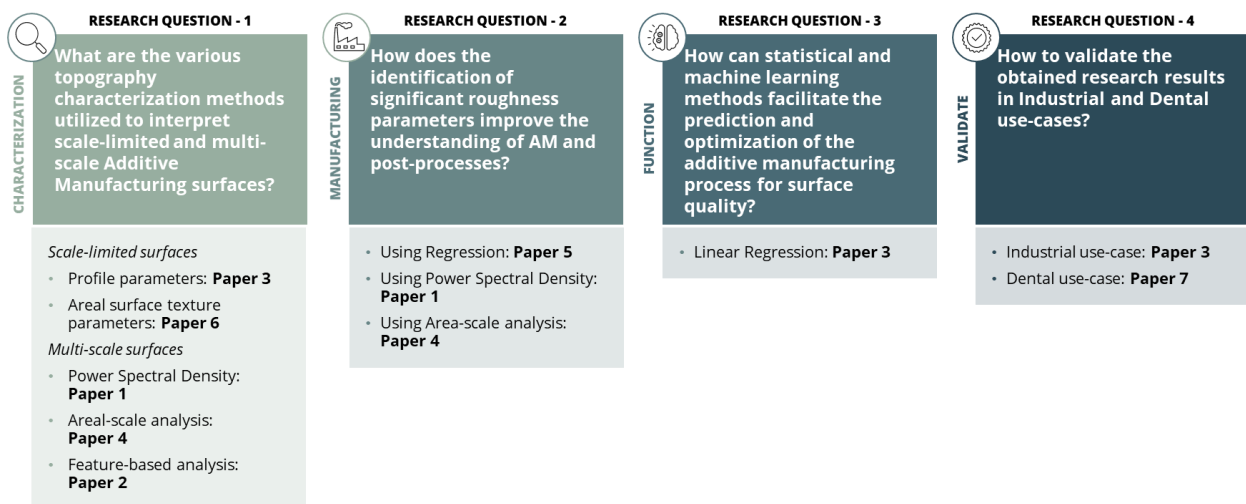
Figure 28. *Classification of appended research papers as per the framed research questions based on the surface control loop.*

6.2 CHARACTERIZATION AND RESEARCH QUESTION 1

This section addresses research question 1 by gathering relevant appended papers that describe various characterization methods employed for discriminating the scale-limited and multi-scale surfaces. The scale-limited surface characterization usually includes profile and areal surface

texture parameters whereas, multi-scale characterization involves more advanced methods such as Power spectral density, Scale-sensitive fractal analysis, and Feature-based analysis. An excerpt from research papers is presented to answer RQ1 in the following sub-sections.

6.2.1 Scale-limited: Profile parameters characterization (Paper 3)

The primary focus of this paper was to study the influence of post-processing methods such as Shot-blasting (SB), Laser-assisted finishing (LAF), and Acetone Vapour Deposition (AVD) on the surface topography of Fused Deposition Modeling (FDM) parts mainly to enhance the product surface quality required for its end application. For this purpose, the surface topographies of the FDM parts in as-built and post-processed conditions were measured and compared to the reference injection molding parts. The injection molding parts had a smooth texture with a matte surface finish, which meets the industrial aesthetic requirement. To achieve these conditions, it was necessary to study and experiment with different post-processing parameters. In this paper, a design of experiments was established for various manufacturing control variables and a linear regression model was implemented to study its influence on surface texture. A methodology was developed to identify the significant profile roughness parameter for the characterization of AM and post-processed surfaces. Finally, the knowledge gained through experimentation served as a guideline to implement the best approaches for finishing the FDM parts for industrial application and more advanced methods of characterization such as Power Spectral Density (PSD) were utilized to discriminate the final surface finish. However, for the first research question, the focus is concentrated on characterizing the FDM surfaces using profile parameters and hence only points related to this are discussed.
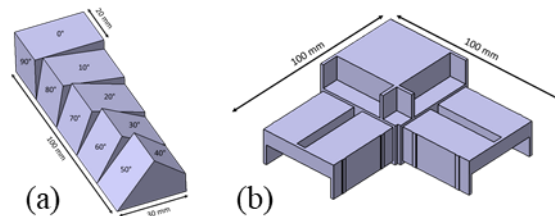
Figure 29. *CAD models of (a) Surface specific artefact and (b) TylöHelö sauna corner knot* [44].

The experiments were performed using a surface test artefact [130] with varying build inclination from 0° to 90° in steps of 10° as shown in Figure 29a and an industrial product as shown in Figure 29b served as a final product to test the results. The profile measurements were performed using a Stylus Profilometer with a stylus tip radius of 2µm and a total of 10 measurements were obtained at each slope angle in the surface test artefact. The profile measurements were refined to remove form using leveling operator by least squares methods and the waviness was removed using the Robust Gaussian method with cut-off values (λ_c = 2.5mm for 0° to 30° and λ_c = 0.8mm for 40° to 90° build inclination) obtained as per the ISO 4287 standards [92]. The design of experiments as per Taguchi's L9 orthogonal array was composed for each post-processing method to generate an optimal set of experiments to study its effect on the surface topography of FDM parts. The process control variables for the Shot-blasting process include blasting time and blasting media. Similarly, for the AVD process, the time of acetone exposure to the FDM parts was varied and results were recorded. For the LAF process, laser power, laser speed, and resolution were analyzed. The best possible FDM print settings were chosen and kept constant to eliminate their influence on surface topography.

Multiple linear regression was utilized for identifying the relationship between post-process settings and profile roughness parameters and based on regression methodology the Rp, Maximum peak height parameter was considered to be most relevant for analyzing the effects of post-processing on surface topography.

The results from the profile measurements are discussed by considering the Laser-assisted finishing (LAF) post-processing method as an example, further, the discussion on various other post-processing methods can be found in the appended paper. Table 3 displays the experimental design utilized for the LAF process.

Table 3. *Design of Experiments with L9 (3³) Taguchi's orthogonal design* [44]

Experimental Units	Laser-assisted finishing		
	Laser Power in %	Laser Speed in %	Resolution (PPI)
1	60	50	500
2	80	65	500
3	100	80	500
4	60	50	750
5	80	65	750
6	100	80	750
7	60	50	1000
8	80	65	1000
9	100	80	1000
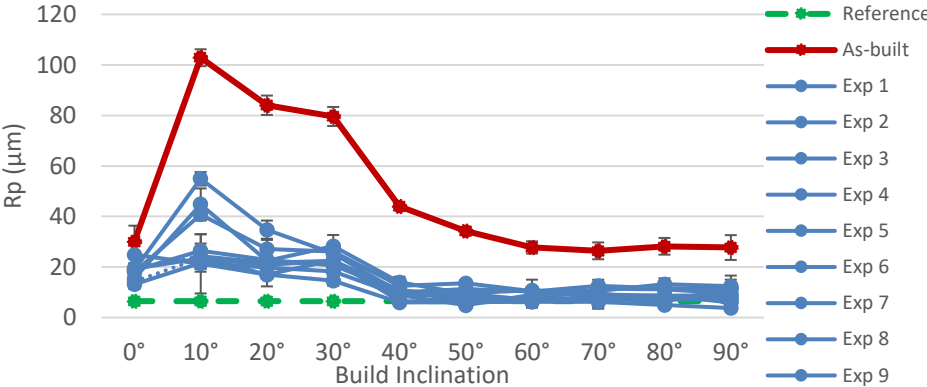
Figure 30. *The maximum peak height of FDM surfaces finished by the LAF process at various build inclinations along with as-built and reference injection moulding measurements.* [44]

Figure 30 presents the variation of the Rp parameter as per the changes in build inclination for as-built, reference injection moulding, and laser-finished surfaces for each experiment performed in accordance with the DOE. It can be seen that Rp increases with a decrease in build inclination this is mainly due to the presence of the "stair-step" effect at lower build inclinations with an exception at 0° build inclination since it is comprised of a raster pattern that provides a slightly different surface texture [131][132]. Also, the value of the Rp parameter is substantially reduced from the initial as-built conditions upon the application of the laser finishing process for all the experimental runs. However, it has failed to fully reach the reference injection moulding surface conditions at lower build inclinations of 0° to 30°, whereas the roughness values are close to reference conditions at higher build inclinations (40° to 90°). From the statistical analysis, it was found that laser power and laser speed have the maximum influence on the profile roughness, and resolution had a negligible effect. It can be visualized from the

profile measurements as shown in Figure 31. The Rp or the peak on the profile measurement decreases with an increase in laser power and with a decrease in laser speed.
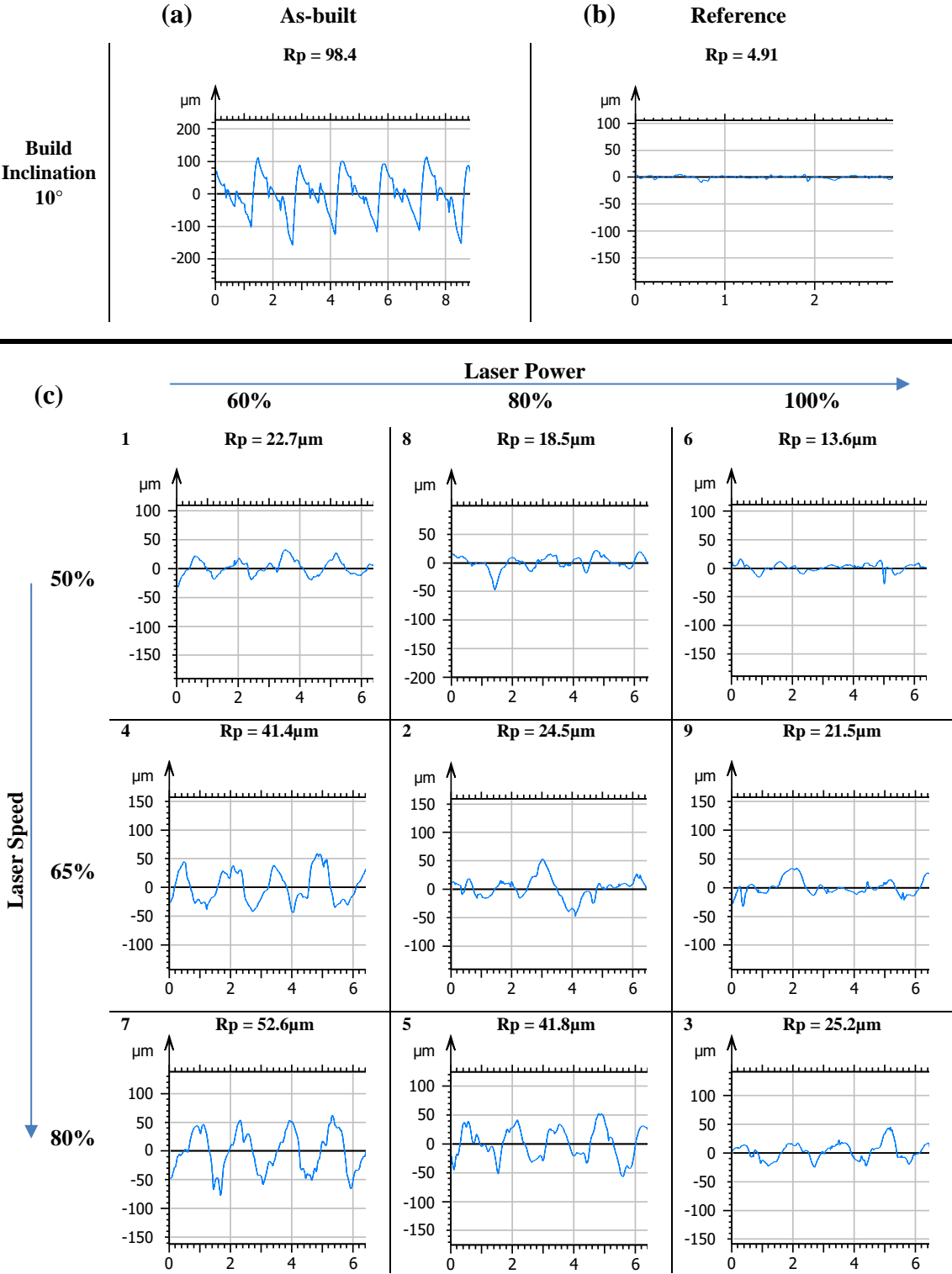
Figure 31. *Profile measurements at 10° build inclination (a) As-built FDM profile (b) Reference injection moulding profile (c) Profiles measured as per DOE after laser-assisted finishing.* [44]

The *laser speed* demonstrates the amount of time the laser is in touch with the sample surface. At lower laser speeds the laser contact with the sample will be resulting in higher melt rates and thus provide lower roughness values. It can be said that the laser speed is directly proportional

to the Rp parameter. On the contrary, the *laser power* is indirectly proportional to the Rp parameter. This is quite obvious since high laser power results in higher melting rates, thus lowering the roughness values. The *resolution* in PPI (points per inch) indicates the number of pulsed laser points per inch in length. The results showed that the resolution did not have any influence on the Rp parameter, this is because the chosen resolution had high PPI values which imply closer spacing of these laser points resulting in excessive local melting and evapouration of surface features leading to the creation of randomness on the surface profile [54]. To fully realize the effect of resolution on surface topography, firstly, a better selection of PPI values is necessary, and secondly, other forms of topography characterization preferably areal surface texture parameters are required which could capture this randomness of the surface effectively.

Furthermore, the use of the post-processing method significantly reduced roughness but it still produced surfaces that did not aesthetically meet the industrial requirement. The LAF process ignited the top layer of the surface during melting which led to discoloration of the part. This aspect cannot be captured in profile measurements hence, it is often combined with visual comparison or more advanced characterization methods for analysis. Although profile measurements provide topography information limited to only one direction (measured across the dominant wavelength), they can still provide adequate information about the surface texture to understand the manufacturing process under investigation.

6.2.2 Scale-limited: Areal Surface Texture Characterization (Paper 6)

In this thesis, the areal surface texture parameters as per ISO 25178-2:2021 [89] have mostly been utilized in combination with advanced characterization methods for the effective characterization of AM surfaces. However, in paper 6, the surfaces of metal FDM samples are simply explained using areal surface texture parameters alone.

Paper 6

This paper focuses on performing a feasibility study of the FDM process to produce bronze (CuSn10)-infused PLA components. The surface topographical, dimensional, physical, mechanical, and microstructural properties of FDM parts were analyzed and reported in this paper. For this purpose, the tensile test artefact (TS-bar) as per ISO 527-2 type 1BA [133] shown in Figure 32 was employed for analysis. Based on the previous research and initial experimentation, ideal FDM print settings were utilized to produce these TS bars. The printed TS-bars formed the green parts which were then subjected to thermal de-binding and sintering processes to get the final metallic bronze product. Figure 32 displays the as-built and sintered tensile test artefact. The surface measurements were performed using an Interferometer and the measurements were performed on the top surfaces of the TS bars for both the as-built and sintered surfaces.
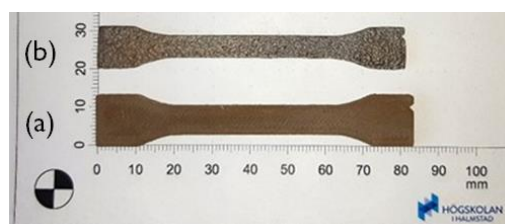
Figure 32. *The FDM printed tensile test artefact in (a) as-built and (b) sintered conditions.* [134]

a) Printed, top, S_a=1.8 µm, S_{10z}=24.5 µm.   b) Sintered, top, S_a=13.0 µm, S_{10z}=122 µm
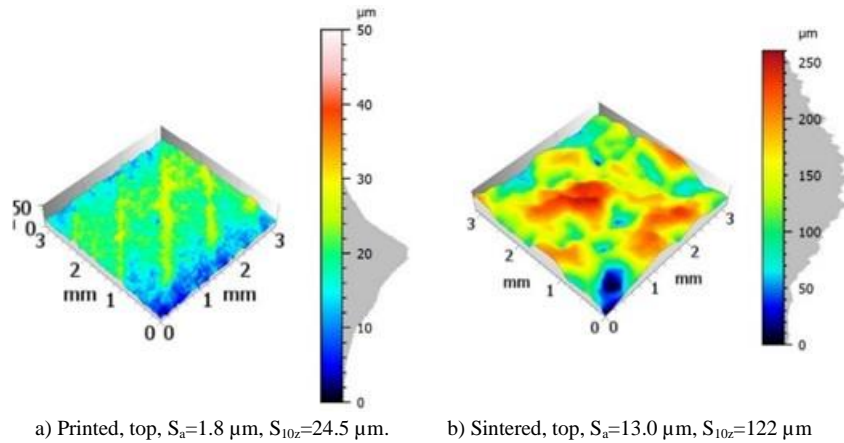
Figure 33. *Three-dimensional topography appearance of as FDM-3D printed and sintered TS-bars.* [134]

Figure 33 shows the 3D view of the surface topography of the as-built and sintered TS bars measured on top surfaces. The average roughness, Sa, and the ten-point height, S10z parameters were utilized to discriminate these measured surfaces. The Sa parameter provides the measure of the overall surface texture and S10z provides the measure of the average maximum height of the surface features. From the figure, it can be noticed that S_a=1.8 µm, and S_{10z}=24.5 µm for the as-built FDM part, it appears to be smoother due to the operation of ironing employed for producing the FDM parts. The ironing operator involves running the heated nozzle of the FDM printer repeatedly over the top surface and this removes the raster pattern smoothening the top surface layer. However, in reality, the ironing operator does not completely remove the raster pattern and this can be witnessed visually in Figure 33a. The sintered tensile bars have a surface topography appearance similar to that of a sintered powder metallurgy metal surface. It can be noticed from Figure 33b that the surface roughness is higher with S_a=13.0 µm and S_{10z}=122 µm compared to the as-built conditions. The surface topography formation with high waviness may be due to the occurrence of thermal effects during the sintering process. At de-binding temperatures, the polymer material melts and evaporates causing imperfections on the sample surface. The 3D printing inaccuracies can lead to the formation of porosities during the sintering process. Additionally, the uneven metal powder distribution in the green parts can cause uneven shrinkages resulting in rough surfaces [135]. The inclusion of refractory materials on the top surface layer during an improper sintering cycle can also lead to an increase in surface roughness [136].

6.2.3 Multi-scale: Power Spectral Density (Paper 1)

This section presents paper 1 where Power Spectral Density (PSD) was utilized to discriminate the surfaces measured on a roughness calibration standard using various surface metrology instruments. The initial purpose of this paper was to assess the capability of the 3D SEM method for capturing complex AM surfaces, but it was first necessary to check the fidelity of these 3D SEM measurements with CSI before measuring the AM surfaces. With this study, it was understood that employing PSD could be very useful for the characterization of the multi-scale AM surfaces which was then introduced successfully to study the AM surfaces in paper 3. The

following section describes the use of PSD in the context of showing it as a powerful method for characterizing surface features.

Paper 1

In this paper, the surface topography of a roughness calibration standard was measured using Coherence Scanning Interferometer (CSI) and Scanning Electron Microscope (SEM). The CSI measurements formed the reference optical measurement to which the SEM measurements were compared. Typically, the SEM measurements provide false grey scale images mostly utilized for qualitative analysis, however, in this study 3D surface topography from SEM images was produced for comparison. This can be achieved by employing various algorithms (TA-Triangulation and PMF-Piazzesi Model Function) that allows the 3D reconstruction of SEM images captured at different viewing angles and PSD analysis was performed to assess the degree of fidelity of 3D SEM images.

The roughness calibration standard chosen for this purpose was anisotropic with a dominant texture in the Y direction as shown in Figure 34. The measurements were performed using CSI with 10X magnification with a lateral resolution of 1.1x1.3µm. The SEM measurements were performed at 150X magnification with a lateral resolution of 0.33µm and a field of view of 750x500µm was maintained for both measurements. One-dimensional PSD was plotted both along (X-direction) and across the lay or surface texture direction (Y-direction). For ease of comparison, the 3D SEM surfaces were resampled to match the CSI measurements, and PSD was plotted for each texture direction, as shown in Figure 35.
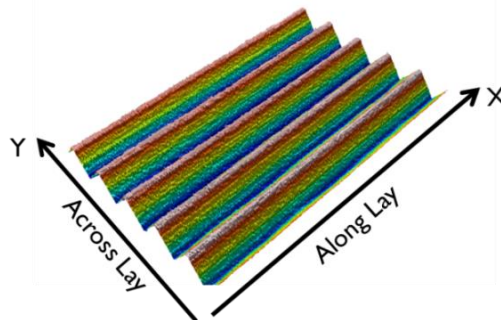
Figure 34. *The surface texture direction of the measured roughness calibration standard* [71]

It can be clearly witnessed from Figure 35a, that there is a huge difference between the CSI and 3D SEM (TA & PMF) measurements along the texture direction (X-direction). This may be caused due to the following reasons. Firstly, the 3D SEM reconstruction of the surfaces containing smaller amplitudes is often difficult and may require large tilt angles. Secondly, the disparity in the X-direction should theoretically be zero since the tilt angles were along the Y-direction. In reality, it is impossible to completely avoid the disparity in X-direction due to inaccuracies in tilting and matching images during reconstruction. Whereas, in Y-direction i.e. across the surface texture direction, the 3D SEM measurements had a very good replication of the reference roughness standard and were comparable to the CSI measurements as seen in Figure 35b. This is mostly due to the presence of dominant wavelength components which are usually quite easy to reconstruct. Therefore, for further analysis, the surface features belonging to the Y-direction were compared.
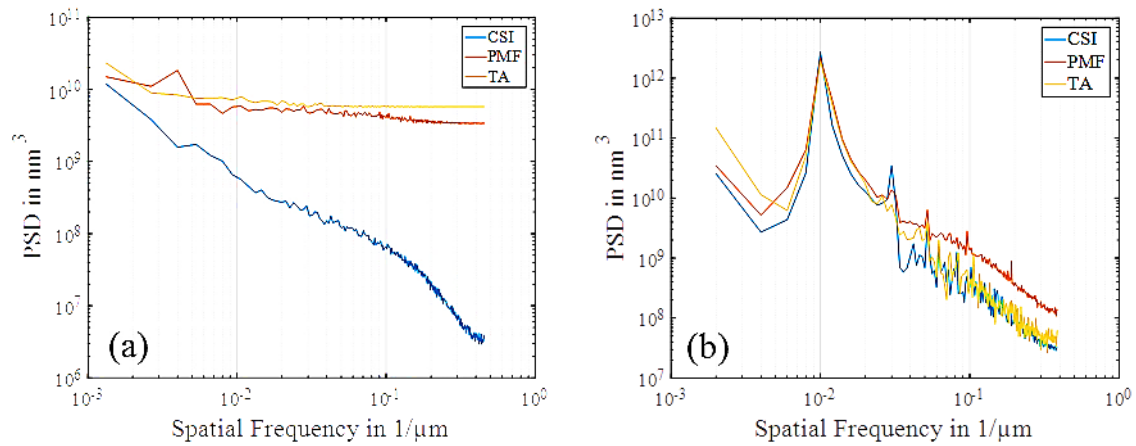
Figure 35. *One-dimensional averaged power spectral density plots in X (left) and Y (right) directions, performed on a roughness calibration standard.* [71]

To carry out the parametric analysis, the surfaces were filtered to remove the features in the X-direction. Figure 36 displays the surface topography of CSI and 3D SEM measurements representing the wavelength components in the Y-direction of the frequency spectrum. These surfaces were obtained after the application of the Fast Fourier Transform filter to the original surfaces with nesting indexes corresponding to the wavelength range in the X-direction of the frequency spectrum (2µm to 375µm). Figure 37 represents the residual surface after the filtration process mainly representing the wavelength components in the X-direction of the frequency spectrum.
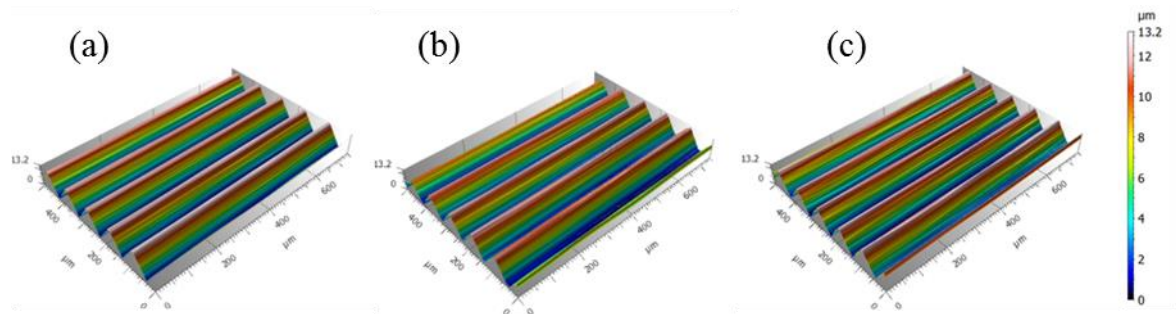
Figure 36. *Areal surface topography of (a) CSI; and reconstructed SEM images from (b) PMF and (c) TA considering only the dominant wavelength.* [71]
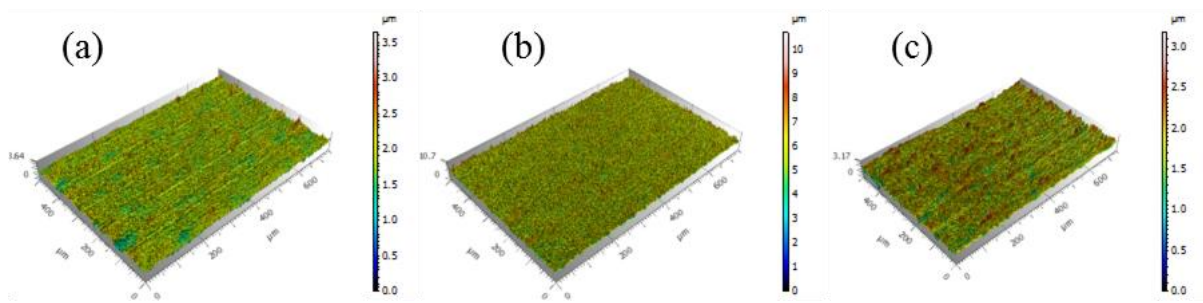
Figure 37. *Areal surface topography of the filtered residue of (a) CSI; and reconstructed SEM images from (b) PMF and (c) TA algorithms.* [71]

6.2.4 Multi-scale: Scale-sensitive fractal analysis (Paper 4)

The focus of this paper is to utilize area-scale analysis to characterize the surface topography of Laser-Based Powder Bed Fusion of Metals (PBF-LB/M) before and after the shot-blasting process. Additionally, this multi-scale approach helps in understanding the influence of geometrical design variations and shot-blasting behaviour on surface topography. To carry out the necessary analysis, the truncheon artefact was utilized with varying building inclinations as shown in Figure 38.
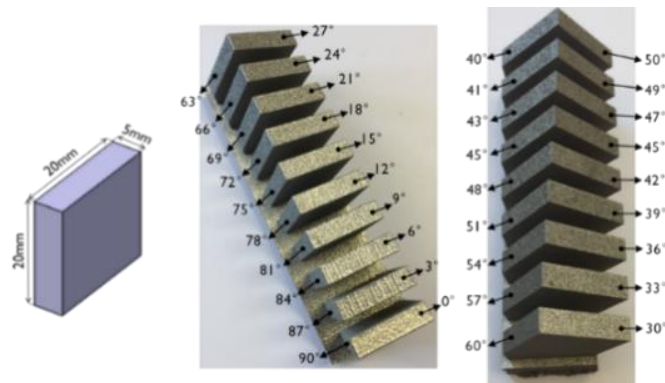
Figure 38. *Surface-specific artefact with varying build inclination* [40]

Two sets of surface test artefacts (truncheon artefact) made of 316L stainless steel material were produced using standard default settings in the EOS M290 metal AM machine with a layer thickness of 20µm. One set was subjected to post-processing by shot blasting while the other was retained in as-built conditions without any physical modifications. A confocal fusion optical microscope that combines both Confocal microscopy and Focus variation for imaging was utilized for capturing the surface topography of PBF-LB/M samples. The field of view was maintained at 2.5x2.5mm with a lateral resolution of 0.65µm. The captured images were refined to fill in the non-measured points, tilt errors were removed using the least squares method and the noise was eliminated using a denoising spatial filter with a window size of 5x5 pixels. It must be noted that surfaces of only a few selected build inclinations representing most of the surface conditions in the PBF-LB/M process were utilized for analysis.

Relative area analysis
The relative area plots of as-built and shot-blasted PBF-LB/M surfaces for various build inclinations are depicted in Figure 39. It can be witnessed from the plots that the relative area increases with the increase in spatial intricacy of surface texture. At larger scales, the relative area is close to unity because this region corresponds to the waviness of the measured surface comprising a smoother surface texture. At fine scales, the surface texture gets complex and rougher and the transition between the waviness to roughness is called smooth-rough crossover (SRC) [137]. It is clear from Figure 39a, that the surface topography can be easily discriminated from scales smaller than 10000 µm2 (SRC) for all the build inclinations. It is important to note that the magnitude of the relative area plot of the as-built surface is more than that of shot-blasted AM surfaces, indicating the extent of surface smoothening offered by the shot-blasting process. Furthermore, a clear pattern can be recognized in Figure 39a, the relative area increases with an increase in build inclinations up to a 15° build angle, beyond this the pattern diminishes. Also, a disparity in the relative area curves can be witnessed between 15° and 30° build angles. This is mainly because at lower build inclinations below 15°, the surfaces are influenced by the

stair-stepping effect and raster patterns with relatively low inclusions of powder particles. On the contrary, at higher build inclinations the surfaces are dominated by powder particles increasing the surface roughness. Due to this reason, the relative area values also increase, and it is especially pronounced at finer scales. This can be visualized in Figure 40a.
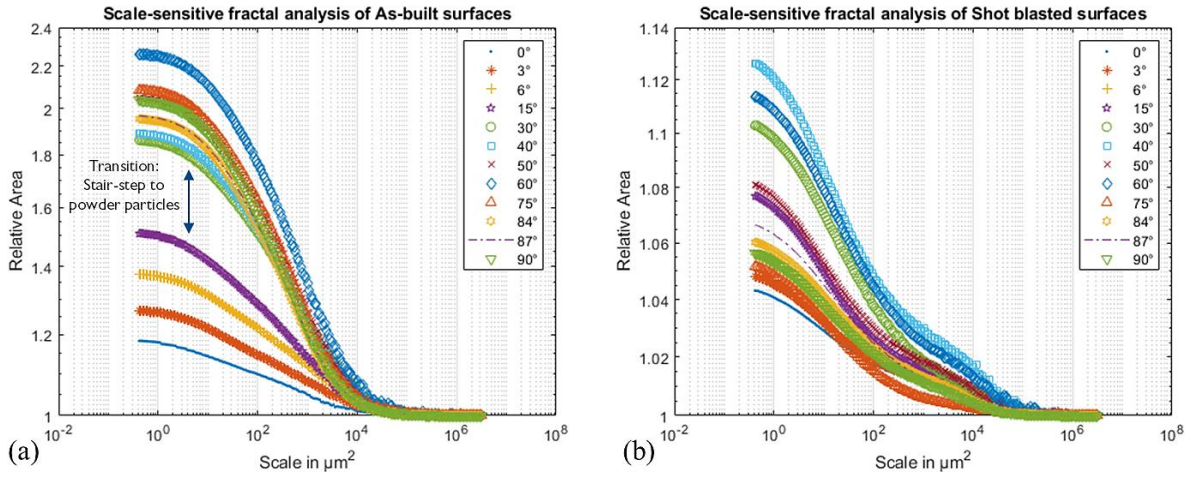
Figure 39. *The relative area plots of PBF-LB/M surfaces at various build inclinations (a) in as-built conditions and (b) in shot-blasted conditions* [40]

On the other hand, the relative area plot of shot-blasted surfaces does not exhibit a trend (see Figure 39b). This is due to the elimination of stair-stepping, raster patterns, and powder particles from the surface topography by the shot-blasting process, resulting in a relatively smooth surface texture as seen in Figure 40b.
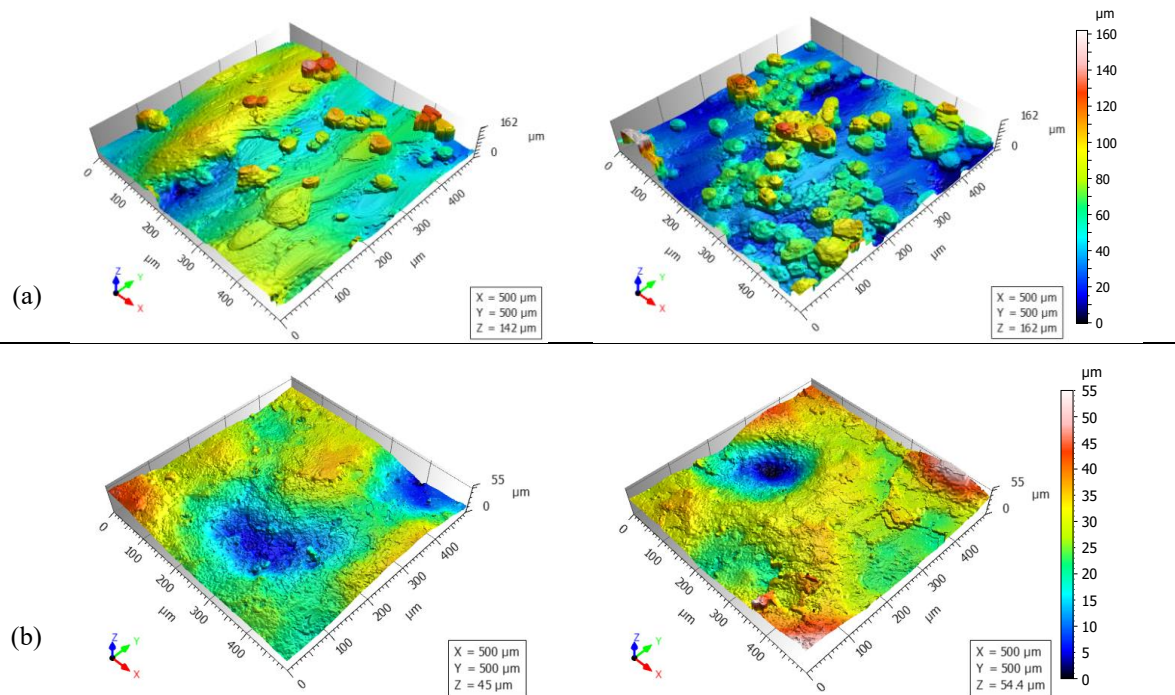
Figure 40. *Extracted surface topography of PBF-LBM sample at build inclination 15° and 30° for (a) as-built and (b) shot-blasted samples.* [40]

Complexity plots

The shot-blasting process not only eliminates the dominant features on the surface texture but also imparts new features due to the impact of abrasive media. This effect can be analyzed using the complexity plots. The complexity plot gives the rate of change of surface intricacy at each scale. Figure 41 shows the complexity plots of as-built and shot-blasted AM surfaces. It can be noticed that the complexity plots of as-built surfaces (see Figure 41a) contain a sharp peak representing the Scale of Maximum Fractal Complexity (SMFC). The SMFC varies slightly for different build inclinations, however, collectively for all the build inclinations the SMFC can be identified at approximately 600 µm² scale. From the SMFC value, a certain scale range can be identified that mostly represents the surface complexity scale. For as-built surfaces, the scales range from approx. 70 to 3000 µm² was selected which nearly contains the most complex features on the surface. Figure 42 displays the surface topography obtained for 3° and 60° after the application of the filter corresponding to the identified scale range. It can be noticed that within this scale range the most complex features comprising "stair-steps", raster patterns, and powder particles can be found.

Similarly, for the shot-blasted surfaces, the complexity curves contain two peaks and reach SMFC at approximately 10 µm². Although there are two peaks, the complexity of a surface is highest around the SMFC and so the scale range around it is considered important for analysis. Figure 43 shows the magnified image of the filtered surface per the identified scale range. It can be noticed that the shot-blasting process eliminated the "stair-steps" and other PBF-LB/M footprints and instead created new footprints from the shot-blasting process due to the impact of blasting media on surface texture. To conclude, SSFA allows the visualization of the surface topography at various scales and reveals important scales for analysis.
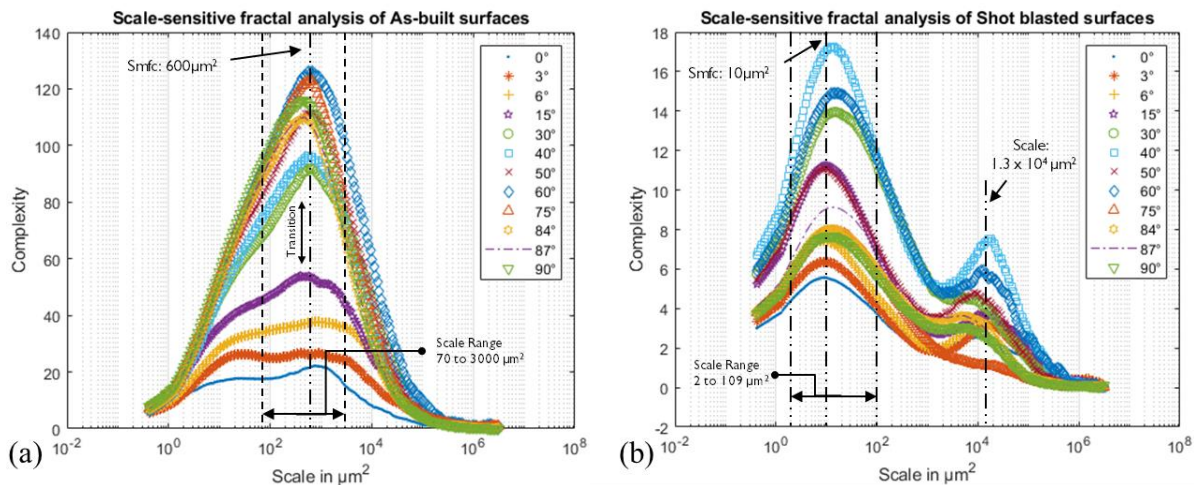
Figure 41. *Complexity plots of (a) as-built and (b) shot-blasted PBF-LBM surfaces at various build inclinations.* [40]
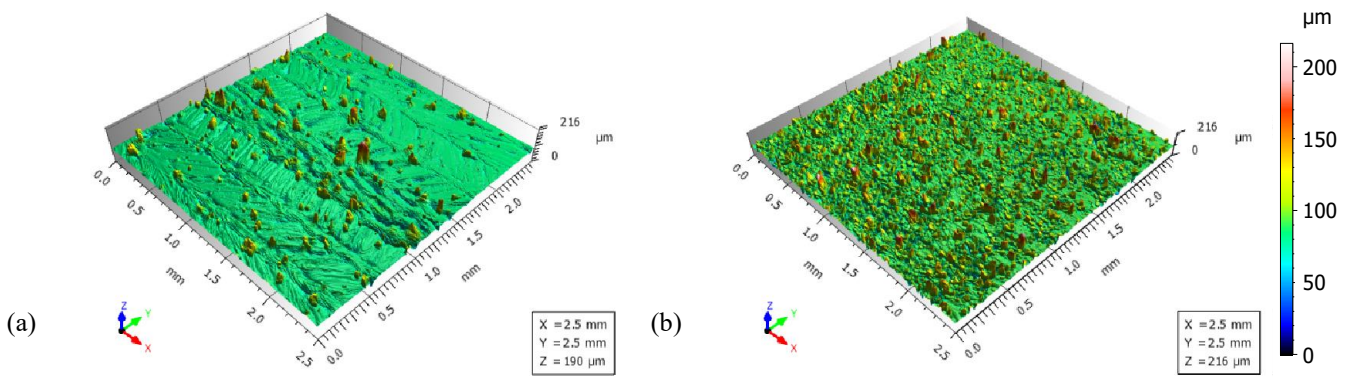
Figure 42. *3D surface view of as-built PBF-LBM samples at build inclination (a) 3° and (b) 60° after bandpass filtration with nesting indexes 12 and 77 μm.* [40]
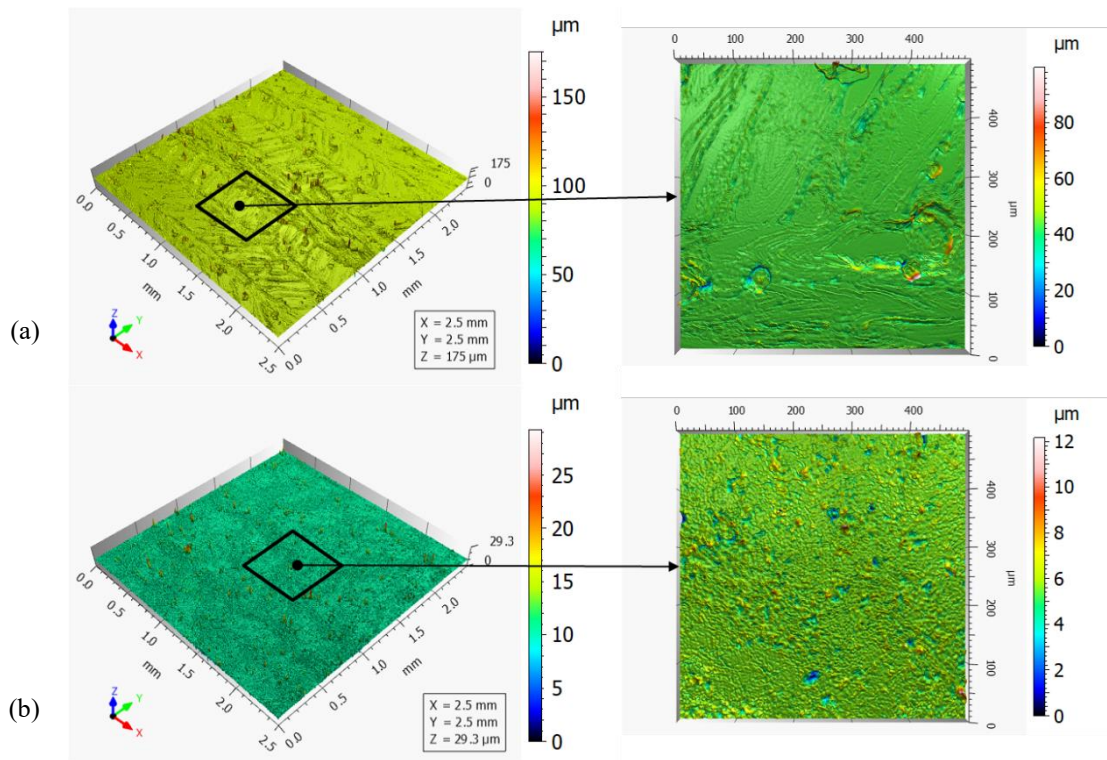
Figure 43. *3D surface topography view of bandpass filtered PBF-LBM sample with nesting indexes of 2 and 15μm at 3° build inclination (a) original as-built surface and (b) shot blasted surface.* [40]

6.2.5 Multi-scale: Feature-based characterization (Paper 2)

This paper focuses on presenting a novel characterization method to tackle the challenges of defining the complex surface topography of AM samples. For this reason, the surface topography of samples produced by the Laser Based Powder Bed Fusion of Metals (PBF-LB/M) process was utilized and the feature-based characterization method was selected for effective description of the surface quality. In this paper, surface-specific artefact or truncheon artefact was produced using 316L stainless steel material containing surfaces at various slopes ranging from angles 0° to 90° in steps of 3° increments as shown in Figure 44. The sample was manufactured using the EOS M290 SLM (Selective Laser Melting) system with a layer

thickness of 20µm and the rest of the print settings were kept in default mode. The stainless-steel powders were gas atomized with particle size distribution ranging from 20 to 53µm.
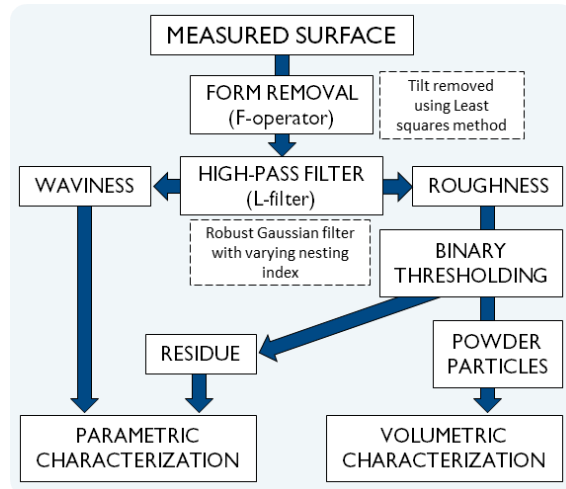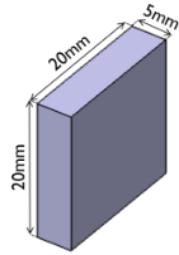
Figure 44. *Surface-specific artefact* [138]   **Figure 45.** *Feature-based characterization strategy* [138]

The areal surface topography of SLM samples was measured using a stylus profilometer and the captured surface was subjected to a string of operators as shown in the workflow strategy in Figure 45 and which is explained in the following paragraph.

The measured surface was first processed to remove the form and then a high-pass filter using the robust Gaussian method was utilized for removing the waviness. Since the measured surfaces vary due to the changes in build inclination, the nesting index chosen for the separation of waviness from roughness also varies. The value of the nesting index was chosen carefully based on the degree of accuracy of waviness separation and also to ensure that the roughness surface is as flat as possible for further processing. The next step involved using a binary thresholding operator to isolate the powder particles from the roughness surface by moving a cutting plane from the highest peak on the surface to the value of the material ratio corresponding to the Reduced summit parameter (Spk) [11]. This resulted in a surface map containing powder particles and the remaining surface was identified as a residual surface. It must be noted that this method only works efficiently well if the waviness surface has been effectively removed.

Figure 46 shows the segregated surface images after the application of the feature-based characterization method. The waviness (Figure 46b)on the SLM surfaces is mostly caused due two reasons i.e., the "stair-step" effect caused by the build inclination and due to the physical phenomena such as shrinkages or swelling effect that occurs due to thermal conditions during the fabrication process [108]. The roughness surface (Figure 46c) includes partially melted powder particles and other manufacturing footprints. The roughness surface was further processed to separate the powder particles (Figure 46d) and residual surface (Figure 46e). The waviness and the residual surfaces were subjected to areal surface topography characterization as per ISO 25178-2 [89] and powder particles were characterized volumetrically.
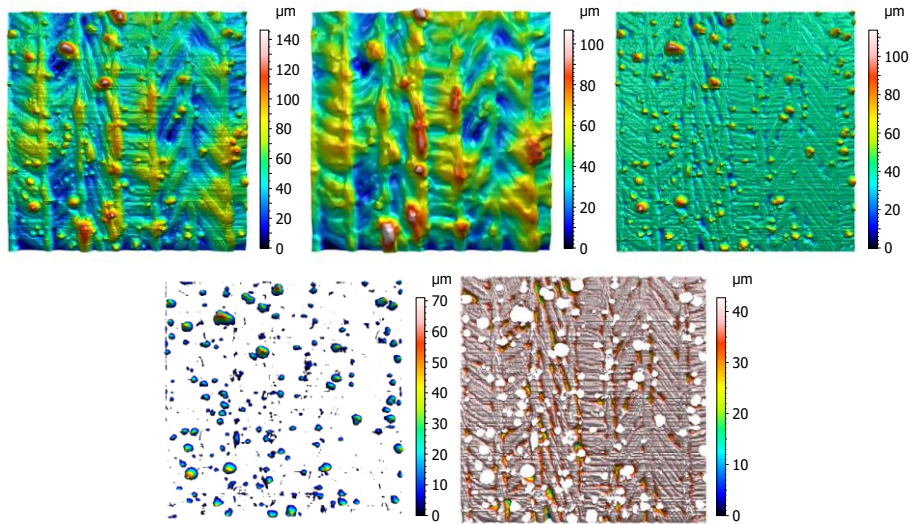
Figure 46. Segregation of powder particles and staircase effect by applying the Robust Gaussian filter. (a) Original surface (b) Waviness surface (c) Roughness surface (d) Powder particles (e) Residual surface. The measurement area of the captured surface is 2.5 x 2.5 mm. [138]

It is evident from Figure 47, that the average roughness of as-built SLM surfaces (Sa – original) increases with an increase in build inclination, which contradicts the model first developed by Reeves and Cobb to predict the average roughness values for AM process [139]. Equation (2) presents a model where the average roughness is a function of layer-thickness (Lt) and build inclination (α). This model was developed to mainly account for the "stair-steps" formation that depends on the layer thickness and build inclination.

$$Ra = \frac{Lt}{4} cos\alpha \tag{2}$$

After the application of the feature-based characterization methodology, the average roughness of the extracted waviness surface (Sa – waviness) has a trend similar to model roughness (Ra – model) implying the presence of a "stair-step" effect and it decreases with an increase in build inclination. From this analysis, it can be understood that the roughness values obtained from as-built conditions may be misleading in understanding the underlying mechanism involved in the SLM process. In an ideal situation, the parts built during the SLM process will have all of the powder particles fully melted leaving behind a surface similar to the extracted waviness surface. However, in reality, the SLM surface may contain partially melted powder particles, spattered powders, and adhered loose powder particles during its building process which contributes to increased roughness.

The presence of powder particles on the SLM surfaces increases with an increase in build inclination. Since the fabrication takes place in a powder bed, the contact between the surface and powder particles increases with an increase in slope angle (refer to section 2.1.1, Figure 5). It can be noticed by observing the volumetric curve in Figure 48. Furthermore, there is an inverse relationship between the residual surface roughness and the volume of powder particles present on the SLM surfaces. The higher the volume of the powder particles, the lower the roughness of the residual surface. An illustration of the deterministic-stochastic nature of AM surfaces can be witnessed in Figure 49. At lower build inclinations, the volume of powder particles is less and hence the residual roughness is more indicating the dominance of stair-step effect representing the deterministic nature. A transition takes place between 6° to 9° build

60

angles and from 9° to 15° powder particles start to dominate with a slight presence of stair-step effect, indicating the deterministic-stochastic nature. Beyond 15° build inclination, the method used in this study fails to recognize the residual surface since it is completely dominated by powder particles mostly signifying the stochastic nature of AM surfaces.
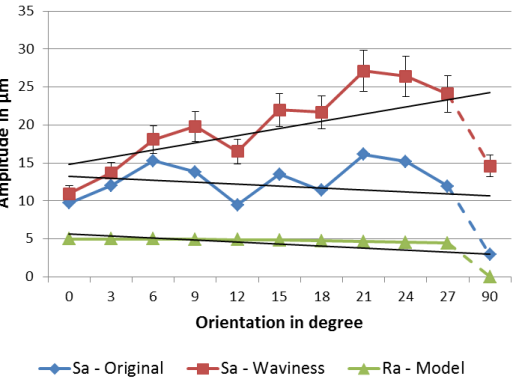
Figure 47. *Average roughness curve* [138]
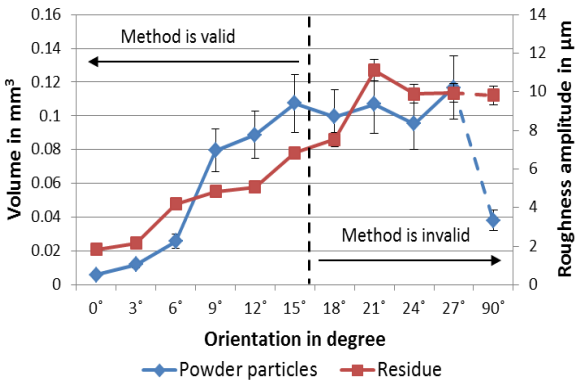
Figure 48. *Volume curve of the powder particles and Sa of residue plotted against the build orientation.* [138]
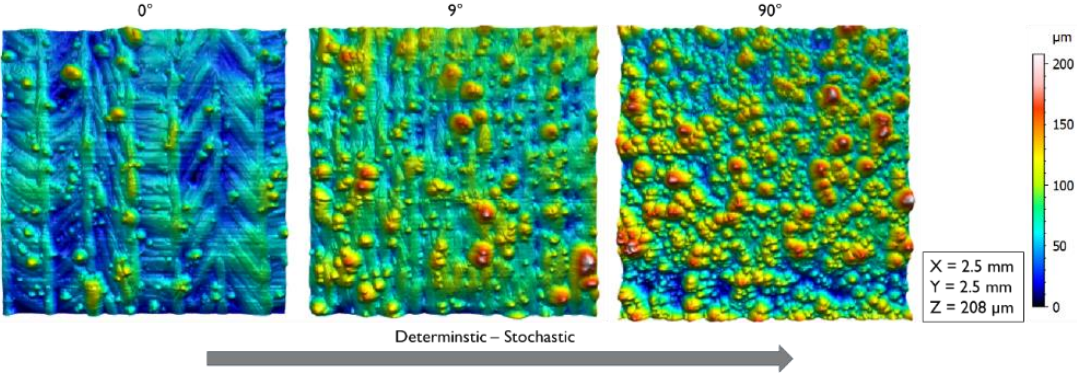
Figure 49. *Areal surface topography representation of SLM surfaces*

6.3   MANUFACTURING AND RESEARCH QUESTION 2

This section answers research question 2 by using the developed research methodology to identify the significant roughness parameters, thereby, providing a better interpretation of AM processes. For this purpose, papers 1, 4, and 5 were chosen. Paper 5 identifies significant parameters using a regression for scale-limited surfaces, and paper 1 and 4 establishes the significant parameters using PSD and SSFA respectively for multi-scale surfaces.

6.3.1 Identification of significant parameters using Regression (Paper 5)

In this paper, the focus is provided to understand the effect of the FDM process parameters on surface texture and identify significant profile parameters for characterizing FDM surfaces. Investigations were performed using a surface-specific artefact [130] with varying build inclination from 10° to 90° in steps of 10°. A design of experiments was formulated using Taguchi's orthogonal arrays [140] with factors containing mixed levels. The factors include layer thickness, print speed, and material infill. A stylus profilometer was utilized for retrieving quantitative profile measurements for analyzing the FDM surfaces. The 2D roughness parameters were obtained after processing each profile measurement to remove tilt errors using the least squares method, and waviness using the robust Gaussian filter. Linear regression was implemented to study the relationship between the profile parameters and the FDM process variables and also to identify the most significant profile parameters for characterization using the developed methodology (refer to section 5.2.4, Figure 25).

The results from the developed methodology using regression identified the Rp, Rv, Rz, Ra, RSm, Rdc, and Rpc as significant profile roughness parameters. The definition of all of these parameters is included in [92]. These parameters mostly describe the amplitude and spacing of geometrical features on the measured profile. These parameters except Rpc (Peak count) decrease with an increase in build inclination and increase with an increase in layer thickness. On the contrary, the material infill and print speed were found to have a negligible effect on the surface texture.

The formation of surface texture in the FDM process is in the form of "stair-steps" and "raster" patterns primarily due to the layer-by-layer process of building components [141][132]. As a result, the measurements made contain a wave-shaped profile which constitutes the roughness. Due to the nature of manufacturing, the amplitude and spacing of such wave-shaped profiles decrease with an increase in build inclination, thereby, increasing the number of "stair-steps". Conversely, an increase in layer thickness will increase the amplitude and spacing which reduces the number of "stair-steps". This behavior can be observed both qualitatively and quantitatively from the profile measurements, as shown in Figure 50 and Figure 51.
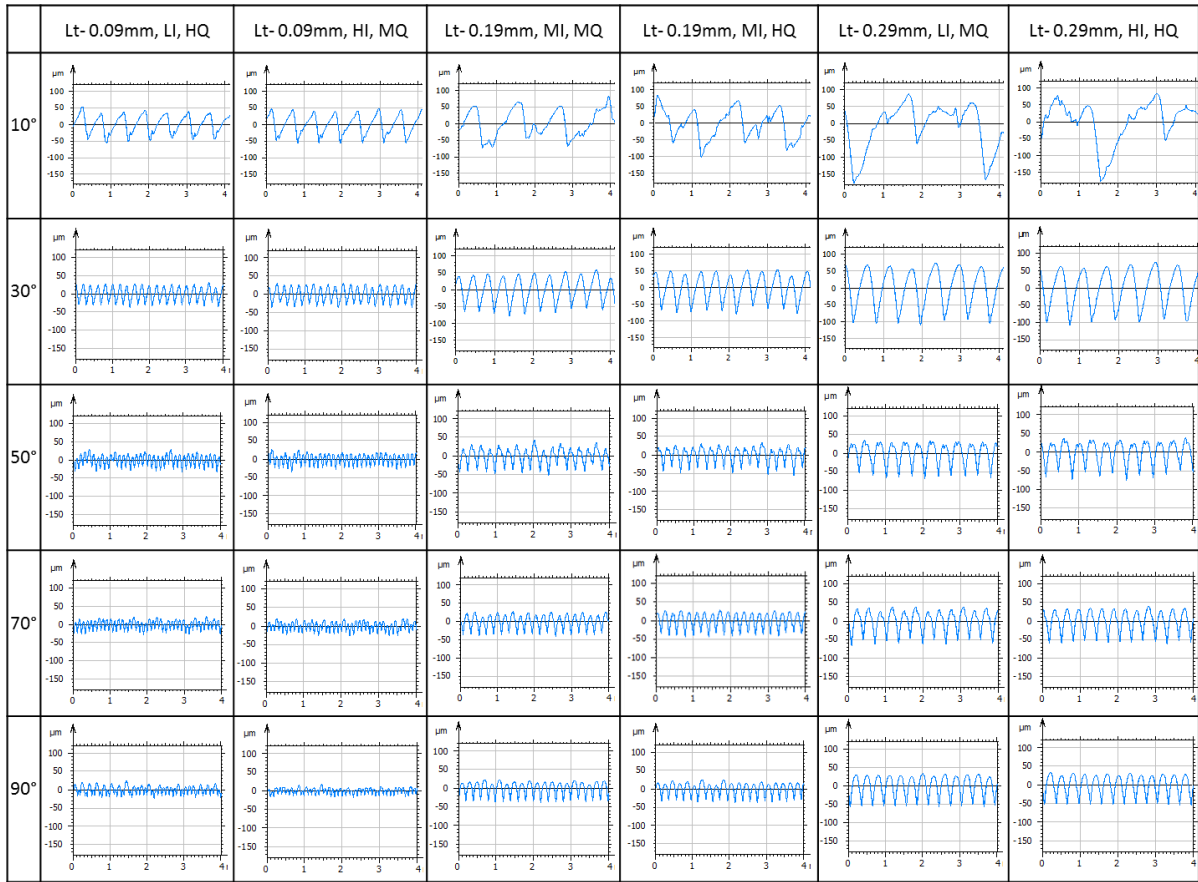
Figure 50. *Roughness profile measurements* [41]

Profile measurements provide surface roughness information in only one direction which can be insufficient in cases where the surface is anisotropic. The FDM surfaces are anisotropic since they have high directionality in their surface texture due to the nature of manufacturing in layers, however, the representative surface roughness of the FDM parts is usually obtained by measuring normal to the direction of its dominant texture. Hence, in the case of FDM, profile measurements may be sufficient to provide enough information for analysis. Nonetheless, measuring the areal surface texture could provide more information about other physical phenomena such as waviness due to shrinkages, material flow tracks, and other manufacturing footprints, which may be necessary for optimizing the process for surface quality. However, it must be noted that the occurrence of these phenomena is random since it depends on uncontrollable factors such as print temperature fluctuations, machine vibrations, environmental temperature, humidity, and so on. It does not fall under the current scope of research, however, the use of areal surface texture measurements could provide more accurate surface information for improving the accuracy of prediction, optimization, and control of surface quality.
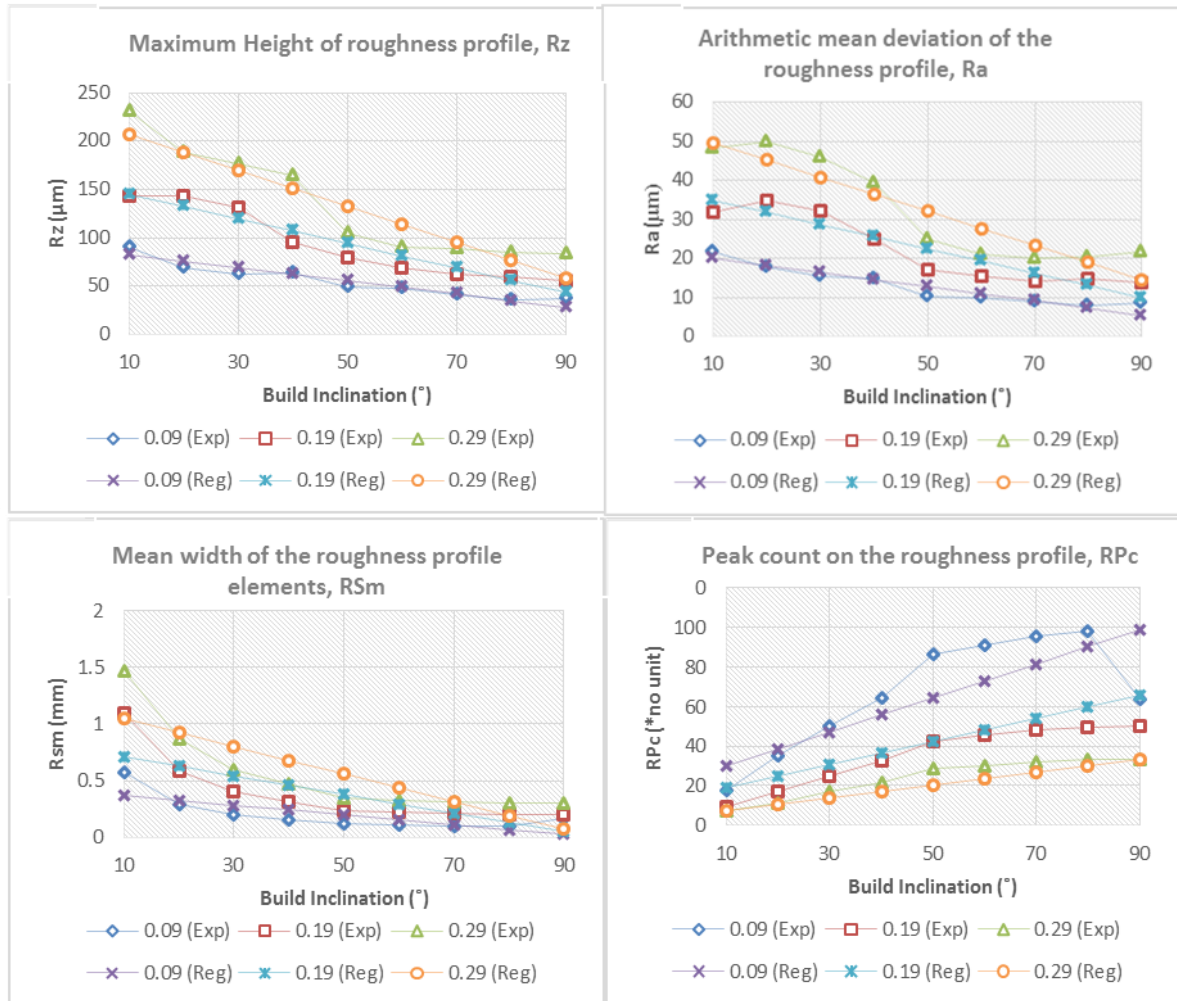
Figure 51. Mean and predicted values of significant- amplitude and spacing parameters. [41]

6.3.2 Identification of significant parameters using PSD (Paper 1)

Before proceeding towards discussing the results in paper 1, it is first necessary to state the relevance of this paper to research question 2 and Additive Manufacturing surfaces. This paper presents a method where the Power Spectral Density (PSD) was utilized to derive the most significant surface parameters by analyzing the frequency spectrum and identifying the crucial wavelength components representing the significant surface features required for analysis. This developed method is discussed in detail in section 5.2.4. This method was first tested in paper 1 using a reference standard sample to assess its capability and later implemented for identifying the crucial wavelength corresponding to important surface features for characterizing AM surfaces. The following passage describes this method used in paper 1.

In this paper, the focus was provided to gauge the fidelity of 3D reconstructed SEM images to the reference CSI measurements made on a roughness calibration standard. Power spectral density (PSD) was utilized for this purpose. The PSD analysis allows the possibility to identify the significant wavelength components comprising surface texture based on the research objective. In this paper, one-dimensional PSD in the Y-direction i.e. across the dominant surface texture was considered for analysis (see Figure 34) since the PSD curves for 3D SEM and CSI are similar in the Y-direction (see Figure 35). Hence, the surface features corresponding to the X-direction were filtered and the resulting surfaces were subjected to

characterization to understand not only the capabilities of surface metrology instruments but also to perceive the underlying mechanism of the surface creation process.

As per the methodology (refer to Figure 27), Table 4 displays the significant parameters that have a percentage difference between the original and filtered surfaces of less than 2% for both CSI and 3D SEM measurements. These significant or robust sets of parameters are insensitive to the micro surface texture in the X direction, this implies that these parameters can be utilized to characterize the 3D SEM surface directly without the need for filtration.

Table 4. Percentage difference between the original surface and the filtered surface for CSI and 3D reconstructed SEM. [71]

Parameter Group	Height							Functional			Spatial			Hybrid	
Parameters	Sq	Ssk	Sku	Sp	Sv	Sz	Sa	Smr	Smc	Sdc	Sal	Str	Std	Sdq	Sdr
CSI	0.3%	0.5%	0.7%	8.3%	6.1%	7.2%	0.2%	107.2%	0.6%	0.6%	0.1%	0.1%	0.1%	22.6%	40.9%
SEM(PMF)	1.8%	3.8%	4.2%	41.2%	52.3%	47.3%	1.4%	200.0%	0.1%	4.0%	0.6%	0.6%	0.8%	76.7%	138.7%
SEM(TA)	0.2%	1.0%	0.5%	0.8%	2.0%	1.4%	0.1%	0.9%	0.0%	0.5%	0.0%	0.0%	0.5%	13.1%	24.0%

Parameter Group	Volume						Feature								
Parameters	Vm	Vv	Vmp	Vmc	Vvc	Vvv	Spd	Spc	S10z	S5p	S5v	Sda	Sha	Sdv	Shv
CSI	1.4%	0.6%	1.4%	0.2%	0.6%	0.6%	200.0%	-	-	-	-	-	-	-	-
SEM(PMF)	36.5%	0.5%	36.5%	0.5%	0.1%	7.3%	199.7%	195.5%	-	-	-	190.5%	197.6%	158.7%	193.1%
SEM(TA)	2.5%	0.1%	2.5%	0.2%	0.0%	1.7%	171.4%	123.1%	-	-	-	-	78.1%	-	85.5%

■ Significant parameters	■ Parameters having a percentage difference of less than 2%

By definition, the average amplitude parameters, Sa and Sq describe the overall texture of the surface topography [11], and these parameters mostly depend on the large wavelength features. Due to this reason, these parameters were selected as significant since these parameters are insensitive to the variations of the short wavelength high frequency features present along the texture direction in the X axis (See Figure 34). On the other hand, maximum amplitude parameters such as Sz, Sp, and Sv that depend on the extreme points on the measured surface were found to be insignificant since the micro surface features in the X direction can influence these parameters. However, it must be noted that these parameters for the Triangulation Algorithm (TA) utilized for 3D SEM reconstruction appear to have a percentage difference less than the set threshold of 2% mainly because the surface features in the X direction have a very fine surface texture which does not largely affect the extreme points on the surface required for calculating the maximum amplitude parameters. Furthermore, the Kurtosis (Sku) and the Skewness (Ssk) parameters that describe the sharpness of peaks and symmetry of surface amplitude distributions can be unstable since these parameters have higher-order powers in their mathematical expression which make them very sensitive to the variations in the surface texture [11].

The Areal material ratio [], Smc parameter at material ratio p=10% provides bearing area height after removing 10% of the top layers or peaks of the surface. Hence, the micro-roughness features present along (X direction) the dominant wavelength does not influence this parameter

and therefore, it was obtained as significant. On the contrary, the Inverse material ratio [], Smr parameter returns a material ratio value at the default height of c=1μm beneath the highest peak. It is due to this reason this parameter is highly sensitive to the micro-roughness features in the X direction. Furthermore, the section height difference parameter [], Sdc (p=50%, q=97.5%) provides the material height after removing 50% and 2.5% of the peak and valley respectively. It was found to be significant for CSI and TA reconstructed SEM measurements, whereas, the opposite for the PMF-reconstructed SEM measurement since it has a relatively rougher texture (see Figure) along the X direction, making the Sdc parameter insignificant as it would necessitate the removal of additional layers in the valley region.
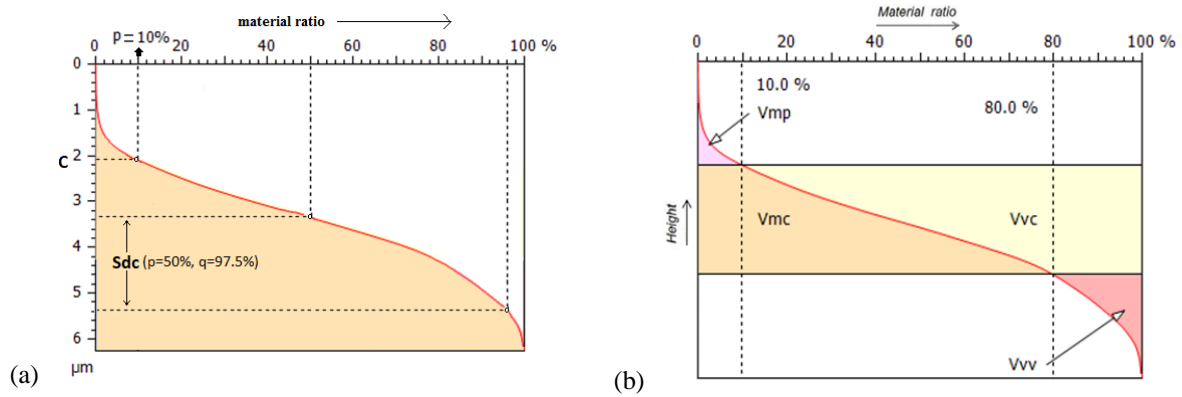
Figure 52. *(a) Material ratio curve and (b) the Volume curve of a surface.* [71]

From the above results, it can be understood that the surface features in the X direction tend to affect the parameters that depend on extreme points on the measured surface texture and have negligible influence on the average and core parameters. Hence, the volume parameters such as Void volume (Vv), Core material volume (Vmc), and Core void volume (Vmc) are significant and the Dale void volume (Vvv) and Peak material volume (Vm, Vmp) are insignificant.

Similarly, the auto-correlation length (Sal), Texture Aspect Ratio (Str), and Texture direction (Std), by definition depend on the large wavelength features of the surface and hence were obtained as significant. The hybrid and feature parameters are very sensitive to the variation of surface features in the X direction and hence excluded from the study.

6.3.3 Identification of significant parameters using SSFA (Paper 4)

This paper aims to utilize scale-sensitive fractal analysis through area-scale analysis to discriminate the PBF-LB/M surfaces before and after the shot-blasting process. Previously, in section 6.2.4, in paper 4, the relative area and complexity plots were utilized to individually interpret the AM surfaces, whereas, in this section, importance is given to simplifying this procedure by using a developed research method to identify the importance scales and significant parameters to then characterize the AM surface for enhancing understanding of the manufacturing process.

As per the methodology (refer to section 5.2.4, Figure 26), the identification of significant scales can be established by using the "transfer function" of a complexity plot. The "transfer function" is obtained by simply taking the ratio of complexity plots of as-built and shot-blasted surfaces for all build inclinations. The resulting graph describes the effects of the shot blasting process on the as-built surface conditions at each scale. Figure 53 represents the transfer function of the complexity plot which identifies three significant scale ranges for comparison. A significant

peak can be observed at the mid-scale range, this suggests that there is a huge disparity between the as-built and shot-blasted surfaces. At a finer scale range, the complexity values in the "transfer function" plot reaches unity, indicating the similarity of the surface features in both as-built and shot-blasted conditions. At the higher scale range, it can be observed that the complexity values are close to unity and then varies chaotically at the highest scales. This is because both the as-built and shot-blasted surfaces are similar at scales that correspond to the waviness caused by the "stair-stepping" effect and raster patterns formed during the fabrication process. However, at the highest scales, the waviness due to thermal effects (shrinkages and swelling effect) occurs which vary randomly for various build inclinations. To further interpret the surface behaviour, visual and parametric characterization were considered.
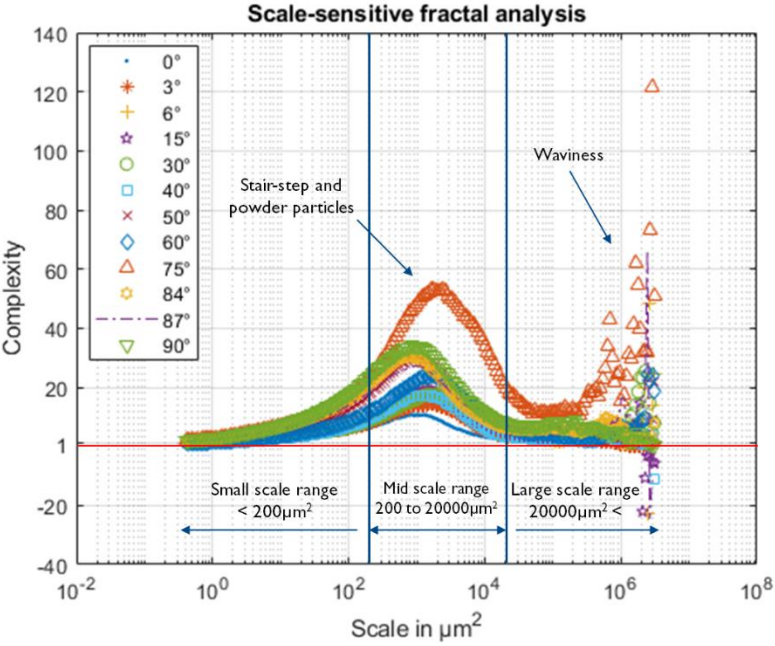
Figure 53. *The transfer function of the complexity plots of the PBF-LB/M surfaces at various build inclinations* [40]

The surfaces corresponding to the identified scale regions were filtered using a robust Gaussian filter. Figure 54 shows the filtered surfaces of both as-built and shot-blasted PBF-LB/M surfaces. It can be noticed visually that the highest difference in surface texture is in the mid-scale range compared to the other two scale ranges.
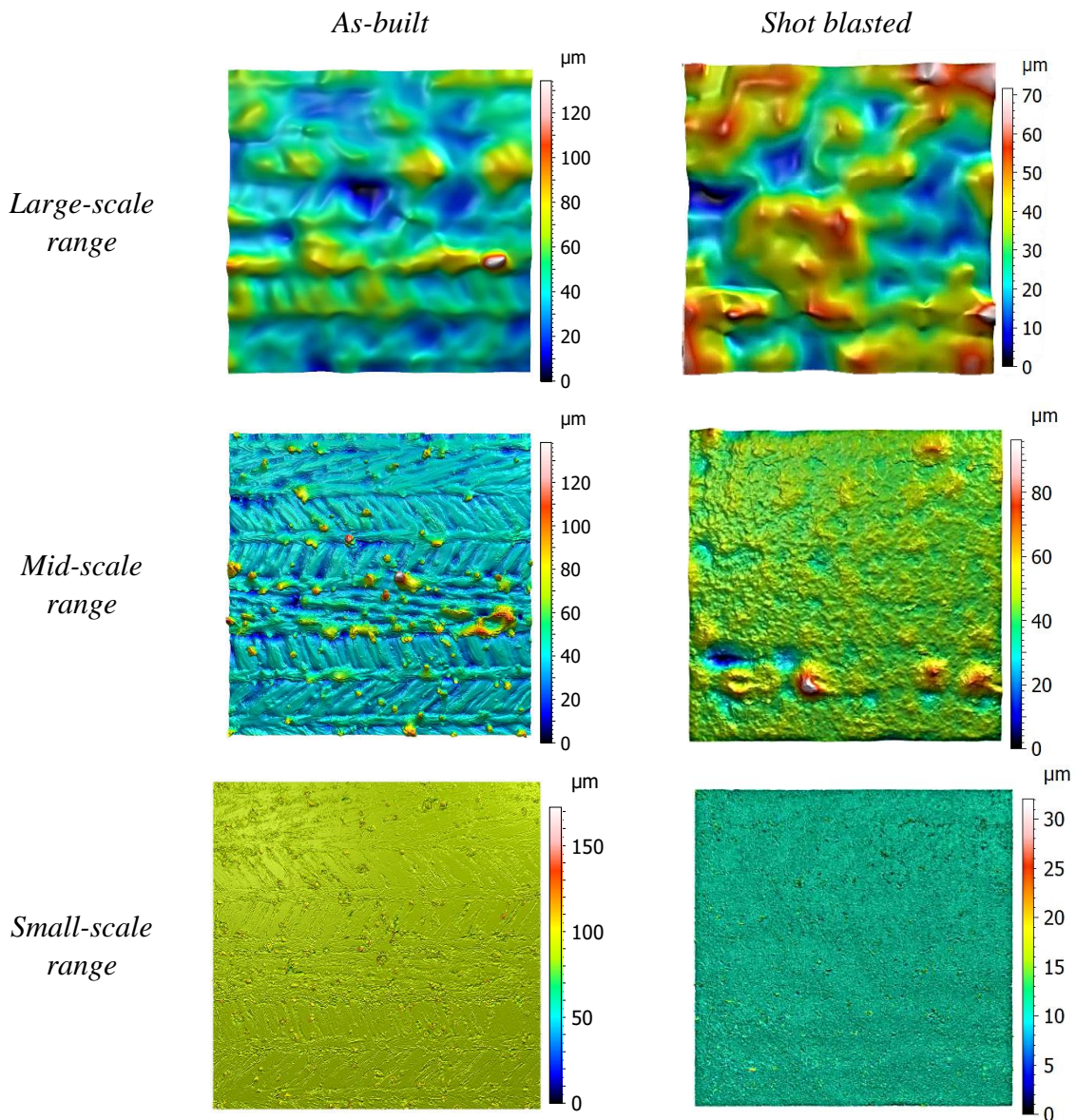
Figure 54. *Filtered surface topography of as-built and shot blasted sample at 3° build inclination for large, mid and small scale ranges. The measurement area was maintained at 2.5 x 2.5mm.* [40]

Furthermore, the methodology allows for identifying the significant parameters within the three important scale ranges. Figure 55 shows the coefficient of determination for areal surface texture parameters at each scale. This was obtained by linearly regressing the complexity values to the values of each surface parameter at each scale. A threshold was set at 70% implying that any parameter within the identified scale range has a coefficient of determination higher than the threshold was selected as the significant parameter. The parameters such as Sa, Sq, Smc, Vmc, Vvc, and Vv have a high correlation within the large-scale ranges, implying that these parameters mostly depend on the waviness surfaces, and parameters such as Sdr, Sdq, Sal, and Str have a high correlation in the small and mid-scale ranges. These significant parameters were utilized to compare the filtered surface as per the identified scales.
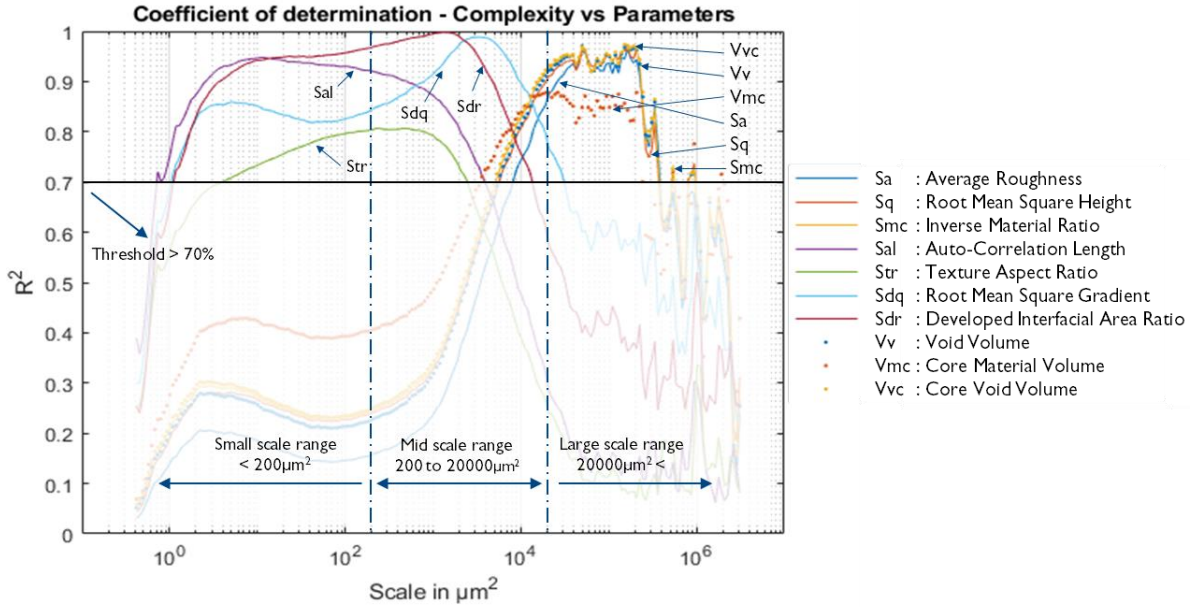
Figure 55. *The coefficient of determination (R²) of significant parameters was obtained by taking correlations between the complexity values and areal surface texture parameters at every scale.* [40]

From the developed methodology using the SSFA technique, it can be understood that:

- The shot blasting method as shown in Figure 54, has a negligible effect on surface features corresponding to the largest scales because it is unable to effectively eliminate the waviness. As a result, the waviness surfaces of both as-built and shot-blasted samples are identical, as indicated by the Sa values in Figure 56a. Shot blasting may not be a viable option for finishing products for high-precision applications. Sa is inversely proportional to build inclination and is highest at build inclinations lower than 15°. Hence, it is advised to avoid orienting the object with these build angles.

- At intermediate scales, the hybrid parameter (Sdr) that provides the perception of surface complexity has a positive correlation with the build inclination for as-built surface conditions (see Figure 56b). This is because the Sdr parameter is influenced by the powder particles which increases with an increase in build inclinations. On the contrary, the shot-blasting eliminates the stair-step, raster pattern, and powder particles (see Figure 54, mid-scale range), hence, the Sdr parameter value is mostly constant for all the build inclinations. However, as-built surfaces at lower build inclinations may not require as much blasting as those at higher build inclinations. Blasting time can be adjusted for different surfaces to achieve optimal results.

- At finer scales, a slight anisotropic property can be observed on the as-built surfaces at lower build inclinations, however, it is entirely eliminated by the blasting process since the shot-blasted surfaces exhibit high isotropic properties for all the build inclinations. Visually, the effects of shot-blasting owing to the abrasive action at finer scales are apparent (see Figure 54, small-scale range), but parametrically, there is no substantial change.

69
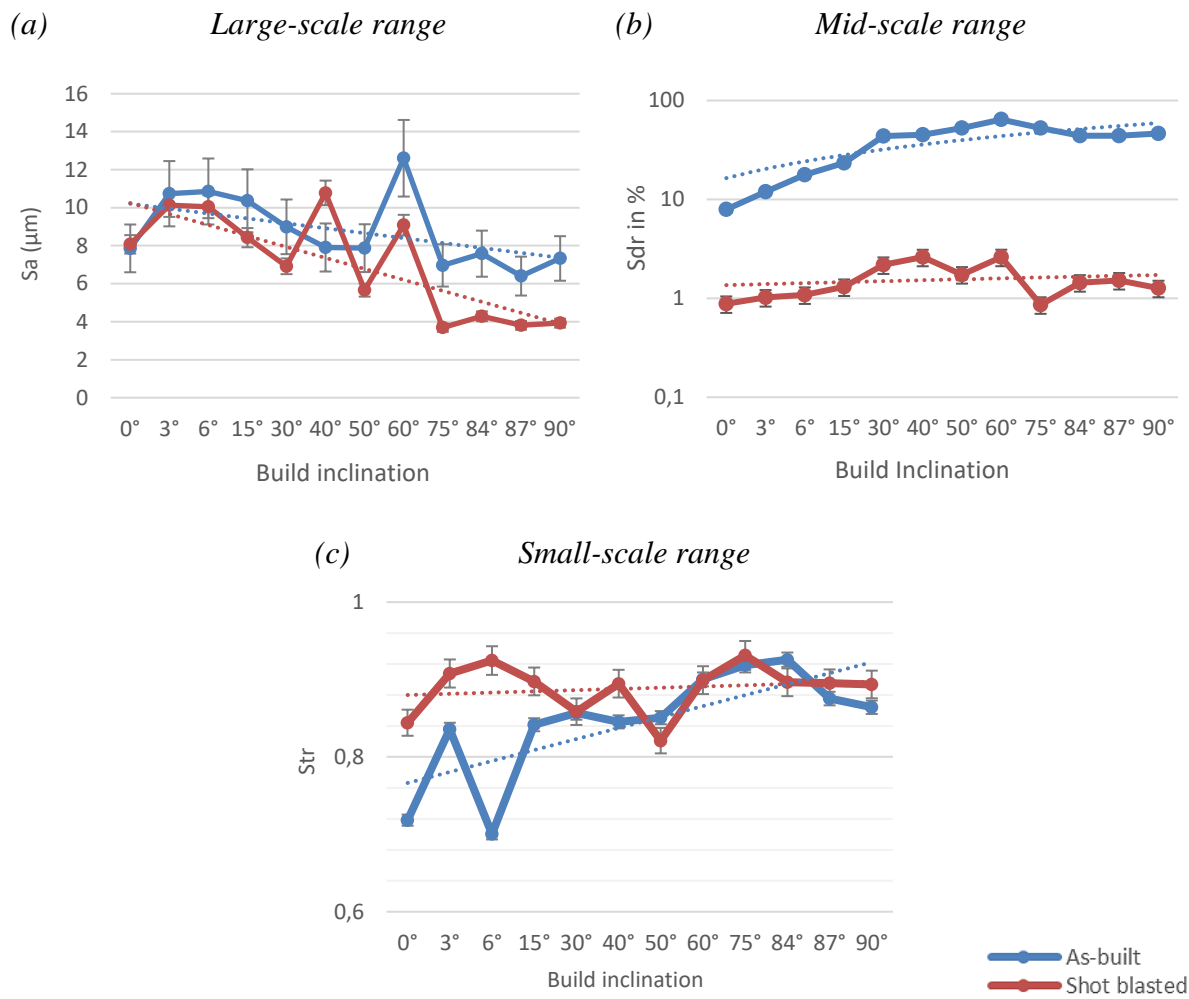
Figure 56. *Variation of selected significant parameters concerning build inclination in corresponding scale ranges.* [40]

6.4   FUNCTION AND RESEARCH QUESTION 3

This section tackles the third research question by using the regression method as a means of predicting and optimizing the manufacturing process to achieve the required surface function. It is important to establish the relationship between the process control variables and the surface topography and once it is established then it can be conveniently optimized to achieve the required function. Hence, the focus is mostly provided to establish this relationship required for optimization.

6.4.1 Process optimization using regression (Paper 3)

In this paper, multiple linear regression was utilized to obtain the relationship between the post-processing settings and surface topography of FDM parts. As previously mentioned, three post-processing methods namely Acetone Vapour Deposition (AVD), Laser-assisted finishing (LAF), and Shot-blasting (SB) were utilized to finish the surface as per the industrial requirement. However, only the LAF process is selected for illustrating the process prediction and optimization.

The surface test artefact (truncheon artefact) was utilized for analysis as it provides the roughness information at various build inclinations. Table 5 displays the design of experiments (DOE) based on Taguchi's orthogonal array for the LAF process. The number of truncheon artefacts required for analysis depends on the number of experimental units in the DOE.

Table 5. *Design of experiments 3^3 Taguchi's orthogonal array.* [44]

No. of Experiments	Laser-Assisted Finishing		
	Laser power in %	Laser speed in %	Resolution (PPI)
1	60	50	500
2	80	65	500
3	100	80	500
4	60	65	750
5	80	80	750
6	100	50	750
7	60	80	1000
8	80	50	1000
9	100	65	1000

The experiments were performed as per the DOE and the surface topography was captured and the profile roughness parameters were noted. The variables in DOE formed the independent variables upon which the dependent variables i.e. roughness parameters depend. The relationship between these variables was retrieved by performing ANOVA. As per the regression methodology (refer to section 5.2.4, Figure 25), Table 6 reveals the ANOVA results for profile parameters that have the highest adjusted R values with a significance F having a p-value less than 0.05 for a confidence interval of 95%. For ease of analysis, the Rp, Maximum peak height parameter was chosen as a significant parameter for assessing the surface quality

obtained from the LAF process. From the p-statistics in Table 6, it can be understood that all of the LAF process variables (Laser speed, Laser power, and Resolution) including build inclination have a considerable effect on the Rp parameter since the p-values are less than 0.05.

Furthermore, by observing the ANOVA coefficients obtained for the Rp parameter in Table 7, a linear regression model can be formulated to predict its value. The linear prediction model is based on the equation

$$Rp = 17.264 - 0.265BI - 0.087LP + 0.189LS + 0.0067R \qquad (3)$$

Where, BI – Build Inclination, LP – Laser Power, LS – Laser Speed, and R – Resolution.

From the coefficients obtained from ANOVA, the value of Rp decreases with an increase in build inclination and laser power due to the negative sign associated with its coefficients and similarly, Rp increases with an increase in Laser speed and Resolution due to the positive coefficients. As per the functional requirement, Rp parameter values can be varied by inserting various values of independent variables using this equation. However, it must be noted that the accuracy of the prediction depends on the chosen model. In this context, the degree of prediction can be poor due to the use of a linear model, and adjusted R values will determine the accuracy of prediction. As a future step, it may be necessary to utilize complex models and they can be trained using machine learning for improved prediction and optimization.

Table 6. *ANOVA results from Laser-Assisted Finishing* [44]

2D parameters	Description	Adj. R²	Sig. F	P-value			
				Build Inclination	Laser Speed	Laser Power	Resolution
Rp	Maximum peak height	56%	9.69E-72	1.71E-66	5.68E-12	1.61E-05	3.30E-05
Rv	Maximum valley depth	55%	4.38E-68	1.87E-48	6.25E-21	4.07E-17	8.30E-08
Rz	Maximum Height	58%	1.16E-74	1.42E-61	1.62E-18	1.92E-12	2.99E-07
Rdq	Root-mean-square slope of the roughness profile.	58%	4.6E-74	2.5E-09	4.8E-38	1.3E-40	1.9E-18
Rdc	Section Height difference	51%	9.65E-62	4.37E-48	1.03E-16	2.23E-12	2.50E-05

Table 7. *ANOVA coefficients for the selected parameter Rp* [44]

Intercept	Build Inclination (BI in °)	Laser Power (LP in%)	Laser Speed (LS in %)	Resolution (R in PPI)
17.264	-0.265	-0.087	0.189	0.0067

6.5   VALIDATION AND RESEARCH QUESTION 4

This section addresses the final research question by gathering relevant appended papers that provide use cases from industries and dentistry to test the characterization approaches in practice. Paper 3 presents a use case from the industry and paper 7 presents a dental application.

6.5.1 Industrial use-case (Paper 3)

In the previous section, paper 3 was introduced where the focus was to find the best finishing process to achieve surface properties close to that of the injection molding process. For this purpose, various post-processing methods with different settings were tested and two-dimensional profile roughness parameters were utilized for characterization. Statistical data analysis through regression helped in identifying the most significant parameters and also in establishing the relationship between the various post-process settings and the surface topography of FDM parts. Finally, after thorough experimentation and analysis, the best post-processing methods and ideal process settings were identified, and also it was realized that the combination of post-processing methods worked the best both in terms of surface finish and aesthetic properties.

In this section, an excerpt from paper 3 is presented where the results from regression were implemented on an industrial product. The TylöHelo sauna product (see Figure 58d), was originally produced using the injection moulding process, and hence, it was taken as a reference object to which the 3D printed and post-processed sauna products were compared. The identified best post-processing methods and settings from regression analysis were implemented on the 3D printed industrial product and the surface topography of these products was measured and PSD was plotted as shown in Figure 57. This figure displays the PSD curves for as-built FDM surfaces, post-processed surfaces, and the reference industrial product surface for comparison.
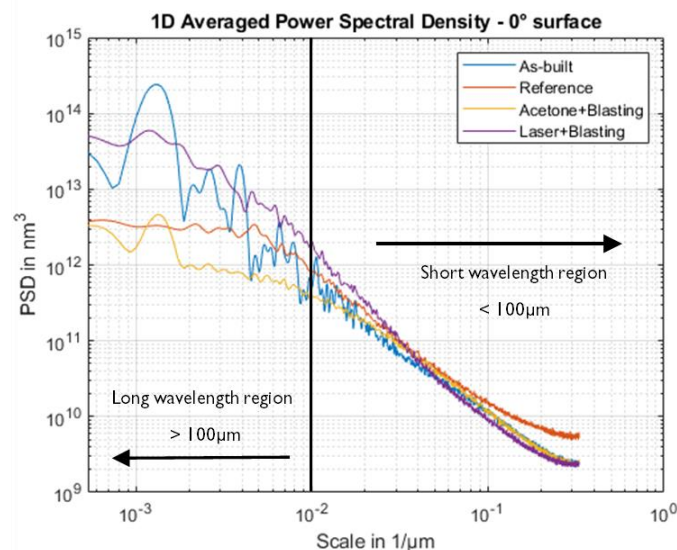
***Figure 57.** One dimensional averaged power spectral density of As-built, Reference injection moulding, Acetone+Blasting, Laser+Blasting surfaces at 0° build inclination.* [44]

It can be witnessed that the features below the wavelength of 100µm are similar for all the surfaces since there are no significant deviations in this region. The most important difference

between the surfaces lies in the larger wavelength regions of the frequency spectrum. The surface features corresponding to wavelengths above 100µm are filtered to study the differences in detail. Figure 58 shows the TylöHelo sauna produced in as-built, reference injection moulding, and post-processes conditions along with the topography of original and filtered surfaces. It can be observed that acetone+blasted surfaces have a slightly better finish than the reference injection moulding samples. Laser+blasting processes have a surface finish closer to as-built conditions, however, the strong directionality of the as-built surface texture was completely removed. Also, the acetone utilized for smoothening the surface can only work with samples that are reactive to it, in other cases, the laser finishing process can be found beneficial.

TylöHelo corner knot	Unfiltered 0° surfaces	Filtered 0° surfaces
(a)	Sa = 15.7µm	(a) Sa = 14.3µm; Str = 0.129
(b)	Sa = 4.7µm	(b) Sa = 2.59µm; Str = 0.316
(c)	Sa = 14.2µm	(c) Sa = 12.0µm; Str = 0.951
(d)	Sa = 6.5µm	(d) Sa = 3.03µm; Str = 0.922
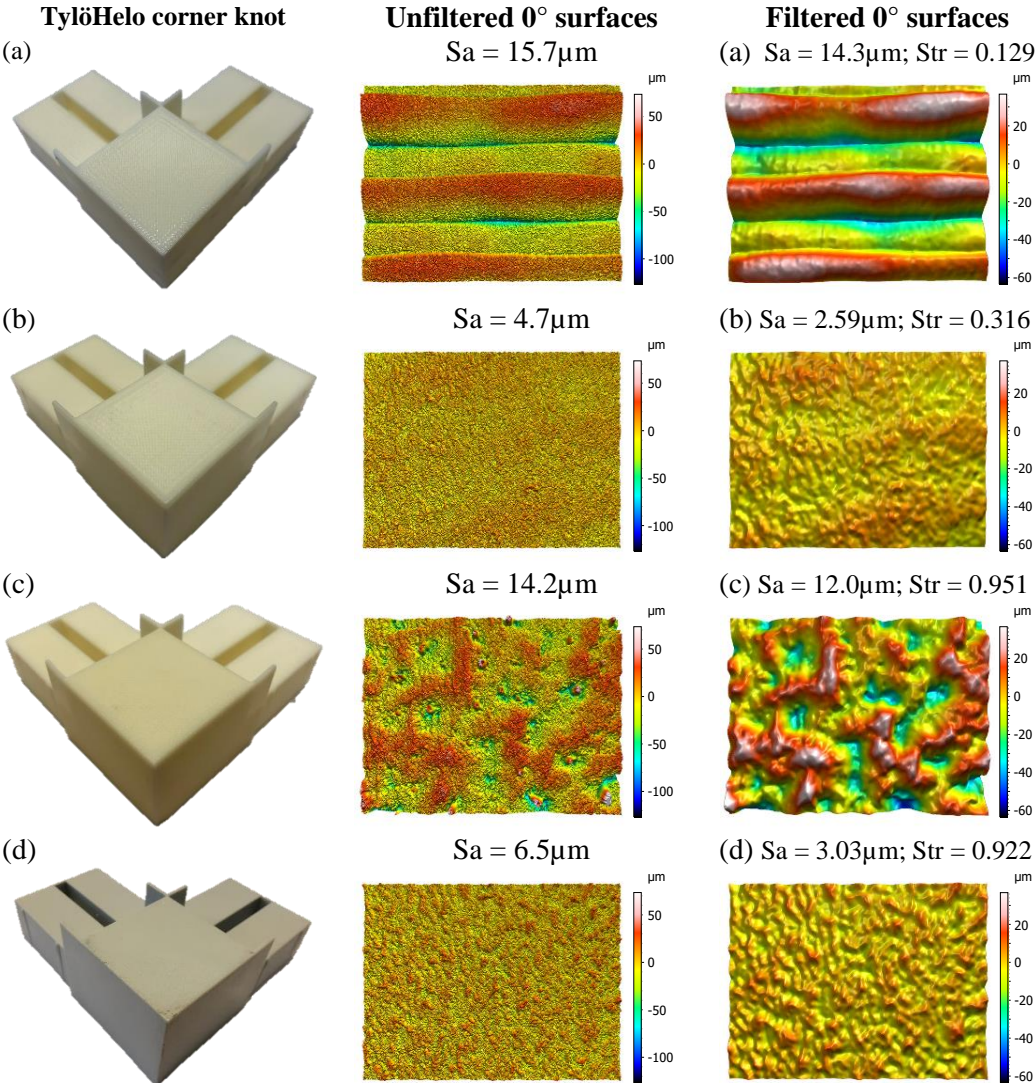
Figure 58. TylöHelo sauna corner knot with unfiltered and filtered surfaces (a) As-built FDM surface (b) Acetone + glass blasted surface (c) Laser + glass blasted surface (d) Reference injection moulding surface. The measurement area of the captured surfaces is 2.5 x 2.5mm. [44]

In conclusion, this paper provided a statistical tool (regression) for quick surface quality assessment and to visualize the effects of post-processing on surface texture. Based on the initial experimentation, the post-processing methods and their settings were optimized and validated by implementing them on an industrial product to get a good finish. Finally, an advanced

characterization tool through PSD was utilized to further analyze the surface quality of the end products.

6.5.2 Dental use-case (Paper 7)

The main focus of this paper is to provide a detailed part quality analysis in terms of surface topography, dimensional accuracy, and mechanical properties of Stereolithography (SLA) biocompatible materials required for Dental/Bio-medical applications. The analysis also includes investigating the produced SLA samples before and after the sterilization process (Autoclave steam sterilization). Finally, the knowledge gained during the experimentation is implemented on an actual dental sample utilized for animal testing and the results are compared with the reference control sample.

Several test artefacts are defined in the standard ISO/ASTM 52902:2019 [130] for assessing the geometric capability of AM systems. However, the criteria for selecting the test artefacts for analysis were dependent on the typical geometrical designs used for guided bone regeneration (Dental/bio-medical application) in animal testing as shown in Figure 59. Based on this design several geometrical artefacts were selected, however, in this context since the focus is solely on surface quality, the surface test artefact shown in Figure 60 was utilized for analysis
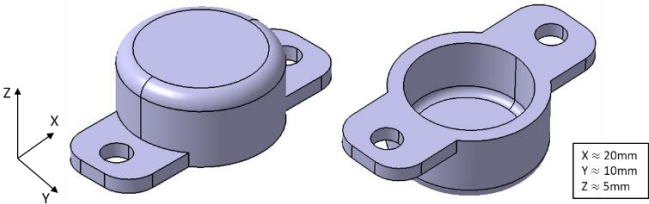
Figure 59. *The dental barrier typically used in animal testing for Guided Bone Regeneration (GBR). Image is taken from paper 7.*
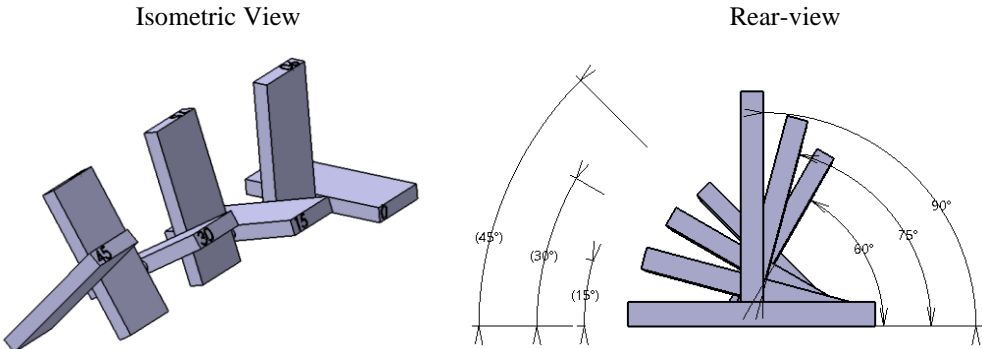
Figure 60. *Surface test artefact with varying build inclination from 0° to 90° in steps of 15°. Image is taken from paper 7.*

The surface test artefact [130] comprises seven flat tabs with different build inclinations ranging from 0° to 90° in steps of 15°. A total number of 5 surface test artefacts were produced to study the repeatability of the SLA printer and also to have statistically reliable results a total of 10 measurements were performed on each tab on each surface artefact at random locations on the up skin surfaces using the CSI microscope and summing up to 50 surface measurements on each build inclinations. The objective of 50X with a measurement area of 0.17x0.17mm and

lateral resolution of 0.17µm were utilized for studying the micro-roughness. The measured surface was processed to remove the form and waviness by the gaussian filtering method with the nesting index discussed in the following section.

Numerous studies have been conducted to identify the influence of the microroughness of dental implants and dental barriers on bone growth responses [142][143][144]. Most of the research has shown that there is a positive relationship between micro-surface roughness and hard tissue regeneration in dental applications. However, it is frequently found in the literature that exact roughness values that correspond to effective bone growth are difficult to identify. It is also important to note that apart from surface topography, other surface characteristics such as hydrophilicity, nano-roughness, and chemical bonding also influence bone growth [143]. Nevertheless, in this thesis, the focus is restricted to the influence of surface topography on bone regeneration.

Furthermore, Anderud et al. [145] utilized milled ceramic-based Zirconia and Hydroxyapatite dental barriers for analyzing bone formation in animal testing. These samples were measured and filtered using a gaussian method with a nesting index of 50µm. The results indicated that Zirconia material with moderately rough surfaces with a Sa value of 1.1±0.1µm and Sdr of 30±2% produced larger volumes of new bone compared to surfaces with smooth roughness less than 0.4µm. Hence, in this paper, Zirconia is utilized as a reference control for analyzing the surface roughness of SLA-based biocompatible material.

Figure 61. *The graphs of (a) Average roughness, Sa, and (b) Developed Interfacial Area Ratio, Sdr for various build inclinations. Measurements were obtained after removing the outliers and by applying a Gaussian filter with a 50µm nesting index. Graphs from paper 7.*

Figure 61 shows the Sa and Sdr values for SLA samples for various build inclinations along with the reference control values. The Sa parameter, average roughness provides a measure of overall surface texture, and Sdr is the developed interfacial area ratio which provides a measure of surface complexity [11]. It can be noticed that the AM surfaces differ with variations in build inclinations, and also the underlying mechanism of surface formation is different in AM compared to other traditional manufacturing processes. Hence, enforcing a Gaussian filter of 50 µm nesting index for SLA surfaces might not effectively remove the waviness, and therefore, for certain build inclinations, the Sa values exceed the control limit. On the contrary, the parameter Sdr has values less than the control implying that the surface topography of SLA samples appears to be less intricate than the Zirconia surfaces. It can also be observed from Figure 61, that the sterilization has minimal effect on the Sa parameter for all the build

inclinations, whereas, there is a significant effect on the Sdr parameter. The effect of sterilization on the surface topography of SLA parts can further be scrutinized by using the complexity "Transfer function" plot, shown in Figure 62.
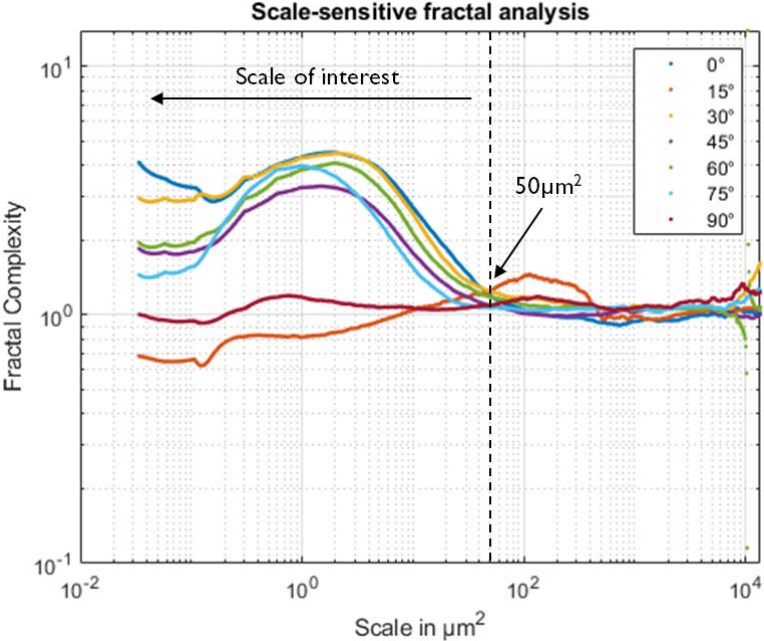
Figure 62. Transfer function plot depicting the effect of sterilization on the SLA samples. The image is taken from paper 7

The transfer function plot was obtained as per the methodology presented in section *5.2.4,* where the ratio of complexity plots of Unsterilized to Sterilized SLA surfaces was taken for all the build inclinations to determine the effect of sterilization. This ratio is close to unity if the as-built and sterilized surfaces are similar, a ratio greater than unity indicates the dominance of the sterilization effect and vice versa for ratios less than unity. It can be noticed from Figure 62, that there is a clear deviation in the fractal complexity for scales less than 50 μm^2. This implies that the Autoclave steam sterilization process effectively alters the micro surface topography features upon the application of heat and pressure. This effect can be visualized in Figure 63 and from the deviation in the Sdr parameter in Figure 61b.

(a) Sa = 0.5 and Sdr = 8.3%   (b) Sa = 0.5µm and Sdr = 3.2%
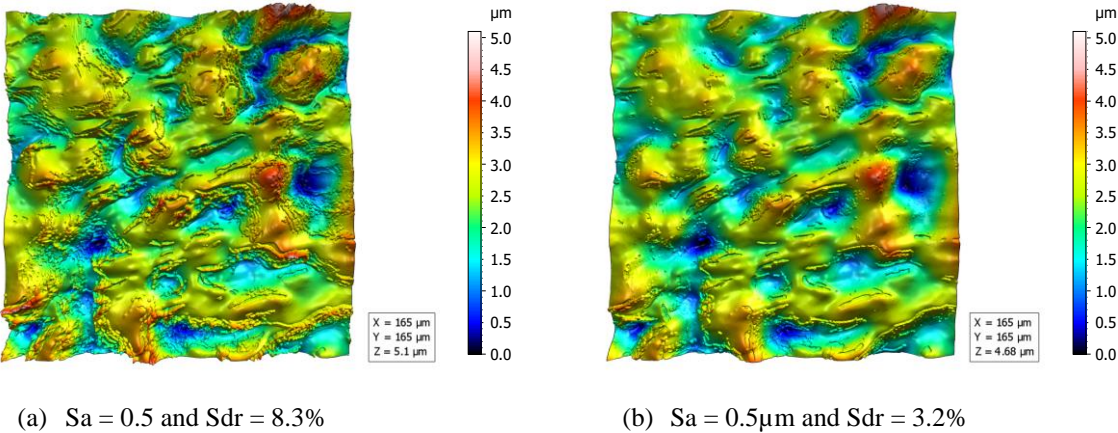
Figure 63. 3D view of relocated surface topography of SLA BioMED material at 0° build inclination in (a) Unsterilized and (b) Sterilized conditions. Surface topography was obtained after applying a Gaussian filter with a 50 µm nesting index. Images were taken from paper 7.

The surface features that correspond to scales higher than 50µm² remain unaffected by the sterilization process since the complexity curves are closer to unity. This implies that the region corresponding to the scales 50µm² and above can be termed waviness region since sterilization only affects the micro-roughness features. Thus by applying a gaussian filter with a nesting index of 10µm that corresponds to a 50µm² scale, waviness can be separated. Figure 64 shows the results after applying the gaussian filter. It can be noticed that the micro-roughness, Sa is well below the control limit, however, the Sdr parameter remains unchanged this is because the Sdr parameter is mostly defined by surface features at lower scales. As mentioned earlier, the literature points out that smooth surfaces having roughness values less than 0.4 often have low bone responses. It may be necessary to perform post-processing to achieve the required surface roughness for effective bone growth. However, further research is required to fully establish the correlation between bone responses and surface topography at various scales, to fully realize the relationship between them.
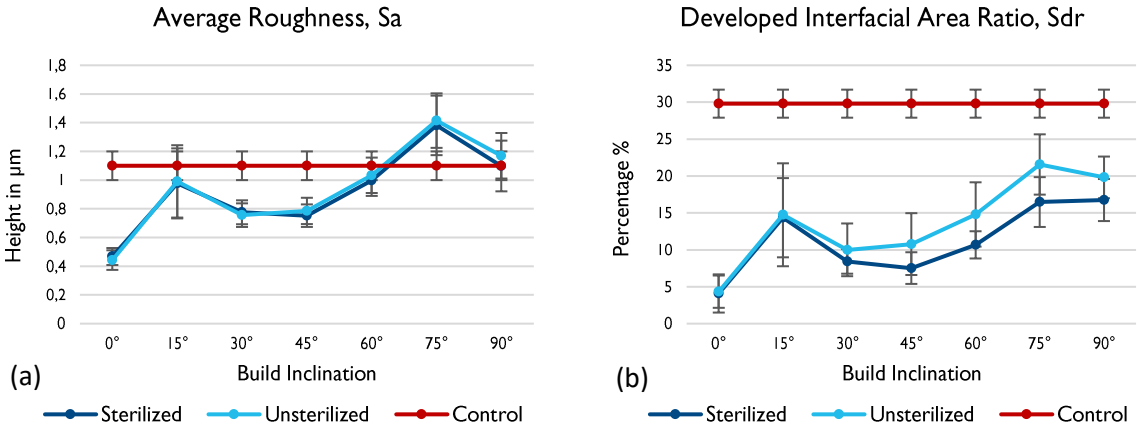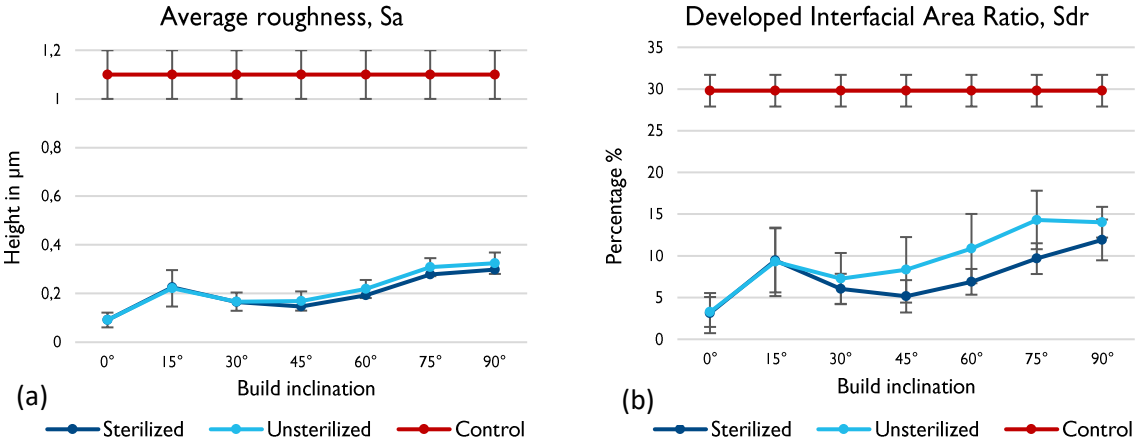

Figure 64. *The graphs of (a) Average roughness, Sa, and (b) Developed Interfacial Area Ratio, Sdr for various build inclinations. Measurements were obtained after removing the outliers and by applying a Gaussian filter with a 10µm nesting index as per the transfer function plot. Graphs are taken from paper 7.*

Validation of results using Dental barriers

In this section, the knowledge gained from the initial experimentation with the artefacts for assessing the surface topography quality is implemented in the actual dental barrier specimen utilized for animal testing. The surface analysis involved measuring the inner and wall surface topography of the printed SLA dental barriers before and after the sterilization process. Figure 65 displays the non-relocated surface images obtained from unsterilized and sterilized SLA samples. Figure 66 presents the Sa and Sdr values obtained after removing the outliers and by applying a Gaussian filter of 10µm nesting index. It can be noticed that these parameter values are well within the control limit, complying with the results obtained from initial experimentation on the test artefacts.
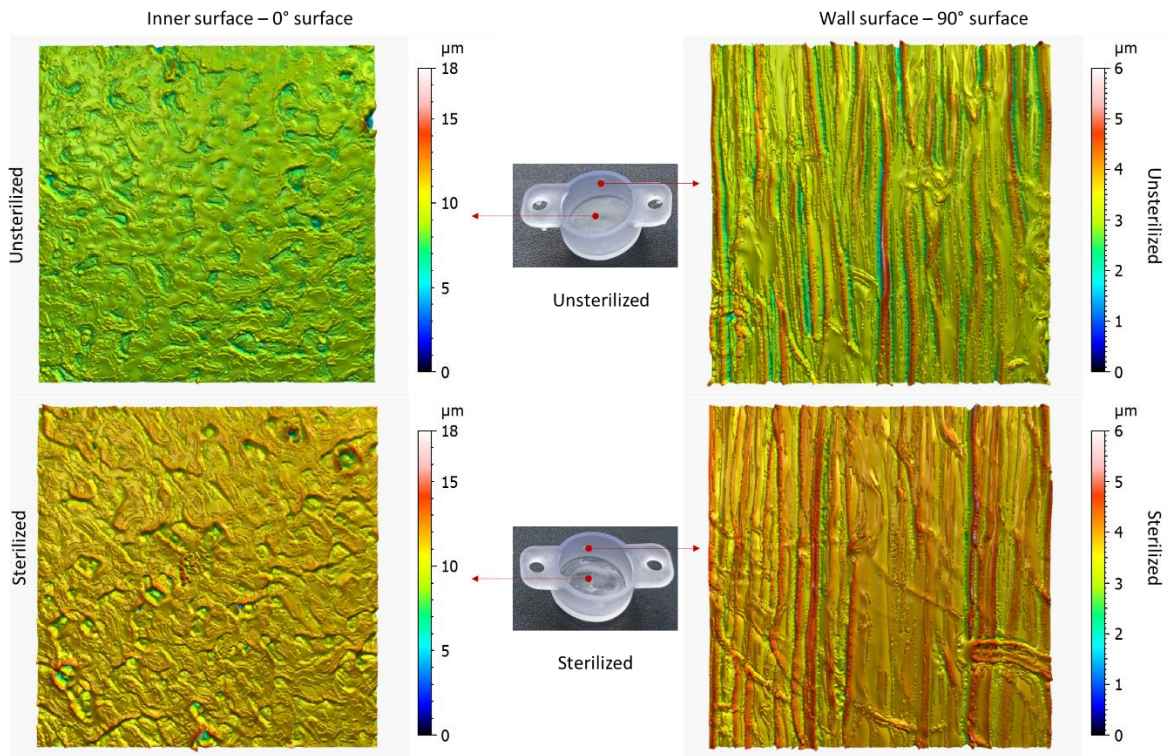
Figure 65. *3D view of the surface topography of the inner and wall surface of the fabricated Dental barrier before and after the sterilization process. Image is taken from paper 7.*
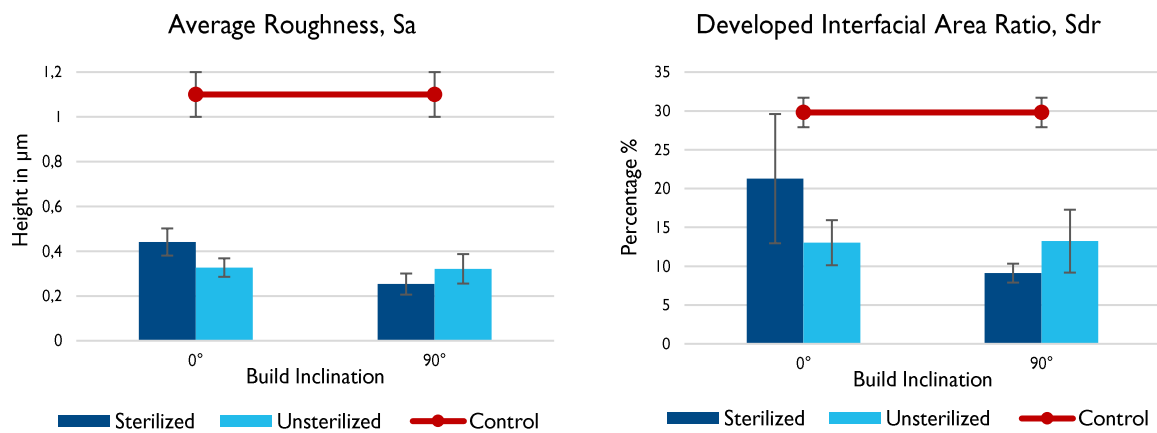
Figure 66. *The graphs of (a) Average roughness, Sa, and (b) Developed Interfacial Area Ratio, Sdr for various build inclinations as measured on the inner surface (0° surface) and wall (90° surface) of the printed dental barriers. Graphs are taken from paper 7.*

At the inner surface or 0° surface, both the Sa and Sdr values are higher for sterilized samples compared to the unsterilized samples, this observation slightly contradicts the findings obtained from the artefact testing. The initial surface study on 0° build inclination showed that on average the values of Sa and Sdr parameters were slightly lower for the sterilized samples, although the difference was insignificant. Surface images also showed (see Figure 63) visually the effect of the sterilization process. However, in the case of dental barriers, the unsterilized samples have lower values of Sa and Sdr mainly due to the increased presence of the resin on the inner surfaces of the dental barriers. The geometry of cup-like shaped

dental barriers confines the resin during the printing process and the automated process of washing the specimen in IPA alcohol does not fully remove the resins from its surface topography. The excess resin after the wash gets further cured in the UV chamber, leaving behind a smoother shiny inner surface of the dental barrier. During the sterilization, the steam under pressure may disrupt the smooth surface texture to provide a rougher texture to the samples. Figure 67 shows the presence of resin compared to the resin-free surface before the sterilization process. Hence, manual washing may be necessary to avoid the accumulation of excess resin. The inner walls of the dental barrier have Sa and Sdr values that were similar to the observed results from the initial experimentation with surface-specific test artefacts. This indicates that the excess resin from the inner walls of the dental barriers can be removed after multiple runs in the automated alcohol rinsing. However, it is necessary to optimize the washing process to maximize the removal of resins from such complex geometries.
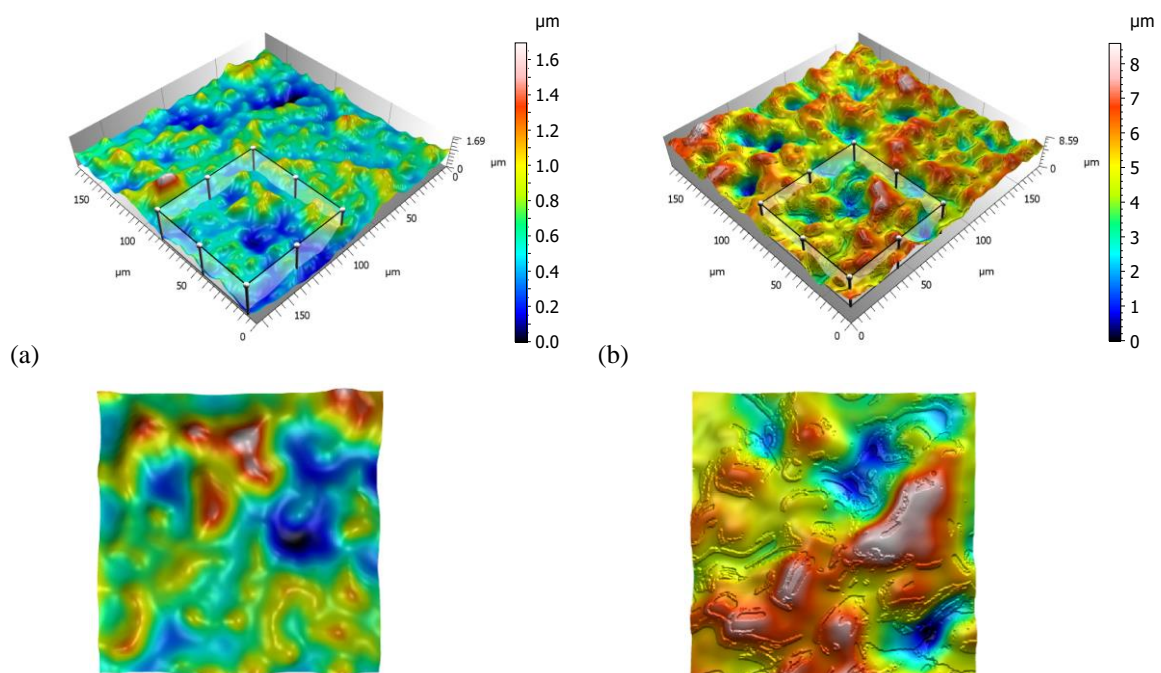
Figure 67. 3D view of the surface topography of the inner surface of the unsterilized SLA dental barriers with an extracted surface view (a) Excess resin on the surface and (b) Resin-free surface. Images adapted from paper 7.

Chapter 7

CONCLUSION AND FUTURE WORK

This is the final chapter of the thesis where the conclusion and future work are presented. The conclusion section is organized to answer the raised research questions and the future work includes the next steps in functional surface research aimed at improving the AM technology for industrial standards.

7.1 CONCLUSION

Globally, there are ongoing attempts to promote AM technology and assure its widespread adoption across industries, since it has shown huge potential in manufacturing and can soon become the industry standard for the production of parts. To achieve such milestones, it is first necessary to address and rectify the downsides of AM. As a consequence, this thesis aims to improve AM processes by addressing the quality-related issues associated with the surface topography of fabricated parts. This thesis compiles and compares diverse research involving various AM technologies, post-processing methods, surface measuring instruments, topography characterization, and statistical methods focused on improving AM surface topography quality and its part function. Additionally, this thesis can be formulated as a guideline for AM users and researchers looking to optimize AM processes for enhanced surface quality. The following passage presents a summary of the whole study by answering the raised research questions.

RQ1: What are the various topography characterization methods that can be used to interpret scale-limited and multi-scale Additive Manufacturing surfaces?

The characterization section in the previous chapter pointed out various appended papers comprising different characterization methods and their effectiveness in interpreting the Additive Manufacturing surfaces. The quality of information that can be extracted from the surface topography depends on the sophistication of characterization methods. For instance, the description of AM surface based on profile parameters (ISO 4287) may not fully reflect the functional behaviour due to its technique of providing waviness and roughness information only in one direction i.e., along the measuring direction. On the other hand, characterization through areal surface texture parameters (ISO 25178-2) provides the missing surface information from profile measurements that could improve the explanation of surface functional behaviour. However, the majority of these parameters are a direct counterpart of the profile parameters, and the literature has shown that average parameters are mostly employed for surface description which often does not fully correlate to the product performance. Hence, either a combination of areal surface texture parameters or advanced characterization approaches must be utilized for describing AM surfaces. The multi-scale characterization methods map the surface topography either as a function of scales or as a function of spatial frequency which helps in identifying the significant scales or wavelengths representing the most crucial surface features affecting the function. Characterizing these surface features not only strengthens the correlation between the surface and its functional performance but also improves the representation of AM surfaces as a whole. To summarize, this thesis provides a contrast between various characterization methods. The profile and areal surface texture parameters were utilized to mainly describe scale-limited AM surfaces and the multi-scale surfaces were

characterized using more advanced methods such as Power spectral density, Scale-sensitive fractal analysis, and Feature-based analysis.

RQ2: How does the identification of significant roughness parameters improve the understanding of AM and post-processes?

As mentioned earlier, several surface texture parameters are required to establish a complete geometrical description of AM surfaces and it is important to note that not all of these surface parameters are required to understand the underlying mechanism of surface formation in AM processes, and definitely not all to necessarily explain the surface function. It is, therefore, important to identify only a few parameters that describe the crucial surface features which can provide meaningful interpretation of the manufacturing process. With that said, it is also important to outline, that most of the research involves using average roughness parameters (Ra or Sa) to describe the AM surfaces. Using a single parameter to describe the surface will limit the understanding of manufactured surfaces. Hence, in this thesis, a research methodology is developed (refer to section 5.2.4) to identify the most significant surface/profile roughness parameters representing the "footprints" on the surface, unique to each manufacturing process. This is done efficiently by using a regression for scale-limited surfaces, where the significant parameters are identified by observing the coefficient of determination (R^2) value. For multi-scale surfaces, significant parameters are identified either by analyzing the significant scales obtained from the "transfer function" of complexity plots or by scrutinizing the power spectral density maps.

RQ3: How can the statistical data analysis method facilitate the optimization of the additive manufacturing processes for achieving its intended surface function?

The unique features of the surface topography highly influence the function of the part. It is, therefore, necessary to fully understand these features and their relation to the manufacturing process to establish control over the function of the part. Once this information is fully established the manufacturing process control variables can be varied to adjust the formation of surface features to achieve its intended function, thus enabling process optimization.
For instance, Multiple regression statistical methods help in achieving this goal by identifying the influence of AM print settings (layer thickness, print temperature, Infill settings, and so on) and post-process settings (shot-blasting, laser-finishing, and acetone process settings) on surface topography. By observing the regression coefficients, an equation can be derived that links the process variables to the concerned roughness parameter and as per the functional requirements, the process settings can be varied to achieve the desired result.

RQ4: How to validate the obtained research results in Industrial and Dental use cases?

Paper 3 and 7 presented two use cases from industrial and dental applications. In paper 3, a TylöHelo sauna product was utilized for analysis, where the functional requirement was to restore the original injection moulding properties particularly related to aesthetic aspects (matte finish). The developed research method of using regression aided not only in identifying the significant parameters for characterization but also in identifying the best post-processing methods and their respective process control variables. Using the acquired knowledge from the statistical methods and by visual inspection, the best-suited post-processing method was selected and implemented on the industrial sauna product. It was found that combining multiple post-processing methods yielded the best results that were comparable to the reference injection moulding product.

In paper 7, the focus was provided on generating surface topographical properties that are suitable for bone regeneration required for a dental application. For this purpose, surface test artefacts were produced by using SLA AM technology using biocompatible material and the micro surface topography of as-built and sterilized samples were analyzed and compared to the reference milled Zirconia dental barriers. The developed method using area-scale analysis helped in identifying the important scales and roughness parameters for characterization. The obtained results were utilized to optimize the printing process to produce dental barriers that resulted in surface roughness within the required specification for facilitating bone growth in the dental application.

7.2 FUTURE WORK

The focus of this thesis was to establish a framework to mainly characterize the Additive Manufacturing and post-processing surfaces, thereby enabling the prediction and optimization of the surface quality to achieve its intended component function. Future work involves mainly addressing the de-limitations mentioned in this thesis. The surface analysis performed in this research was confined to only three of seven AM process categories and to generalize the findings into a framework other AM processes need to be investigated. However, the selected three AM processes i.e., Powder Bed Fusion, Material Extrusion, and Vat-photopolymerization for analysis are most widely used in industries, medical and dental sectors. In this thesis, all the results were restricted to the up-skin surfaces of AM samples mostly including surface features corresponding to "stair-steps" and raster patterns. It is necessary to study the influence of re-entrant surface features on the functional performance of the produced samples. These features are typically present on the down skin surfaces. This then points out the fact that the utilized surface measuring instruments often fail to capture these re-entrant features and hence other methods of surface acquisition namely computed tomography may be necessary to analyze the AM surfaces. Furthermore, it may be necessary to analyze the form effects on AM product functional performance, since the current methods of characterization especially the surface parameters and filtering conditions are mainly designed to analyze nominally flat surfaces. Finally, the most important future step would be to integrate Artificial Intelligence for the surface analysis of AM products. AI through Machine Learning allows the utilization of complex modeling algorithms that provides better prediction and optimization of AM process variables and surface function.

REFERENCES

[1]   I. Gibson, D. Rosen, B. Stucker, and M. Khorasani, *Additive Manufacturing Technologies*. Springer, 2021. doi: 10.1007/978-3-030-56127-7

[2]   "ISO/ASTM 52900:2015(en), Additive manufacturing — General principles — Terminology," Geneva, 2015.

[3]   "The Sustainable Development Goals Report." *Sustain. Dev. goals Rep. 2016*, 2016, doi: 10.29171/azu_acku_pamphlet_k3240_s878_2016.

[4]   M. Wiese, S. Thiede, and C. Herrmann, "Rapid manufacturing of automotive polymer series parts: A systematic review of processes, materials and challenges," *Addit. Manuf.*, vol. 36, p. 101582, Dec. 2020, doi: 10.1016/j.addma.2020.101582.

[5]   B. Blakey-Milner *et al.*, "Metal additive manufacturing in aerospace: A review," *Mater. Des.*, vol. 209, p. 110008, Nov. 2021, doi: 10.1016/J.MATDES.2021.110008.

[6]   M. A. Ali, M. Rajabi, and S. Sudhir Sali, "Additive manufacturing potential for medical devices and technology," *Current Opinion in Chemical Engineering*, vol. 28. Elsevier Ltd, pp. 127–133, Jun. 01, 2020, doi: 10.1016/j.coche.2020.05.001.

[7]   R. Galante, C. G. Figueiredo-Pina, and A. P. Serro, "Additive manufacturing of ceramics for dental applications: A review," *Dental Materials*, vol. 35, no. 6. Elsevier Inc., pp. 825–846, Jun. 01, 2019, doi: 10.1016/j.dental.2019.02.026.

[8]   C. J. Bae, A. B. Diggs, and A. Ramachandran, "Quantification and certification of additive manufacturing materials and processes," in *Additive Manufacturing: Materials, Processes, Quantifications and Applications*, Elsevier, 2018, pp. 181–213.

[9]   A. Townsend, N. Senin, L. Blunt, R. K. Leach, and J. S. Taylor, "Surface texture metrology for metal additive manufacturing: a review," *Precision Engineering*, vol. 46. Elsevier Inc., pp. 34–47, Oct. 01, 2016, doi: 10.1016/j.precisioneng.2016.06.001.

[10]   R. K. Leach, "The measurement of surface texture using stylus instruments.," *Meas. Good Pract. Guid. No. 37*, no. 2, p. 100, 2001, [Online]. Available: http://publications.npl.co.uk/npl_web/pdf/mgpg37.pdf.

[11]   R. Leach, "Characterisation of areal surface texture," *Characterisation Areal Surf. Texture*, vol. 9783642364, pp. 1–353, 2013, doi: 10.1007/978-3-642-36458-7.

[12]   A. Thompson, I. Maskery, and R. K. Leach, "X-ray computed tomography for additive manufacturing: A review," *Meas. Sci. Technol.*, vol. 27, no. 7, Jun. 2016, doi: 10.1088/0957-0233/27/7/072001.

[13]   A. Townsend, L. Blunt, L. Pagani, and P. Scott, "Measurement and characterisation of additively manufactured re-entrant surfaces," *undefined*, 2017.

[14]   F. Zanini, L. Pagani, P. J. Scott, E. Savio, and S. Carmignato, "Measurement of additively manufactured surfaces with re-entrant features by x-ray computed tomography," *Proc. - 2018 ASPE euspen Summer Top. Meet. Adv. Precis. Addit. Manuf.*, no. July, pp. 222–225, 2018.

[15]   K. J. Stout and E. J. Davis, "Surface topography of cylinder bores - the relationship between manufacture, characterization and function," *Wear*, vol. 95, no. 2, pp. 111–125, 1984, doi: 10.1016/0043-1648(84)90111-X.

[16]   N. H. Harun, M. S. Kasim, M. Z. Z. Abidin, R. Izamshah, H. Attan, and H. N. Ganesan, "A study on surface roughness during fused deposition modelling: A review," *J. Adv. Manuf. Technol.*, vol. 12, no. Specialissue1, pp. 25–36, 2018.

[17]   T. Grimm, G. Wiora, and G. Witt, "Characterization of typical surface effects in additive manufacturing with confocal microscopy," *Surf. Topogr. Metrol. Prop.*, vol. 3, no. 1, p. 014001, Jan. 2015, doi: 10.1088/2051-672X/3/1/014001.

[18]   M. Ziaee and N. B. Crane, "Binder jetting: A review of process, materials, and

methods," *Additive Manufacturing*, vol. 28. Elsevier B.V., pp. 781–801, Aug. 01, 2019, doi: 10.1016/j.addma.2019.05.031.

[19]   B. Dutta, "Directed Energy Deposition (DED) Technology," *Encycl. Mater. Met. Alloy.*, pp. 66–84, Jan. 2022, doi: 10.1016/B978-0-12-819726-4.00035-1.

[20]   S. C. Daminabo, S. Goel, S. A. Grammatikos, H. Y. Nezhad, and V. K. Thakur, "Fused deposition modeling-based additive manufacturing (3D printing): techniques for polymer material systems," *Materials Today Chemistry*, vol. 16. Elsevier Ltd, p. 100248, Jun. 01, 2020, doi: 10.1016/j.mtchem.2020.100248.

[21]   S. C. Ligon, R. Liska, J. Stampfl, M. Gurr, and R. Mülhaupt, "Polymers for 3D Printing and Customized Additive Manufacturing," *Chemical Reviews*, vol. 117, no. 15. American Chemical Society, pp. 10212–10290, Aug. 09, 2017, doi: 10.1021/acs.chemrev.7b00074.

[22]   B. Khoshnevis, "Automated construction by contour crafting - Related robotics and information technologies," in *Automation in Construction*, Jan. 2004, vol. 13, no. 1, pp. 5–19, doi: 10.1016/j.autcon.2003.08.012.

[23]   F. Hamidi and F. Aslani, "Additive manufacturing of cementitious composites: Materials, methods, potentials, and challenges," *Construction and Building Materials*, vol. 218. Elsevier Ltd, pp. 582–609, Sep. 10, 2019, doi: 10.1016/j.conbuildmat.2019.05.140.

[24]   A. Paolini, S. Kollmannsberger, and E. Rank, "Additive manufacturing in construction: A review on processes, applications, and digital planning methods," *Additive Manufacturing*, vol. 30. Elsevier B.V., p. 100894, Dec. 01, 2019, doi: 10.1016/j.addma.2019.100894.

[25]   J. Malda *et al.*, "25th anniversary article: Engineering hydrogels for biofabrication," *Advanced Materials*, vol. 25, no. 36. John Wiley & Sons, Ltd, pp. 5011–5028, Sep. 01, 2013, doi: 10.1002/adma.201302042.

[26]   S. V. Murphy and A. Atala, "3D bioprinting of tissues and organs," *Nature Biotechnology*, vol. 32, no. 8. Nature Publishing Group, pp. 773–785, 2014, doi: 10.1038/nbt.2958.

[27]   A. Habib and B. Khoda, "Development of clay based novel hybrid bio-ink for 3D bio-printing process," *J. Manuf. Process.*, vol. 38, pp. 76–87, Feb. 2019, doi: 10.1016/j.jmapro.2018.12.034.

[28]   J. Y. Lee, J. An, and C. K. Chua, "Fundamentals and applications of 3D printing for novel materials," *Applied Materials Today*, vol. 7. Elsevier Ltd, pp. 120–133, Jun. 01, 2017, doi: 10.1016/j.apmt.2017.02.004.

[29]   "ISO - ISO/ASTM 52911-1:2019 - Additive manufacturing — Design — Part 1: Laser-based powder bed fusion of metals." https://www.iso.org/standard/72951.html (accessed Nov. 14, 2022).

[30]   L. E. Murr *et al.*, "Fabrication of metal and alloy components by additive manufacturing: Examples of 3D materials science," *Journal of Materials Research and Technology*, vol. 1, no. 1. Elsevier Editora Ltda, pp. 42–54, Apr. 01, 2012, doi: 10.1016/S2238-7854(12)70009-1.

[31]   S. Yuan, F. Shen, C. K. Chua, and K. Zhou, "Polymeric composites for powder-based additive manufacturing: Materials and applications," *Progress in Polymer Science*, vol. 91. Elsevier Ltd, pp. 141–168, Apr. 01, 2019, doi: 10.1016/j.progpolymsci.2018.11.001.

[32]   S. Cooke, K. Ahmadi, S. Willerth, and R. Herring, "Metal additive manufacturing: Technology, metallurgy and modelling," *Journal of Manufacturing Processes*, vol. 57. Elsevier Ltd, pp. 978–1003, Sep. 01, 2020, doi: 10.1016/j.jmapro.2020.07.025.

[33]   S. Yi, F. Liu, J. Zhang, and S. Xiong, "Study of the key technologies of LOM for

functional metal parts," in *Journal of Materials Processing Technology*, Jul. 2004, vol. 150, no. 1–2, pp. 175–181, doi: 10.1016/j.jmatprotec.2004.01.035.

[34] A. Bournias-Varotsis, X. Han, R. A. Harris, and D. S. Engstrøm, "Ultrasonic additive manufacturing using feedstock with build-in circuitry for 3D metal embedded electronics," *Addit. Manuf.*, vol. 29, p. 100799, Oct. 2019, doi: 10.1016/j.addma.2019.100799.

[35] H. Wu *et al.*, "Recent developments in polymers/polymer nanocomposites for additive manufacturing," *Progress in Materials Science*, vol. 111. Elsevier Ltd, p. 100638, Jun. 01, 2020, doi: 10.1016/j.pmatsci.2020.100638.

[36] F. Li *et al.*, "Digital light processing 3D printing of ceramic shell for precision casting," *Mater. Lett.*, vol. 276, p. 128037, Oct. 2020, doi: 10.1016/j.matlet.2020.128037.

[37] A. R. Johnson *et al.*, "Single-step fabrication of computationally designed microneedles by continuous liquid interface production," *PLoS One*, vol. 11, no. 9, Sep. 2016, doi: 10.1371/journal.pone.0162518.

[38] P. Gu, X. Zhang, Y. Zeng, and B. Ferguson, "Quality analysis and optimization of solid ground curing process," *J. Manuf. Syst.*, vol. 20, no. 4, pp. 250–263, Jan. 2001, doi: 10.1016/S0278-6125(01)80045-5.

[39] J. S. Taylor, "Physical processes linking input parameters and surfacemorphology in additivemanufacturing," *ASPE Spring Top. Precis. Toler. Addit.*, pp. 70–1, 2015.

[40] A. V. Krishna, O. Flys, V. V. Reddy, J. Berglund, and B. G. Rosen, "Areal surface topography representation of as-built and post-processed samples produced by powder bed fusion using laser beam melting," *Surf. Topogr. Metrol. Prop.*, vol. 8, no. 2, p. 024012, Jun. 2020, doi: 10.1088/2051-672X/ab9b73.

[41] V. Reddy, O. Flys, A. Chaparala, C. E. Berrimi, V. Amogh, and B. G. Rosen, "Study on surface texture of Fused Deposition Modeling," in *Procedia Manufacturing*, 2018, vol. 25, pp. 389–396, doi: 10.1016/j.promfg.2018.06.108.

[42] Stephen Oluwashola Akande, "Dimensional Accuracy and Surface Finish Optimization of Fused Deposition Modelling Parts using Desirability Function Analysis," *Int. J. Eng. Res.*, vol. V4, no. 04, pp. 196–202, 2015, doi: 10.17577/ijertv4is040393.

[43] D. Ahn, H. Kim, and S. Lee, "Surface roughness prediction using measured data and interpolation in layered manufacturing," *J. Mater. Process. Technol.*, vol. 209, no. 2, pp. 664–671, Jan. 2009, doi: 10.1016/j.jmatprotec.2008.02.050.

[44] A. V. Krishna *et al.*, "Influence of different post-processing methods on surface topography of fused deposition modelling samples," *Surf. Topogr. Metrol. Prop.*, vol. 8, no. 1, p. 014001, Feb. 2020, doi: 10.1088/2051-672X/AB77D7.

[45] J. Khodaii and A. Rahimi, "Improving the surface roughness in stereolithography by controlling surface angle, hatch spaces, and postcuring time," *Eng. Reports*, vol. 2, no. 6, p. e12193, Jun. 2020, doi: 10.1002/ENG2.12193.

[46] "Sustainable Manufacturing | US EPA." https://www.epa.gov/sustainability/sustainable-manufacturing (accessed Nov. 15, 2022).

[47] S. H. Huang, P. Liu, A. Mokasdar, and L. Hou, "Additive manufacturing and its societal impact: A literature review," *International Journal of Advanced Manufacturing Technology*, vol. 67, no. 5–8. Springer, pp. 1191–1203, Jul. 16, 2013, doi: 10.1007/s00170-012-4558-5.

[48] R. E. Williams and V. L. Melton, "Abrasive flow finishing of stereolithography prototypes," *Rapid Prototyp. J.*, vol. 4, no. 2, pp. 56–67, 1998, doi: 10.1108/13552549810207279.

[49] K. F. Leong, C. K. Chua, G. S. Chua, and C. H. Tan, "Abrasive jet deburring of

jewellery models built by stereolithography apparatus (SLA)," *J. Mater. Process. Technol.*, vol. 83, no. 1–3, pp. 36–47, Nov. 1998, doi: 10.1016/S0924-0136(98)00041-7.

[50]   A. P. Nagalingam, H. K. Yuvaraj, and S. H. Yeo, "Synergistic effects in hydrodynamic cavitation abrasive finishing for internal surface-finish enhancement of additive-manufactured components," *Addit. Manuf.*, vol. 33, p. 101110, May 2020, doi: 10.1016/j.addma.2020.101110.

[51]   O. FLYS *et al.*, "Heat transfer and flow performance in additively manufactured cooling channels with varying surface topography," *J. Japan Soc. Precis. Eng.*, vol. 86, no. 1, pp. 71–79, Jan. 2020, doi: 10.2493/jjspe.86.71.

[52]   A. V. KRISHNA, "Towards Topography Characterization of Additive Manufacturing Surfaces," 2020, Accessed: Nov. 14, 2022. [Online]. Available: https://research.chalmers.se/en/publication/519478.

[53]   R. C. Mulhall and N. D. Nedas, "Impact blasting with glass beads," *Met. Finish.*, vol. 105, no. 10, pp. 65–71, Jan. 2007, doi: 10.1016/S0026-0576(07)80319-9.

[54]   M. Taufik and P. K. Jain, "Laser assisted finishing process for improved surface finish of fused deposition modelled parts," *J. Manuf. Process.*, vol. 30, pp. 161–177, Dec. 2017, doi: 10.1016/j.jmapro.2017.09.020.

[55]   E. Yasa, J. Deckers, and J. P. Kruth, "The investigation of the influence of laser re-melting on density, surface quality and microstructure of selective laser melting parts," *Rapid Prototyp. J.*, vol. 17, no. 5, pp. 312–327, Aug. 2011, doi: 10.1108/13552541111156450.

[56]   S. Hallmann, T. Wolny, and C. Emmelmann, "Post-processing of additively manufactured cutting edges by laser ablation," in *Procedia CIRP*, Jan. 2018, vol. 74, pp. 276–279, doi: 10.1016/j.procir.2018.08.110.

[57]   A. Lalehpour, C. Janeteas, and A. Barari, "Surface roughness of FDM parts after post-processing with acetone vapor bath smoothing process," *Int. J. Adv. Manuf. Technol.*, vol. 95, no. 1–4, pp. 1505–1520, Mar. 2018, doi: 10.1007/s00170-017-1165-5.

[58]   V. R. Sastri, "Material Requirements for Plastics Used in Medical Devices," *Plast. Med. Devices*, pp. 65–112, Jan. 2022, doi: 10.1016/B978-0-323-85126-8.00008-4.

[59]   J. I. Sasaki and S. Imazato, "Autoclave sterilization of dental handpieces: A literature review," *J. Prosthodont. Res.*, vol. 64, no. 3, pp. 239–242, 2020, doi: 10.1016/j.jpor.2019.07.013.

[60]   D. Whitehouse, "Handbook of Surface and Nanometrology," *Handb. Surf. Nanometrology, Second Ed.*, no. May, pp. 171–254, 2010.

[61]   D. J. Whitehouse, "Surface metrology," *Meas. Sci. Technol.*, vol. 8, no. 9, pp. 955–972, 1997, doi: 10.1088/0957-0233/8/9/002.

[62]   R. Leach, "Surface Texture," in *CIRP Encyclopedia of Production Engineering*, L. Laperrière and G. Reinhart, Eds. Springer Berlin Heidelberg, 2014, pp. 1–4.

[63]   "ISO 25178-6:2010(en), Geometrical product specifications (GPS) — Surface texture: Areal — Part 6: Classification of methods for measuring surface texture." https://www.iso.org/obp/ui#iso:std:iso:25178:-6:ed-1:v1:en:biblref:13 (accessed Aug. 05, 2020).

[64]   "ISO 3274:1997, Geometrical Product Specifications (GPS) — Surface texture: Profile method — Nominal characteristics of contact (stylus) instruments." https://www.iso.org/obp/ui/#iso:std:iso:3274:ed-2:v1:en (accessed Aug. 07, 2020).

[65]   K. Creath, "V Phase-Measurement Interferometry Techniques," *Prog. Opt.*, vol. 26, no. C, pp. 349–393, Jan. 1988, doi: 10.1016/S0079-6638(08)70178-1.

[66]   G. E. Sommargren, "Optical heterodyne profilometry," *Appl. Opt.*, vol. 20, no. 4, p. 610, Feb. 1981, doi: 10.1364/ao.20.000610.

[67] J. M. Eastman and J. M. Zavislan, "A New Optical Surface Microprofiling Instrument," in *Precision Surface Metrology*, 1983, vol. 0429, pp. 56–64, doi: 10.1117/12.936340.

[68] C. A. Gomez, A. Thompson, J. Disciacca, and Z. Corporation, "Coherence scanning interferometry for additive manufacture," no. June, pp. 3–5, 2017.

[69] R. Wang, A. C. Law, D. Garcia, S. Yang, and Z. Kong, "Development of structured light 3D-scanner with high spatial resolution and its applications for additive manufacturing quality assurance," doi: 10.1007/s00170-021-07780-2/Published.

[70] L. Newton *et al.*, "Areal topography measurement of metal additive surfaces using focus variation microscopy," *Addit. Manuf.*, vol. 25, pp. 365–389, Jan. 2019, doi: 10.1016/j.addma.2018.11.013.

[71] A. V. Krishna, O. Flys, V. V Reddy, and B. G. Rosén, "Surface topography characterization using 3D stereoscopic reconstruction of SEM images," *Surf. Topogr. Metrol. Prop.*, vol. 6, no. 2, p. 024006, May 2018, doi: 10.1088/2051-672X/AABDE1.

[72] G. Ercolano *et al.*, "Additive manufacturing of sub-micron to sub-mm Metal structures with hollow AFM cantilevers," *Micromachines*, vol. 11, no. 1, Jan. 2020, doi: 10.3390/mi11010006.

[73] A. M. Hamouda, "A precise pneumatic co-axial jet gauging system for surface roughness measurements," *Precis. Eng.*, vol. 1, no. 2, pp. 95–100, Apr. 1979, doi: 10.1016/0141-6359(79)90140-5.

[74] "ISO 13696:2022(en), Optics and photonics — Test method for total scattering by optical components." https://www.iso.org/obp/ui/#iso:std:iso:13696:ed-2:v1:en (accessed Nov. 14, 2022).

[75] J. M. Bennett and L. Mattsson, *Introduction to Surface Roughness and Scattering*. Optical Society of America, 1989.

[76] B. J. N, F. R. E, and S. L. Y, "A capacitance-based surface texture measuring system.," *CIRP Ann*, vol. 26, no. 1, pp. 375–377, 1977, Accessed: Aug. 28, 2020. [Online]. Available: https://jglobal.jst.go.jp/en/detail?JGLOBAL_ID=201002027345082954.

[77] R. Leach, Ed., *Optical Measurement of Surface Topography*. Springer Berlin Heidelberg, 2011.

[78] "ISO - ISO 25178-601:2010 - Geometrical product specifications (GPS) — Surface texture: Areal — Part 601: Nominal characteristics of contact (stylus) instruments." https://www.iso.org/standard/42786.html (accessed Aug. 28, 2022).

[79] M. Piska and J. Metelkova, "On the comparison of contact and non-contact evaluations of a machined surface," *MM Sci. J.*, no. June 2014, pp. 476–479, 2014, doi: 10.17973/mmsj.2014_06_201408.

[80] F. Isgrò, F. Odone, and A. Verri, "An open system for 3D data acquisition from multiple sensor," *Proc. - Int. Work. Comput. Archit. Mach. Perception, CAMP*, no. May 2014, pp. 52–57, 2005, doi: 10.1109/CAMP.2005.13.

[81] "ISO - ISO 25178-602:2010 - Geometrical product specifications (GPS) — Surface texture: Areal — Part 602: Nominal characteristics of non-contact (confocal chromatic probe) instruments." https://www.iso.org/standard/43920.html (accessed Aug. 05, 2020).

[82] A. Canette and R. Briandet, "MICROSCOPY | Confocal Laser Scanning Microscopy," *Encycl. Food Microbiol. Second Ed.*, pp. 676–683, Jan. 2014, doi: 10.1016/B978-0-12-384730-0.00214-7.

[83] F. Cabanettes *et al.*, "Topography of as built surfaces generated in metal additive manufacturing: A multi scale analysis from form to roughness," *Precis. Eng.*, vol. 52, pp. 249–265, Apr. 2018, doi: 10.1016/j.precisioneng.2018.01.002.

[84] C. Bermudez, A. Matilla, and A. Aguerri, "Confocal fusion: towards the universal

optical 3D metrology technology," in *EUSPEN - LAMDAMAP*, 2017.

[85] A. Matilla, J. Mariné, J. Pérez, C. Cadevall, and R. Artigas, "Three-dimensional measurements with a novel technique combination of confocal and focus variation with a simultaneous scan," in *Proceedings of the 16th International Conference of the European Society for Precision Engineering and Nanotechnology, EUSPEN 2016*, Apr. 2016, vol. 9890, p. 98900B, doi: 10.1117/12.2227054.

[86] O. Flys, J. Berglund, and B. G. Rosen, "Using confocal fusion for measurement of metal AM surface texture," *Surf. Topogr. Metrol. Prop.*, vol. 8, no. 2, 2020, doi: 10.1088/2051-672X/ab84c3.

[87] A. Khursheed, "Scanning electron microscope optics and spectrometers," *Scanning Electron Microsc. Opt. Spectrometers*, pp. 1–403, Jan. 2010, doi: 10.1142/7094.

[88] L. Blunt and X. Jiang, *Advanced Techniques for Assessment Surface Topography: Development of a Basis for 3D Surface Texture Standards "Surfstand."* Elsevier Inc., 2003.

[89] "ISO 25178-2:2021(en), Geometrical product specifications (GPS) — Surface texture: Areal — Part 2: Terms, definitions and surface texture parameters." https://www.iso.org/obp/ui/#iso:std:iso:25178:-2:ed-2:v1:en (accessed Sep. 15, 2022).

[90] C. A. Brown *et al.*, "Multiscale analyses and characterizations of surface topographies," *CIRP Ann.*, vol. 67, no. 2, pp. 839–862, 2018, doi: 10.1016/j.cirp.2018.06.001.

[91] "Geometrical product specifications (GPS)-Surface texture: Profile-Part 2: ISO 21920-2:2021(E) COPYRIGHT PROTECTED DOCUMENT," 2021, Accessed: Sep. 19, 2022. [Online]. Available: www.sis.se.buytheentirestandardviahttps://www.sis.se/std-80033082.

[92] "ISO 4287:1997(en,fr), Geometrical Product Specifications (GPS) — Surface texture: Profile method — Terms, definitions and surface texture parameters / Spécification géométrique des produits (GPS) — État de surface: Méthode du profil — Termes, définitions et paramètres d'état de surface." https://www.iso.org/obp/ui#iso:std:iso:4287:ed-1:v1:en,fr (accessed Aug. 05, 2020).

[93] T. R. Thomas, *Rough Surfaces*. PUBLISHED BY IMPERIAL COLLEGE PRESS AND DISTRIBUTED BY WORLD SCIENTIFIC PUBLISHING CO., 1998.

[94] "ISO 4288:1996(en), Geometrical Product Specifications (GPS) — Surface texture: Profile method — Rules and procedures for the assessment of surface texture." https://www.iso.org/obp/ui/#iso:std:iso:4288:ed-2:v1:en:sec:B (accessed Aug. 09, 2020).

[95] "ISO 16610-21:2011(en), Geometrical product specifications (GPS) — Filtration — Part 21: Linear profile filters: Gaussian filters." https://www.iso.org/obp/ui/#iso:std:iso:16610:-21:ed-1:v1:en (accessed Aug. 09, 2020).

[96] M. C. Salcedo, I. B. Coral, and G. V. Ochoa, "Characterization of Surface Topography with Abbott Firestone Curve," *Contemp. Eng. Sci.*, vol. 11, no. 68, pp. 3397–3407, 2018, doi: 10.12988/ces.2018.87319.

[97] ASME, *B46.1:2002 Surface Texture (Surface Roughness, Waviness, and Lay) - ASME*. 2002.

[98] R. N. Youngworth, B. B. Gallagher, and B. L. Stamper, "An overview of power spectral density (PSD) calculations," *Opt. Manuf. Test. VI*, vol. 5869, no. August 2005, p. 58690U, 2005, doi: 10.1117/12.618478.

[99] E. Sidick, "Power spectral density specification and analysis of large optical surfaces," *Model. Asp. Opt. Metrol. II*, vol. 7390, no. June 2009, p. 73900L, 2009, doi: 10.1117/12.823844.

[100] T. D. B. Jacobs, T. Junge, and L. Pastewka, "Quantitative characterization of surface topography using spectral analysis," *Surf. Topogr. Metrol. Prop.*, vol. 5, no. 1, 2017, doi: 10.1088/2051-672X/aa51f8.

[101] O. Flys, "On surface structure characterization and application on additive manufacturing," 2020, Accessed: Aug. 07, 2020. [Online]. Available: https://research.chalmers.se/en/publication/516839.

[102] C. A. Brown, W. A. Johnsen, R. M. Butland, and J. Bryan, "Scale-Sensitive Fractal Analysis of Turned Surfaces," *CIRP Ann. - Manuf. Technol.*, vol. 45, no. 1, pp. 515–518, Jan. 1996, doi: 10.1016/S0007-8506(07)63114-X.

[103] J. Berglund, *Characterisation of Functional Pressing Die Surfaces*. Chalmers University of Technology, 2011.

[104] C. A. Brown *et al.*, "Multiscale analyses and characterizations of surface topographies," *CIRP Ann.*, vol. 67, no. 2, pp. 839–862, Jan. 2018, doi: 10.1016/j.cirp.2018.06.001.

[105] C. A. Brown, "Areal fractal methods," in *Characterisation of Areal Surface Texture*, vol. 9783642364587, Springer-Verlag Berlin Heidelberg, 2013, pp. 129–153.

[106] N. Senin, A. Thompson, and R. Leach, "Feature-based characterisation of signature topography in laser powder bed fusion of metals," *Meas. Sci. Technol.*, vol. 29, no. 4, p. 045009, Mar. 2018, doi: 10.1088/1361-6501/aa9e19.

[107] S. Lou, W. Zeng, L. Pagani, H. Abdul-Rahman, X. Jiang, and P. J. Scott, "Development of Surface Characterisation Toolbox for Additive Manufactured Components: from Planar Layer Surfaces to Complex Functional Surfaces." Accessed: Aug. 17, 2020. [Online]. Available: www.euspen.eu.

[108] A. Boschetto, L. Bottini, and F. Veniali, "Roughness modeling of AlSi10Mg parts fabricated by selective laser melting," *J. Mater. Process. Technol.*, vol. 241, pp. 154–163, Mar. 2017, doi: 10.1016/j.jmatprotec.2016.11.013.

[109] B. G. Rosen, A. Fall, S. Rosen, A. Farbrot, and P. Bergström, "Topographic modelling of haptic properties of tissue products," in *Journal of Physics: Conference Series*, 2014, vol. 483, no. 1, doi: 10.1088/1742-6596/483/1/012010.

[110] S. Chatterjee and J. S. Simonoff, *Handbook of Regression Analysis*. Somerset, UNITED STATES: John Wiley & Sons, Incorporated, 2012.

[111] R. Malhotra, "Empirical Research in Software Engineering : Concepts, Analysis, and Applications," *Empir. Res. Softw. Eng.*, Mar. 2016, doi: 10.1201/B19292.

[112] V. Bairagi and M. . Munot, Eds., *Research Methodology: A Practical and Scientific Approach (1st ed.)*. 2019.

[113] K. Tanner, "Experimental research," *Res. Methods Information, Syst. Context. Second Ed.*, pp. 337–356, 2018, doi: 10.1016/B978-0-08-102220-7.00014-5.

[114] D. C. Montgomery and J. Wiley, "D esign and Analysis of Experiments Eighth Edition," 2013, Accessed: Aug. 23, 2022. [Online]. Available: www.wiley.com/go/permissions.

[115] C. Gatti, *Design of Experiments for Reinforcement Learning*. Springer International Publishing , 2015.

[116] R. H. Myers, D. C. Montgomery, and C. M. Anderson-Cook, *Response Surface Methodology : Process and Product Optimization Using Designed Experiments*. New York, UNITED STATES: John Wiley & Sons, Incorporated, 2016.

[117] J. E. Gentle, "Computational Statistics," *Int. Encycl. Educ.*, pp. 93–97, Jan. 2010, doi: 10.1016/B978-0-08-044894-7.01316-6.

[118] M. E. Buchanan, "Methods of data collection," *AORN J.*, vol. 33, no. 1, 1981, doi: 10.1016/S0001-2092(07)69400-9.

[119] O. Flys, "Calibration Procedure and Industrial Applications of Coherence Scanning

Interferometer," Chalmers University of Technology, Gothenburg, Sweden, 2016.

[120] "ISO 16610-1:2015(en), Geometrical product specifications (GPS) — Filtration — Part 1: Overview and basic concepts." https://www.iso.org/obp/ui/#iso:std:iso:16610:-1:ed-1:v1:en (accessed Aug. 07, 2020).

[121] "ISO/TS 16610-1:2006(en), Geometrical product specifications (GPS) — Filtration — Part 1: Overview and basic concepts." https://www.iso.org/obp/ui/#iso:std:iso:ts:16610:-1:ed-1:v1:en (accessed Sep. 15, 2022).

[122] "ISO 16610-40:2015(en), Geometrical product specifications (GPS) — Filtration — Part 40: Morphological profile filters: Basic concepts." https://www.iso.org/obp/ui/#iso:std:iso:16610:-40:ed-1:v2:en:term:3.7 (accessed Sep. 15, 2022).

[123] M. H. Nasab, D. Gastaldi, N. F. Lecis, and M. Vedani, "On morphological surface features of the parts printed by selective laser melting (SLM)," *Addit. Manuf.*, vol. 24, no. October, pp. 373–377, 2018, doi: 10.1016/j.addma.2018.10.011.

[124] L. Blunt and X. Jiang, *Numerical Parameters for Characterisation of Topography*. Kogan Page Limited and contributors, 2003.

[125] S. Chatterjee and J. S. Simonoff, "Handbook of Regression Analysis.," p. 252, 2013, Accessed: Sep. 15, 2022. [Online]. Available: https://www.wiley.com/en-us/Handbook+of+Regression+Analysis-p-9780470887165.

[126] M. Douglas C., P. Elizabeth A., and V. G. Geoffrey, "Introduction to Linear Regression Analysis, Fifth Edition," *A JOHN WILEY SONS, INC., Publ.*, vol. 81, no. 2, pp. 318–319, 2012, Accessed: Sep. 15, 2022. [Online]. Available: https://www.adlibris.com/se/bok/introduction-to-linear-regression-analysis-9780470542811.

[127] "ISO 16610-71:2014(en), Geometrical product specifications (GPS) — Filtration — Part 71: Robust areal filters: Gaussian regression filters." https://www.iso.org/obp/ui/#iso:std:iso:16610:-71:ed-1:v1:en (accessed Aug. 07, 2020).

[128] G. Piazzesi, "Photogrammetry with the scanning electron microscope," *J. Phys. E.*, vol. 6, no. 4, p. 392, Apr. 1973, doi: 10.1088/0022-3735/6/4/023.

[129] A. Kudryavtsev, "3D Reconstruction in Scanning Electron Microscope : from image acquisition to dense point cloud," Accessed: Sep. 15, 2022. [Online]. Available: https://tel.archives-ouvertes.fr/tel-01930234.

[130] "ISO/ASTM 52902:2019(en), Additive manufacturing — Test artifacts — Geometric capability assessment of additive manufacturing systems." https://www.iso.org/obp/ui/#iso:std:iso-astm:52902:ed-1:v1:en (accessed Aug. 09, 2020).

[131] E. Yasa, O. Poyraz, E. U. Solakoglu, G. Akbulut, and S. Oren, "A Study on the Stair Stepping Effect in Direct Metal Laser Sintering of a Nickel-based Superalloy," *Procedia CIRP*, vol. 45, pp. 175–178, 2016, doi: 10.1016/j.procir.2016.02.068.

[132] G. Strano, L. Hao, R. M. Everson, and K. E. Evans, "Surface roughness analysis, modelling and prediction in selective laser melting," *J. Mater. Process. Technol.*, vol. 213, no. 4, pp. 589–597, 2013, doi: 10.1016/J.JMATPROTEC.2012.11.011.

[133] "ISO - ISO 527-2:2012 - Plastics — Determination of tensile properties — Part 2: Test conditions for moulding and extrusion plastics." https://www.iso.org/standard/56046.html (accessed Sep. 15, 2022).

[134] S. Dizdar and A. V. Krishna, "Microstructural and Mechanical Properties of Polylactic Acid/Tin Bronze Tensile Strength Bars Additive Manufactured by Fused Deposition Modelling," pp. 566–579, 2022, doi: 10.3233/atde220175.

[135] X. Wei, I. Behm, T. Winkler, S. Scharf, X. Li, and R. Bähr, "Experimental Study on Metal Parts under Variable 3D Printing and Sintering Orientations Using Bronze/PLA Hybrid Filament Coupled with Fused Filament Fabrication," *Materials (Basel).*, vol. 15, no. 15, p. 5333, 2022, doi: 10.3390/ma15155333.

[136] Z. Deng, *Study on the Interaction between Refractory and Liquid Steel Regarding Steel Cleanliness*, no. september. 2016.

[137] G. J. Cantor and C. A. Brown, "Scale-based correlations of relative areas with fracture of chocolate," *Wear*, vol. 266, no. 5–6, pp. 609–612, Mar. 2009, doi: 10.1016/J.WEAR.2008.04.069.

[138] A. V. Krishna, O. Flys, V. V. Reddy, A. Leicht, L. Hammar, and B. G. Rosen, "Potential approach towards effective topography characterization of 316L stainless steel components produced by selective laser melting process," *Eur. Soc. Precis. Eng. Nanotechnology, Conf. Proc. - 18th Int. Conf. Exhib. EUSPEN 2018*, no. June, pp. 259–260, 2018.

[139] P. E. Reeves and R. Cobb, "Reducing The Surface Deviation Of Streolithography Using An Alternative Build Strategy," *Rapid Prototyp. J.*, vol. 3, no. 1, pp. 20–31, 1997.

[140] V. Wankhede, D. Jagetiya, A. Joshi, and R. Chaudhari, "Experimental investigation of FDM process parameters using Taguchi analysis," *Mater. Today Proc.*, vol. 27, pp. 2117–2120, 2019, doi: 10.1016/J.MATPR.2019.09.078.

[141] I. Gibson, D. Rosen, and B. Stucker, *Additive Manufacturing Technologies*. New York, NY: Springer New York, 2015.

[142] A. K. Lundgren, D. Lundgren, A. Wennerberg, C. H. Hämmerle, and S. Nyman, "Influence of surface roughness of barrier walls on guided bone augmentation: experimental study in rabbits.," *Clin. Implant Dent. Relat. Res.*, vol. 1, no. 1, pp. 41–48, 1999, doi: 10.1111/j.1708-8208.1999.tb00090.x.

[143] A. Wennerberg and T. Albrektsson, "On implant surfaces: a review of current knowledge and opinions.," *Int. J. Oral Maxillofac. Implants*, vol. 25, no. 1, pp. 63–74, 2009, [Online]. Available: http://www.ncbi.nlm.nih.gov/pubmed/20209188.

[144] G. Kerckhofs, G. Pyka, S. Van Bael, J. Schrooten, and M. Wevers, "Investigation of the influence of surface roughness modification of bone tissue engineering scaffolds," *Status Publ.*, no. January, 2010.

[145] J. Anderud, *On Guided Bone Regeneration Using Ceramic Membranes*. 2016.